

Advanced technologies to control stem-cell based organogenesis

THÈSE N° 7461 (2017)

PRÉSENTÉE LE 27 JANVIER 2017

À LA FACULTÉ DES SCIENCES DE LA VIE

UNITÉ DU PROF. LUTOLF

PROGRAMME DOCTORAL EN BIOTECHNOLOGIE ET GÉNIE BIOLOGIQUE

ÉCOLE POLYTECHNIQUE FÉDÉRALE DE LAUSANNE

POUR L'OBTENTION DU GRADE DE DOCTEUR ÈS SCIENCES

PAR

Nathalie BRANDENBERG

acceptée sur proposition du jury:

Prof. S. Maerkl, président du jury

Prof. M. Lütolf, directeur de thèse

Prof. G. Schwank, rapporteur

Prof. D. Seliktar, rapporteur

Prof. D. Ghezzi, rapporteur



ÉCOLE POLYTECHNIQUE
FÉDÉRALE DE LAUSANNE

Suisse
2017

“Everybody is a genius. But if you judge a fish by its ability to climb a tree, it will live its whole life believing that it is stupid.”

Albert Einstein

ACKNOWLEDGEMENTS

It is with an immense pleasure that I would like to thank all who contributed to make this thesis a success.

First, I would like to express my sincere gratitude to my thesis advisor, Prof. Matthias Lutolf, who, in addition to being available and always excited to bounce ideas, gave me the chance and his support to perform high quality research in a true multidisciplinary environment surrounded by amazingly brilliant people. Thank you!

Secondly, I thank very much my thesis committee, Prof. Dror Seliktar, Prof. Gerald Schwank, Prof. Diego Ghezzi and Prof. Sebastian Maerkl for their participation and their involvement in evaluating my thesis. Having the chance to receive feedback from world experts is most valuable to grow scientific projects.

Also, I would like to give a big thanks to all the scientists and facility staffs who are always here to share their expertise and their passion to push projects forward. The Center for MicroNano Technology (CMI, EPFL), especially Cyrille Hibert, Joeffrey Pernollet and Kaspar Suter, the Histology Core Facility, EPFL, Jessica Dessimoz and Gianni Mancini, the Bioimaging and Optics Platform, EPFL, José Artacho, Olivier Burri, and Romain Giuet, the Electron Microscopy Facility, EPFL, Marie Croisier and Stéphanie Clerc.

A special thanks goes to the Biomolecular Screening Facility at EPFL, especially, to Benjamin Rappaz and Gerardo Turcatti with whom I could develop an exciting application of my research that will continue in the future.

Of course, this journey would have never been as amazing without the people I had the chance to share 90% of my time:

Massi – for teaching me what research is really about and all the fun times together,
Andrea – to have shared all these trips and time together, I particularly enjoy refreshing you how to ski and our endless science/philosophical discussions in the most random places that I really like and hope to continue,

Mehmet – for always being so nice and fun even though I did not manage to make you stop smoking,

Sara – to always be such a source of motivational energy and a great lab mum,

Laura and Simone – for having gone successfully through this PhD together as well as sharing so many good times outside of the lab,

Aline – to share many activities together, it is always more than a pleasure to have you around,

Aleks – to be our lab mate in adoption and for all the fun together,

Guliana – for the time already shared together and more to come,

Josefine – to always be here and take part to our crazy events,

Marlen – for always being picky on the right topics,

Mike – for giving me awesome Russian honey,

Saba and Ji Soo – for being an endless source of kindness and calm,

Vincent – to always be a lot of fun and laughs,

without forgetting, Yuya, Steffen, Samy, Adrian, Andrea and Mukul.

Also, I would like to thank all my students, Marie-Laure, Tunvez, Satomi, Pauline, Aline and Ece that have brilliantly helped me in developing this research.

To Yoji-kun, for being a long lasting friend, whom I consider like my little brother. I am always grateful for the time spent together as well as the work we could achieve.

To Sonja and Delph, who, besides being great friends within the lab, are very close to my heart for the support you give me and your precious friendship.

To Nikolce for being my favorite post-doc without whom my thesis would not look as it does. Thank you for being an amazing friend, always here to support and motivate me. Also, thank you for sharing your addiction to partying and organizing amazeballs well-deserved parties,

To Sylke for being you. Thank you for the unconditional emotional support and never-ending motivation you give me every single day. Thank you for sharing dreams and goals and making them happen with me. The future is exciting and I can't wait to make it happen,

To all my friends beyond the lab:

To Tanja and Prisci for having been here for me, always, as much in the fun time than in the difficult time,

To Nadia and Pauline for having shared great times together, for attempting to take my head off of work and for your precious friendship,

To Cylia for sharing so many great moments together and for your precious friendship,

To Pauline, Felix, Guillaume, Cedric, Arlette, Fabienne, Carole, Jonas, Vivi, Nico, Fabien and all of you for the amazing time and support,

To my entire family:

Thank you for always supporting me. Without you, this PhD would have been much tougher.

The most special thank goes to my parents, who are cherishing me unconditionally and to whom I can go hide anytime. Thank you for being here for me, always. Having you is an invaluable gift,

To both of you and grand-papa, who always wanted to have a Dr. Brandenburg,
I dedicate this thesis.

SUMMARY

Organoids represent the first *in vitro* cell culture systems that closely resemble native tissues in terms of cellular composition, architecture and key aspects of physiology. Through the discovery of these cultures, researchers could demonstrate that stem cells retain *in vitro* their innate tendency to self-organize, thus giving rise to complex structures in processes reminiscent of those driving tissue and organ development.

Until now, most organoid systems have been obtained relying on ill-defined and clinically irrelevant 3D matrices, in which these organoids are homogeneously exposed to biomolecules that induce *in vitro* development. However, tissue growth and specification *in vivo* is a tightly orchestrated process, where a multitude of effectors, from biomolecules to mechanical cues, are presented to the developing tissue in a spatiotemporally controlled fashion. Thus, even though stem and progenitor cells are able to self-organize to striking extents, there is an imminent need to establish new technologies to control the growth of these self-organizing, organ-mimicking structures. The few already described dynamic culture systems, such as microfabricated gradient generators, will have to be considerably revisited to accommodate the final size and the extended culture time of these developing *in vitro* tissues. Considering these limitations, in this thesis two innovative technologies have been developed that provide the expected flexibility to adapt to organoid cultures and that offer control on morphogenesis *in vitro*.

First, a unique method was established to generate microfluidic networks inside naturally derived and synthetic hydrogels. Using short-pulsed lasers, perfusable microchannels can be fabricated in any transparent matrix. This technique has several advantages over conventional microfabrication approaches, as microchannels can be easily fabricated *a posteriori* in 3D cell-laden hydrogels. In addition, the resulting microfluidic network can be varied on demand depending on cellular growth and morphogenetic events, without impairing cell viability. The versatility of this platform technology is exemplified using two cell-based assays: Skeletal stem cells grown in 3D can be locally attracted upon perfusion of chemo-attractants and vasculature-like constructs can be fabricated with previously unmatched ease.

Next, in order to control organoids grown in suspension, a versatile hydrogel-based microwell platform harboring U-shaped microcavities of any size or shape was developed. A wide range of cell types, ranging from embryonic stem cells to numerous cell lines, can be readily aggregated into highly homogenous cellular clusters. The differentiation of retinal organoids can be improved by optimizing the culture substrate in combination with a specific medium formulation, resulting in an increase of photoreceptor progenitors from 60%, using conventional protocols, up to 90% when using the appropriate combination of substrate and nutrient formulation. Furthermore, the novel technology was used to reduce the variability and improve the traceability of current organoid cultures grown in 3D matrices. For example, aggregation of low numbers of intestinal stem cells instead of single cells resulted in more homogenous organoid formation. The improved homogeneity allows for non-

biased analyses at single organoid levels, providing higher resolution to current protocols analyzing differences only at population levels.

Finally, new methods were explored to facilitate the application of these next-generation organoid cultures in pharmacological screenings. Using intestinal organoids derived from a murine disease model of cystic fibrosis, more specifically of the widespread mutation $\Delta F508$, a new label-free method was introduced to precisely read out transepithelial fluid exchanges. By measuring changes in the local molecular density within the organoid lumen, various functional metrics representing transepithelial fluxes can be measured, such as the time of initiation of swelling, the dilution factor inside the lumen, and the fluid uptake rate. Using image analysis approaches, these metrics can be automatically tracked over time. This method allows for the time to capture physiologically relevant 3D measures in organoid cultures without the need of complex or invasive manipulation of the sample.

Taken together, this thesis introduces several cutting-edge technologies that offer the possibility to exert control over in vitro organoid development and should therefore facilitate the translation of organoid technology towards pharmaceutical and clinical applications.

Keywords: Laser micromachining, naturally-derived hydrogel, synthetic hydrogel, polyethylene glycol (PEG), microfluidics, microfabrication, 3D migration, vasculature, U-shaped microwells, cellular aggregate, retinal organoid, intestinal organoid, cystic fibrosis, digital holographic microscopy (DHM), forskolin-induced swelling (FIS), high throughput, drug screening

ZUSAMMENFASSUNG

Organoide sind *in vitro* Zellkultursysteme, welche nativen Geweben in Bezug auf zelluläre Zusammensetzung, Architektur und Physiologie ähneln. Einhergehend mit deren Entdeckung konnten Forscher zeigen, dass Stammzellen *in vitro* ihre angeborene Neigung zur Selbstorganisation beibehalten und sich zu komplexen Strukturen entwickeln können, entlang ähnlicher Prozesse, wie sie während der Gewebe und Organentwicklung stattfinden.

Bis jetzt wurden die meisten Organoid-Systeme durch den Gebrauch schlecht definierter und klinisch irrelevanter 3D-Matrizen etabliert, in denen diese Organoiden homogenen Biomolekülgemischen ausgesetzt sind um ihre *in vitro* Entwicklung zu induzieren. Allerdings unterliegen Gewebewachstum und -entwicklung *in vivo* einem streng koordinierten Prozess, bei dem eine Vielzahl von Effektoren, von Biomolekülen über mechanische Signale, in einer räumlich-zeitlich kontrollierten Art und Weise Zellen in einem Gewebe präsentiert werden. Obwohl also Stamm- und Vorläuferzellen in der Lage sind, sich zu hohem Maße selbst zu organisieren, besteht ein unmittelbarer Bedarf für neue Technologien, mit deren sich das Wachstum dieser selbstorganisierenden Organ-imitierenden Strukturen steuern lässt. Die wenigen bereits beschriebenen dynamischen Kultursysteme, wie beispielsweise mikrogefertigte Gradientengeneratoren, müssen erheblich angepasst werden, um der endgültigen Größe und der verlängerten Kultivierungszeit dieser neuen *in vitro* Gewebe Raum zu bieten. Unter Berücksichtigung dieser Einschränkungen wurden in dieser Arbeit zwei innovative Technologien entwickelt, welche die erforderliche Flexibilität für Organoid-Kulturen liefern und welche Kontrolle über Morphogenese *in vitro* ermöglichen.

Zunächst wurde ein einzigartiges Verfahren etabliert um im Inneren natürlicher und synthetischer Hydrogele Mikrofluidik-Netze zu erzeugen. Mit Hilfe von Kurzpulslasern können perfundierbare Mikrokanäle in jeder transparenten Matrix hergestellt werden. Diese Methode hat mehrere Vorteile gegenüber herkömmlichen Mikrofabrikationsansätzen, da Mikrokanäle nachträglich und auf leichte Art und Weise in zellbeladenen 3D Hydrogelen hergestellt werden können. Darüber hinaus kann das resultierende mikrofluide Netzwerk nach Bedarf, abhängig zum Beispiel vom Zellwachstum und morphogenetischen Ereignissen, angepasst werden, ohne die Lebensfähigkeit der Zellen zu beeinträchtigen. Die Vielseitigkeit dieser Plattform-Technologie wurde mit zwei zellbasierten Testverfahren veranschaulicht: In 3D gezüchtete skeletale Stammzellen können nach Perfusion chemischer Lockstoffe lokal angezogen werden und Blutgefäß-ähnliche Konstrukte können mit bisher unerreichter Leichtigkeit hergestellt werden.

Als nächstes, wurde eine vielseitige Hydrogel-basierte Plattform entwickelt, welche mit U-förmigen Mikrokavitäten jeglicher Form und Größe ausgestattet werden kann, um die Herstellung in Suspension gezüchteter Organoiden zu steuern. Ein breites Spektrum von Zelltypen, reichend von embryonalen Stammzellen zu zahlreichen Zelllinien können leicht in sehr homogene Zellhaufen aggregiert werden. Die Differenzierung retinaler Organoiden kann durch Optimierung des Kultursubstrats in Kombination mit einer spezifischen Medium-Formulierung, anhand einer Erhöhung der Anzahl von Fotorezeptor-Vorläufern von 60% auf 90%, verbessert werden. Darüber hinaus wurde diese neue Technologie verwendet, um die Variabilität aktueller Organoid-Kulturen in 3D-Matrizen zu verringern und deren zeitliche Verfolgbarkeit zu verbessern. Zum Beispiel führte die Aggregation geringer Zahlen von Darm-Stammzellen anstatt einzelner Stammzellen zu homogeneren Organoiden während der gesamten Kultur. Diese verbesserte Homogenität ermöglicht Analysen von einzelnen

Organoiden innerhalb einer Population frei von systematischen Fehlern und bietet eine höhere Auflösung verglichen zu aktuellen Protokolle, welche Unterschiede nur auf dem gesamten Populationsniveau analysieren können.

Schließlich wurden neue Methoden erforscht, um die Anwendung dieser Organoid-Kulturen der nächsten Generation in pharmakologischen Screenings zu erleichtern. Mit Hilfe von Darm-Organoiden, welche von einem Maus-Krankheitsmodell für zystischer Fibrose, spezifisch für die weit verbreitete Mutation $\Delta F508$, isoliert wurden, wurde eine neue markierungsfreie Methode etabliert, um transepithelialen Flüssigkeitsaustausch genau zu bestimmen. Durch Änderungen in der lokalen molekularen Dichte innerhalb des Lumens eines Organoids, lassen sich verschiedene funktionelle Metriken messen, welche transepitheliale Flüsse repräsentieren. So lassen sich zum Beispiel der Eintrittszeitpunkt des Anschwellens, der Verdünnungsfaktor innerhalb des Lumens, und die Fluidaufnahmerate messen. Dank Bildanalyseverfahrens können diese Metriken automatisch über die Zeit ausgelesen und verfolgt werden. Diese Methode ermöglicht es physiologisch relevante 3D Messgrößen in Organoid-Kulturen einzufangen ohne die Notwendigkeit komplexer oder invasiver Probenmanipulationen.

Zusammengenommen stellt diese Doktorarbeit mehrere innovative Technologien vor, um mehr Kontrolle über *in vitro* Organoid-Entwicklung zu gewinnen, um damit die Umsetzung von Organoid-Technologien zu pharmazeutischen und klinischen Anwendungen zu erleichtern.

Schlüsselwörter: Laser-Mikrobearbeitung, natürliche Hydrogele, synthetische Hydrogele, Polyethylenglykol (PEG), Mikrofluidik, Mikrofertigung, 3D-Migration, Gefäße, U-förmige Mikrotitervertiefungen, zelluläre Aggregate, Retina-Organoid, Darm-Organoid, Zystische Fibrose, digitale holographische Mikroskopie (DHM), Forskolin-induzierte Schwellung (FIS) Hochdurchsatz, Wirkstoff-Screening

RÉSUMÉ

Les mini-organes, appelés « organoïdes », représentent la première plateforme de culture de cellules *in vitro* qui ressemble fidèlement aux tissus d'origine en terme de composition cellulaire, d'architecture et récapitule les éléments essentiels de la physiologie. Grâce à la découverte de ce nouveau type de culture cellulaire, les chercheurs ont pu démontrer que les cellules souches gardent *in vitro*, leur capacité innée à s'auto-organiser, ainsi donnant naissance à des structures complexes à l'aide de processus rappelant ceux qui déterminent la formation des tissus et des organes au court du développement embryonnaire.

Jusqu'à présent, la plupart des organoïdes sont fabriqués dans des matrices à trois-dimensions (3D) caractérisées de manière vague et pauvrement validées à l'échelle clinique, dans lesquelles ces organoïdes sont exposés de manière homogène à des biomolécules entraînant le développement *in vitro*. Cependant, la croissance des tissus et la spécification *in vivo* est un processus hautement orchestré, où une multitude d'effecteurs, variant entre des biomolécules et des signaux mécaniques, sont présentée devant le tissu en développement de façon spatialement et temporellement contrôlée. Ainsi, bien que les cellules souches et les cellules progénitrices sont capables de s'auto-organiser en faits marquants, il existe un besoin imminent d'établir de nouvelles technologies afin de contrôler la croissance de ces structures qui ont la capacité de s'auto-organiser et d'imiter les organes. Les rares systèmes de culture cellulaire déjà décrits, tels les générateurs de gradients employant des techniques de microtechnique, doivent être considérablement remis à l'ordre du jour et être adaptés afin de satisfaire la taille finale et la période prolongée nécessaire pour la culture cellulaire de ces tissus en développement *in vitro*. Au regard de ces limitations, dans cette thèse, deux technologies innovatrices ont été développées afin d'assurer la flexibilité attendue pour être adaptée à la culture d'organoïdes et afin d'offrir un contrôle unique sur la morphogénèse *in vitro*.

Dans un premier temps, une méthode unique a été établie afin de créer des réseaux microfluidiques au sein d'hydrogels naturellement dérivés ou synthétiques. En utilisant des lasers à brèves impulsions, des micro-canaux à perfusion peuvent être fabriqués dans une quelconque matrice transparente. Cette technique comporte plusieurs avantages par rapport aux procédés de microfabrication traditionnels, dans la mesure où ces micro-canaux peuvent être facilement fabriqués *a posteriori* dans des hydrogels incorporant des cellules en 3D. De plus, le réseau microfluidique résultant peut être varié sur demande, en fonction de la croissance cellulaire et d'évènements morphogénétiques, sans porter atteinte à la viabilité cellulaire. La souplesse de cette plateforme technologique a été illustrée en utilisant deux essais cellulaires : des cellules souches de muscle squelettique cultivées en 3D peuvent être localement attirées en perfusant des chemo-attracteurs et des matrices imitant le système vasculaire ont pu être conçues avec une facilité précédemment jamais atteinte.

Par la suite, afin de contrôler la croissance des organoïdes en suspension, une plateforme polyvalente basée sur des micro-puits d'hydrogel a été mise en place contenant des micro-cavités en forme de U de toute taille ou toute forme. Une large variété de types cellulaires, allant des cellules souches embryonnaires à de nombreuses autres lignées cellulaires, ont pu aisément être agrégées en groupes de cellules extrêmement homogènes. La différenciation des organoïdes rétiniens a pu être améliorée en optimisant la surface du substrat de culture en combinaison avec une formulation spécifique de milieu. Cette synergie a pu permettre

une hausse de 60% à 90% de création de cellules progénitrices photoréceptrices entre les procédures conventionnelles et notre nouvelle méthode. De plus, notre nouvelle technologie a été utilisée afin de réduire la variabilité entre échantillons et afin d'améliorer la maniabilité des systèmes de culture d'organoïde actuels, mis sous culture en utilisant des matrices 3D. Par exemple, l'agrégation d'un faible nombre de cellules souches intestinales à défaut d'utiliser une seule cellule souche a entraîné la formation d'un nombre bien plus important d'organoïdes homogènes. Cette homogénéité améliorée permet des approches objectives à l'échelle d'un seul organoïde, fournissant une plus haute résolution et une meilleure précision qu'il n'était possible d'obtenir auparavant avec les protocoles classiques qui analysent habituellement les différences seulement aux niveaux des populations.

Enfin, de nouvelles méthodes ont été explorées afin de faciliter l'application de cette nouvelle génération de systèmes de culture d'organoïde dans le domaine du criblage pharmacologique. En utilisant les organoïdes intestinaux dérivés d'un modèle murin de la mucoviscidose, plus spécifiquement en utilisant la mutation $\Delta F508$, la plus largement répandue, une nouvelle méthode sans marquage a été introduite afin d'étudier précisément les échanges de fluides transépithéliales. En mesurant les changements liés à la densité moléculaire locale au sein du lumen d'un organoïde, diverses statistiques représentant les flux transépithéliales peuvent être mesurées, tel le temps d'initiation de gonflement, le facteur de dilution au sein du lumen et le taux d'absorption du liquide. En utilisant des approches d'analyses d'images, ces statistiques peuvent être automatiquement suivies au fil du temps. Cette méthode permet de capturer dans le temps des mesures tridimensionnelles physiologiquement pertinentes de ces cultures d'organoïdes, sans nécessiter la moindre manipulation complexe et invasive de l'échantillon.

Considérée dans son ensemble, ce travail de thèse introduit plusieurs technologies de pointe qui offre la possibilité d'exercer un contrôle précis sur le développement d'organoïde *in vitro* et devrait ainsi faciliter la recherche translationnelle de cette technologie liée aux organoïdes vers des applications pharmaceutiques et cliniques.

Mots clés: Usinage au laser, hydrogel d'origine animale, hydrogel synthétique, polyéthylène glycol (PEG), microfluidique, microfabrication, migration tridimensionnelle, réseau vasculaire, micropuits en forme de U, agrégat cellulaire, organoïde rétinien, organoïde intestinal, mucoviscidose, microscopie holographique digitale (MHD), gonflement induit par la forskolin, haut-débit, criblage pharmacologique

TABLE OF CONTENT

ACKNOWLEDGEMENTS	V
SUMMARY	IX
ZUSAMMENFASSUNG	XI
RÉSUMÉ	XIII
CHAPTER I – INTRODUCTION	1
INTRODUCTION AND MOTIVATIONS	3
Organoids as a major technological advance in the stem cell field	3
Engineering concentration gradients using conventional microtechnology	9
Generating micro-engineered gradients to control stem cell fate	13
Recapitulating tissue function in microengineered systems	19
Open challenges	22
OBJECTIVES	23
REFERENCES	24
CHAPTER II – IN SITU PATTERNING OF MICROFLUIDIC NETWORKS IN 3D	
CELL-LADEN HYDROGELS	31
Abstract	34
Introduction	34
Results and discussion	35
Conclusions	43
Experimental methods	44
References	46
CHAPTER III – STANDARDIZING ORGANOID CULTURES	49
Abstract	52
Introduction	52
Results and discussion	54
Conclusions	65
Experimental methods	66
References	70
CHAPTER IV – ORGANOID IN DRUG SCREENING	73
Abstract	76
Introduction	76
Results and discussion	79
Conclusions	86
Experimental methods	87
References	89
CHAPTER V – DISCUSSION AND OUTLOOK	93
APPENDIX A	XVII
APPENDIX B	XXIX
APPENDIX C	XXXIII

CHAPTER I

INTRODUCTION

INTRODUCTION AND MOTIVATIONS

ORGANOIDS AS A MAJOR TECHNOLOGICAL ADVANCE IN THE STEM CELL FIELD

Since their formal discovery in 1968, stem cells have held the promise of human-relevant drug testing and (stem-)cell therapies¹. Yet, their use in clinics is still limited to a few tissues such as blood or skin. The disappointing translational impact of stem cell biology is to a large extent the result of our inability to grow many stem cell types in vitro without losing their potency, along with our difficulty to control the poorly understood process of differentiation into mature cell types.

Despite our solid knowledge of the self-organizing capacities of mammalian cells in vivo, it is only in recent years that researchers have realized the remarkable ability of adult and pluripotent stem cells to differentiate and self-organize in vitro.

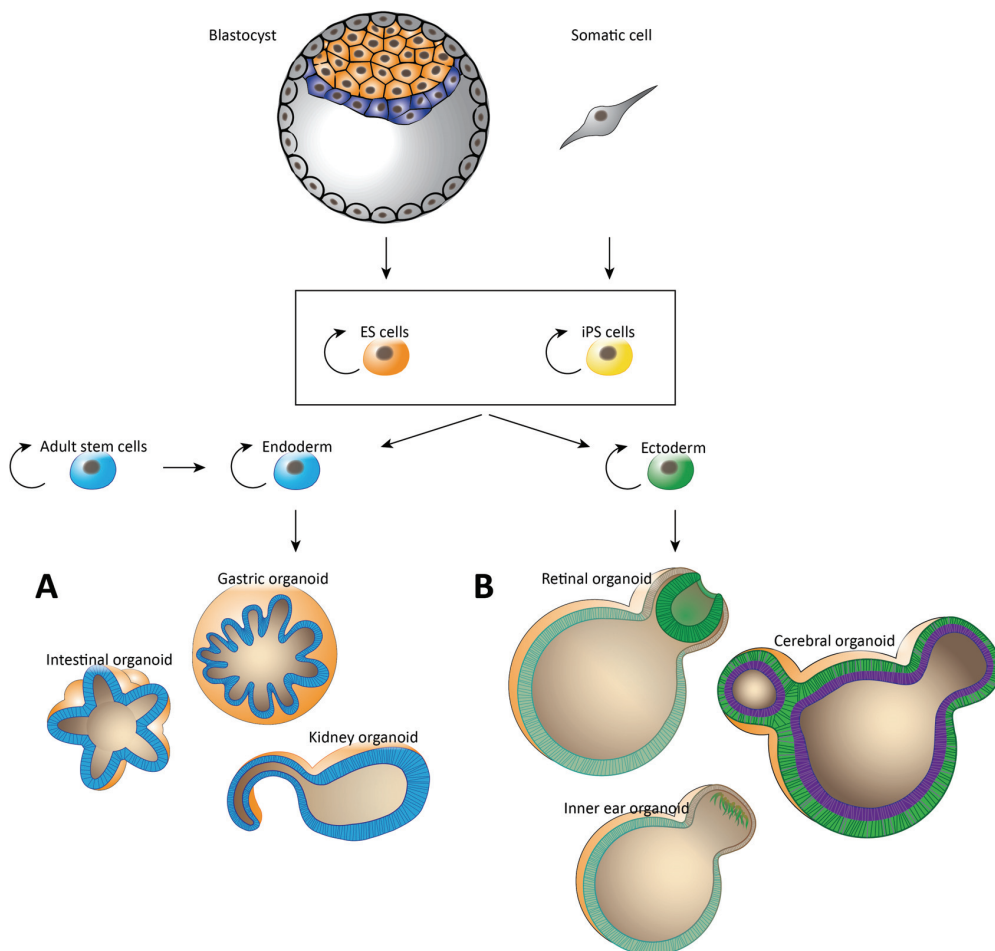


Figure 1: Conceptual scheme of the derivation of organoids. Three-dimensional tissue-mimicking constructs can be obtained from either adult or pluripotent stem cells. These cells have the capabilities to self-organize and differentiate in vitro to recapitulate some key features of the physiology of our organs. They open the door to major advances in drug screening and cell therapy.

When provided with the right signaling molecules at the right time, and when cultured in suitable three-dimensional (3D) microenvironments, many stem cells can develop into organized multicellular constructs, termed organoids, that mimic several features of real organs (see **Figure 1**).

Organoids can be defined as “a collection of organ-specific cell types that develops from stem cells or organ progenitors and self-organizes through cell sorting and spatially restricted lineage commitment in a manner similar to *in vivo*”². One of the pioneering examples of organoids is the intestinal organoid from either biopsied intestinal crypts or even a single intestinal stem cell (ISC) reported by Clevers and colleagues³. Growing these structures required a reliable stem cell marker and a detailed knowledge on the signaling crosstalk between endogenous ISC niche components in order to design culture conditions that allow the maintenance of stem cells, as well as their differentiation into organ-specific progeny. Generally, the growth of organoids relies on two major components: *i*) a cocktail of specific inducers to maintain stem cell potential, and *ii*) a supporting extracellular matrix (ECM), such as Matrigel™, that promotes spatially controlled self-organization similarly to the native tissue.

This first demonstration of organoid formation gave rise to a wave of new tissue-mimicking 3D cultures grown from primary adult stem cells from various regions of the gastrointestinal tract and other tissues with endodermal origin⁴ (see **Figure 1A**). In parallel, tissue-mimicking 3D cultures grown from pluripotent stem cells, exemplified by retinal organoids, or other organoids of tissues with ectodermal origin were being discovered, following similar concepts, notably, by Sasai and colleagues^{4,5} (see **Figure 1B**).

This nascent field holds tremendous promise to create relevant human *in vitro* organ and disease models for drug screening as well as cell therapy and organ replacement^{2,6-8}. Furthermore, deriving these structures from human pluripotent stem cells offers developmental biologists unique insights into human early development^{9,10}.

Yet, organoid systems can thus far only be obtained in relatively ill-defined and clinically irrelevant native ECM-derived microenvironments (e.g. Matrigel™) in which they are homogeneously flooded with biomolecules to induce *in vitro* development. Unsurprisingly, this results in organoid formation that is highly heterogeneous and often poorly reproducible. I hypothesize that controlling organoid development will require to precisely understand how the molecular effectors instruct developing cells in space and in time, and then to recapitulate these mechanisms *in vitro* with good fidelity.

The importance of concentration gradients in biology

Gradients were first proposed to be a critical component of biological processes more than a century ago. Embryologists observed recurrent patterns forming during the development of sea urchins, insects and amphibians, suggesting the presence of graded signals within developing embryos¹¹. Alan Turing coined the term morphogens to describe the organized signals. In addition, he defined them precisely as diffusible molecules that induce different cellular responses in a

concentration-dependent manner¹². Initially, the hypothesis was undermined by the common belief that the rapid development of such systems could not be dictated by diffusion speed, which was known to be slow. However, Crick later provided a mathematical demonstration showing that, in this context, diffusion could in fact correlate with the observed biological phenomena¹³, catalyzing wide-spread study of concentration gradients in the organization of cells.

More recently, the importance of morphogens and even gas gradients was described in diverse adult tissues. A notable example is the initiation of the formation of blood vessels, where, after activation of the endothelium, selected endothelial cells sprout and sense their elongation direction by following a gradient of vascular endothelial growth factor (VEGF) secreted by the surrounding tissue¹⁴⁻¹⁶. Interestingly, graded signals have also been shown to be an important component of several adult stem cell niches in the body. Remarkably, the hematopoietic stem cell (HSC) niche, located in the bone marrow, displays graded signals from the sinusoids to the endosteal surface that are responsible for maintaining long-term HSCs (LT-HSCs)¹⁷. In particular, low oxygen tension in the bone marrow niche appears to be a key regulator of quiescence due to the related low oxidative stress that permits LT-HSCs to maintain their slow proliferation rate¹⁸. Other niches, such as the intestinal stem cell (ISC) niche, maintain their homeostasis with a tightly regulated balance between bone morphogenetic proteins (BMP) and Wnt pathway proteins. BMPs are secreted by the villi mesenchyme while Wnts are secreted in the intervilli crypts. These proteins seem to form an inverse pair of concentration gradients from the bottom of the crypts, where ISCs reside, to the top of the villi, where the fully differentiated cells are located. This maintains the fidelity of the organ structure by keeping the various cellular compartments of the organ in specific locations^{19,20}.

Molecular mass transport through tissues: theoretical considerations

In order to engineer appropriate gradients *in vitro*, engineers must first understand their dynamics and the processes by which tissues establish them. Typically, morphogenesis induced by concentration gradients occurs by the secretion of morphogens from a source followed by the spread of morphogens into the target tissue to then be degraded. While the gradient is being established or remains dynamic, the concentration of effectors will vary in space and time. At equilibrium, the gradient reaches a steady state.

Concentration gradients of both morphogens and chemo-attractants have been characterized in various manners in the literature²¹. Among them, two main hypotheses have been presented. First, the system can be described as discrete entities that individually aid in the transport of a specific effector molecule. While this description gives a high-resolution picture of all of the cellular processes as well as the contribution of each entity in forming the gradient, this type of model is highly specific to the tissues and molecules of interest. Moreover, while the dynamic of a whole tissue is conserved over individuals and species, it is very unlikely that cellular processes between individuals are identical. These complexities render the approach difficult to generalize and, thus, to engineer. An obvious alternative to these discrete models is to describe the dynamic of a tissue as a continuum. Here, the effective

molecules vary continuously in time and space while individual entities of the tissue are not distinguished. In this case, the sum of every entity in the tissue can be recapitulated in specific parameters such as the effective diffusion coefficient of the molecule of interest or its effective degradation rate. It is of high interest to understand and formalize such gradients mathematically in order to engineer devices that accurately generate concentration gradients *in-vitro*.

In 2009, González-Gaitán and colleagues described different diffusion models inspired by embryonic development from a theoretical perspective and mathematically formalized them²². Since most of the gradients studied *in-vivo* display symmetry, the mathematical descriptions are simplified to one spatial dimension. Four different types of gradients are described. The first case study is gradients formed solely by diffusion (**Figure 2A**). In the ideal situation, the molecules produced by the source spread in a manner proportional to their effective diffusion coefficient (D). Having production but not depletion, the concentration in the target tissue increases constantly with time, which leads to the formation of Gaussian gradients that never reach steady state. Even so, transient states of these gradients can instruct cells, as is suggested for the anterior-posterior patterning of *Drosophila* embryos, which we will describe later in more detail.

To achieve steady-state, effector molecules must be degraded. The simplest model considers diffusion coupled with linear degradation (**Figure 2B**). In this case, the molecule is being degraded at a single rate (represented by a constant, k), independent of location. This model is characterized by an analytical solution, which provides the concentration profile at steady-state (solid line). The amplitude of the gradient is proportional to the source concentration, and the decay length is proportional to the effective diffusion coefficient (D) and inversely proportional to the degradation rate (k). During *drosophila* wing development, it has been demonstrated using Fluorescence Recovery After Photobleaching (FRAP) that the gradient of Decapentaplegic (Dpp) behaves similarly to the model of diffusion with linear degradation; the time needed to establish the Dpp gradient is on the same time scale as the time to reach steady-state. In addition, measurements of its degradation rate were observed as constant²³.

However, morphogen degradation rates can also vary non-linearly. Diffusion with non-linear degradation (**Figure 2C**) is typically observed when feedback loop mechanisms depend upon the morphogen concentration. In many cases, such as Hedgehog (Hh) proteins, an intracellular negative feedback loop causes high concentrations of protein to result in higher degradation rates. While linear degradation translates into exponential gradients, non-linear degradation gives rise to power-law gradients. González-Gaitán and colleagues postulate that robustness is the key characteristic that distinguishes exponential from power-law gradients. In the exponential case, there is no limiting factor as the gradient is only proportional to the flux of molecules coming from the source, leading to a general increase of concentration over the whole spatial dimension.

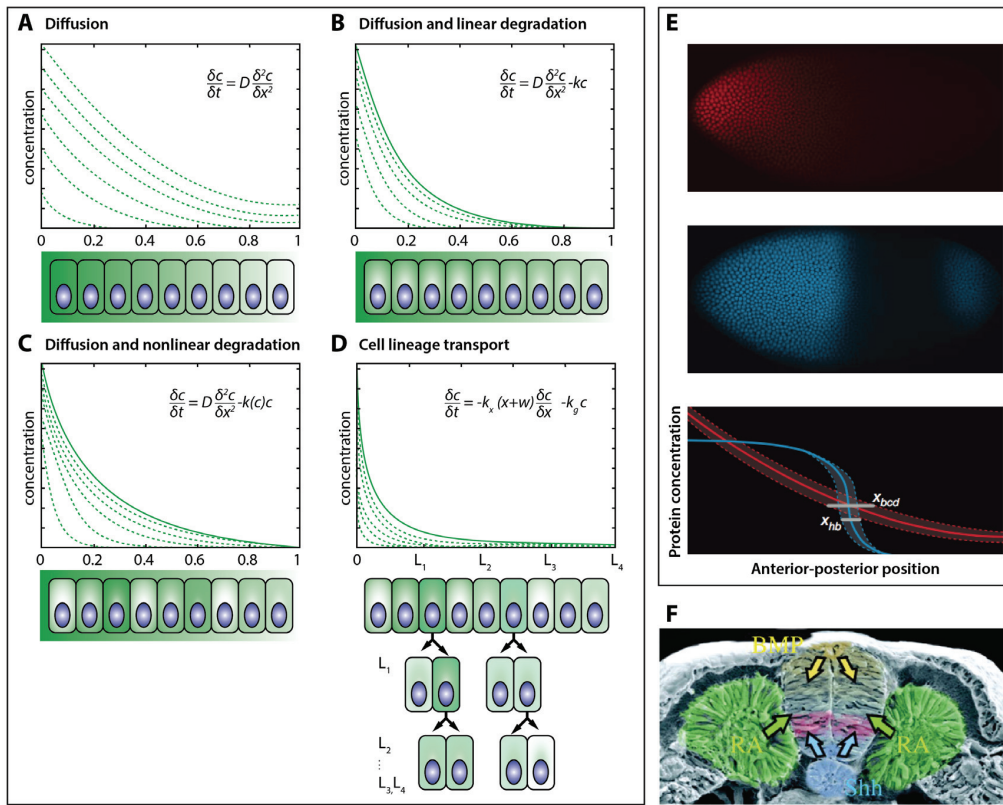


Figure 2: (A) Free diffusion model. The molecules diffuse in the cellular compartment without any interactions with the surrounding tissue. This model does not give rise to a steady state. (B) Diffusion and linear degradation model. The molecules diffuse in the cellular compartment and are being degraded by the cells at an equivalent rate throughout the tissue. This model allows for a steady state gradient with an exponential shape. (C) Diffusion and nonlinear degradation model. The molecules diffuse in the cellular compartment and are being degraded at unequal rates by the different cells composing the tissue. This model allows for a steady state gradient with a power law shape. (D) Cell lineage transport model. The molecules are not secreted in the extracellular space, which forms a gradient through cell growth and division. This model allows for a steady state gradient following a power law as well. Adapted from (22). (E) Fluorescent images of a drosophila embryo at the blastoderm stage of development. Bicoid and Hunchback proteins are fluorescently tagged using immunofluorescence in red and blue, respectively. The protein concentrations are represented as normalized in arbitrary units. Figure reproduced from (24). (F) Scanning electron micrograph of the closed neural tube. Counter gradients of BMPs and SHH contribute to the dorsal-ventral patterning of the cells along the developing neural tube. Image reproduced from (26).

In contrast, in the power-law case, a higher production leads to a higher concentration, which in turn increases the degradation rate. Thus, the effective increase in concentration is smaller than in exponential gradients. The latter model shows a self-regulatory component that has the potential to mimic proteins displaying feedback loop mechanisms. Lastly, gradients can be generated without secretion or diffusion in the target tissues. Cell growth and division itself can propagate effectors and thus establish graded intracellular signals. This cell lineage transport model (Figure 2D) takes single cells as “volume elements” of the tissue. Therefore, concentration is inversely proportional to the volume, which implies that

if an element grows exponentially, the concentration will decrease at the same rate; the molecules get diluted because of growth. The corresponding mathematical model gives a steady-state solution that follows a power law, which is similar to the model of diffusion with non-linear degradation. On a final note, it is important to specify that cellular proliferation during development most likely couples cell lineage transport with gradients established through diffusion, regardless of degradation characteristics. However, if the growth of the tissue is much slower than diffusion turnover, which is often the case, the dilution effect of cell division becomes negligible.

Overall, the models described above are valuable tools since they can recapitulate the fine modulation of gradients that occurs through complex interactions between receptors, extracellular matrix components and inhibitors²² by including these interactions in the model as different variables.

Learning from developing organisms

As a perspective, we will detail two extensively studied examples to illustrate how these models can be relevant for understanding *in-vivo* morphogenesis. In *Drosophila* embryos, anterior-posterior patterning is initiated by a gradient of the transcription factor Bicoid (Bcd) established from maternal Bcd mRNA deposited in the embryonic syncytium. Even though detailed mechanistic studies are still pursued to understand precisely how the gradient develops, Bcd is widely described as a simple diffusion model, where the Bcd protein is produced in the anterior part of the embryo, diffuses and decays throughout the tissue. While it is still debated whether this system reaches a steady-state before instructing the cells, its “instructive state” can be represented by an exponential profile (**Figure 2E**)²⁴. Experimentally, the Bcd profile was found to deviate slightly from the exponential model at the anterior region, since the synthesis of Bcd protein is not localized at a single point source. However, the fidelity of the model is sufficient to recapitulate tissue dynamics such as pattern scaling²⁵.

Vertebrate development is also orchestrated by tightly regulated morphogen gradients. In this context, neural tube patterning has been the gold standard for studying gradient-mediated dorsal-ventral patterning. In developing neural tissue, the source of the ventralizing morphogen, Sonic Hedgehog (SHH), is located outside of the developing tissue and induces the most ventral cells of the forming neural tube to differentiate (**Figure 2F**)²⁶. Interestingly, cell patterning in the neural tube is proportional to SHH concentration as well as the duration of SHH exposure. Thus, the SHH gradient acts in a concentration-dependent manner, and is increasing in amplitude in the neural tube, establishing then an exponential gradient, which resembles to diffusion with linear reaction. However, cells appear to be responsive to SHH only during specific time windows, suggesting mechanisms exist that modify the signaling activity of differentiating cells and desensitize them to the Hedgehog signaling²⁷. These intriguing mechanisms fortify the patterning process of developing tissues, such as the neural tube²⁸.

ENGINEERING CONCENTRATION GRADIENTS USING CONVENTIONAL MICROTECHNOLOGY

Microfluidic technology has unique features that allow the manipulation of incredibly small amounts ($10^{-9} - 10^{-18}$ liters) of fluids at the micrometer scale. Operating fluids at such a small scale provides two major advantages for biological applications: First, fluid behavior at this scale is mostly laminar, which permits the flow to be manipulated with fine control. In a laminar regime, flows do not mix convectively; each particle follows its specific streamline. Thus, mixing can only occur by diffusion within the fluid or across the interface of different fluids. Furthermore, by reducing or eliminating the presence of chaotic turbulent flow, microfluidics and its laminar nature allow users to precisely predict critical geometrical and fluidic parameters²⁹ to engineer relevant devices. Secondly, the order of magnitude of microfluidic devices, which ranges from tens of nanometers to hundreds of micrometers, fits particularly well with the scale at which cellular processes occur³⁰. Moreover, the standardized fabrication process allows an exceptionally high degree of freedom in planar designs and even in multilayered devices, although the fabrication of more intricate features along the z-axis still remains a challenge.

So far, microfluidics has been applied primarily for analytical biology or fabricating microparticles from emulsions. Despite notable elegant demonstrations using robust systems, such as *Drosophila* embryos³¹, microorganisms³², or cell culture^{22,33,34}, coupling living organisms with microfluidics is still a relatively early application of the technology. Today, facilities supporting development of microfluidics technology is common in many institutes around the world where biologists, physicists, chemists and microengineers develop cutting-edge, application-based microfluidic systems.

First, we will give a basic overview of the fluid mechanics knowledge required to build successful microfluidics systems, and then we will study how gradients can be generated using such systems.

Fluid mechanics at the microscale

When studying flows at the microscale, several considerations must be taken into account. Specific, intrinsic parameters define fluids, while the microfluidic channels themselves are subject to physical constraints. Every fluid is characterized by two important parameters; its density, ρ , which measures the ratio of mass to volume, and its viscosity, μ , which represents the flow response of the material. Even though all materials are compressible to some degree, while looking at fluids in motion, especially biological fluids that can be considered analogous to water, their densities remain constant. Thus, they are taken as incompressible, which drastically simplifies the mathematical characterization of the system.

Microfluidic channels display interesting characteristics to consider when calculating flows. First, actuation of flow solely in the horizontal direction and the relatively inconsequential gravitational effects at this dimension renders vertical fluctuations negligible. In addition, most of these devices are fabricated using planar lithography techniques, which gives the channels rectangular cross sections. Thus, they are characterized by the channel width, w , and height, h . Finally, these flows are mostly

pressure driven, and it has been demonstrated extensively that fluids at the surface of the microchannels obey the no-slip boundary condition (i.e. there is no flow at the fluid-channel interface), as they wet the surface³⁵.

The best qualitative measure of a fluid in motion is the Reynolds number, a dimensionless number that assesses the ratio of convective forces to viscous forces. It is described as follow:

$$Re = \frac{\rho \bar{v} D_h}{\mu} \quad (1)$$

where D_h is the characteristic length, and \bar{v} is the average fluid velocity in the channel. Typically, the characteristic length for a rectangular channel can be calculated as follow:

$$D_h = \frac{2wh}{(w+h)} \quad (2)$$

We usually define flow as laminar when Re is lower than 2300. All microfluidic devices possess an Re below this threshold, showing that viscous forces are dominant in this environment.

Lastly, flows can be calculated from the Navier-Stokes equations, whose mathematical development is beyond the scope of this book. However, after simplification, multiple parameters can be calculated using the equations (3) and (4). Flow rates, Q , are typically formalized as a function of the pressure drop, Δp , over a channel length, L , and can be written as follows for rectangular cross sections:

$$Q = \bar{v}A = \bar{v}wh = \frac{wh^3 \Delta p}{12\mu L} \quad (3)$$

It is noteworthy to specify that the pressure drop can be written as a relation between the hydrodynamic resistance in the channel, R_H , and the flow³⁶, mirroring voltage drops in electrical current. From equation (3), this relation can be written as follow:

$$\Delta p = QR_H = Q \frac{12\mu L}{wh^3} \quad (4)$$

Hydrodynamic resistance, which is cumulative like in electrical circuits, is a critical parameter to consider when designing microfluidic devices.

Micromanipulating flows to generate concentration gradients

As described above, flows are laminar in microfluidic devices. Thus, the simplest way to generate a gradient is to bring two streams composed of different molecular species together using a T-shaped or Y-shaped junction³⁷⁻³⁹. However, despite their simplicity, these types of gradient generators are limited to certain profiles, such as sigmoidal shapes. Mixing mediated by microfluidics has been extensively characterized in the literature and has created a foundation for more elaborate gradient generators. Using a premixing microchannel network, Jeon *et al.*⁴⁰ developed the first device capable of generating many distinct profiles. This design—subsequently improved by Dertinger *et al.*⁴¹ and commonly known in the field as the “christmas tree gradient generator”—harbors two main regions (**Figure 3A**). The upper part of the device has a series of bifurcated microchannels that repetitively

split and recombine. As the horizontal channel length was designed to be three orders of magnitude smaller than the vertical channel (V) length, the resistance of the horizontal channel can be neglected, allowing only the serpentine resistance to be considered when modeling the flow being split. In addition, each serpentine channel is congruent, and each branched path has an equal amount of branching layers (B). Thus, the resistance and the flux across each serpentine are equal. Finally, because of its vertical symmetry, the splitting ratios are symmetric at each branching point. Together, these characteristics allow the dilution of the initial concentrations to be precisely calculated across the whole mixing region⁴¹. The lower part of the device is made of a larger channel, in which all of the mixed branches join to create a quasi-continuous gradient over its width, whose cross section, L, represents the analyzed section of the resulting gradient in **Figure 3A**.

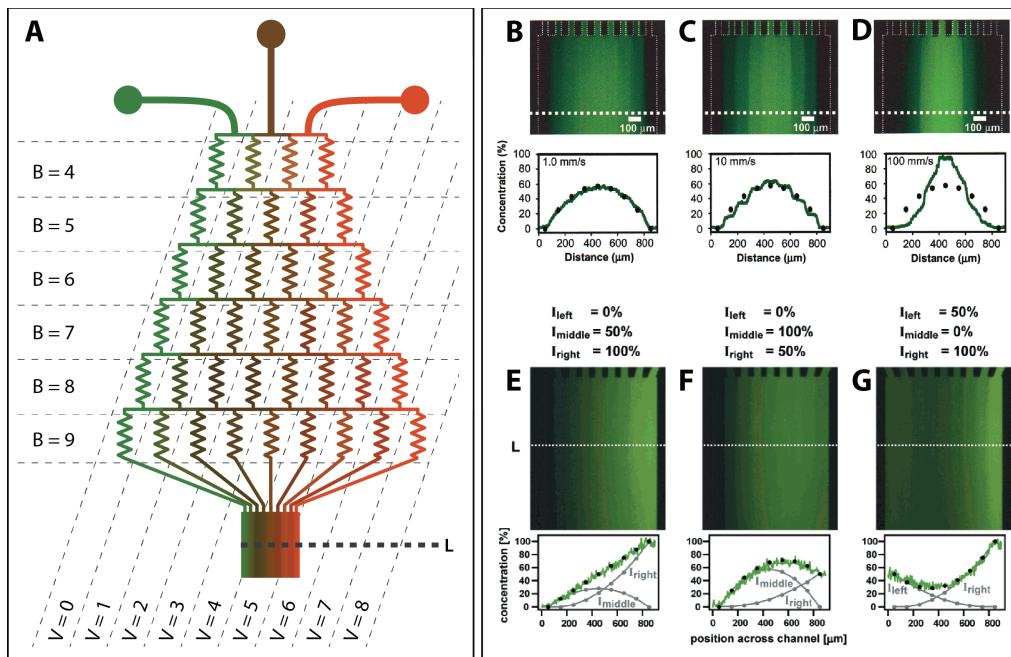


Figure 3: (A) Scheme of the Christmas tree microfluidic design. B represents the number of branching points, V, the number of vertical channels. The resulting gradient is analyzed in L. Adapted from (40). (B)-(G) For every generated gradient, a wide-field fluorescent micrograph is shown with a dashed line indicating where the gradient was analyzed. The concentrations were normalized for comparison purposes. (B)-(D) Gaussian shaped gradient, generated using equal flows in all inlets of 1, 10 and 100 mm/s, respectively. (E) Linear, (F) modified bell shaped and (G) parabolic gradients are generated using different contributions of the inlets. Figure reproduced from (42).

As a result, many profiles can be generated using this device. Two variables can be changed to modify the profiles: the flow rates of the entering fluids, and the contribution of each in the whole system. When the flow rates are all equal and a fluorophore is incorporated only in the middle input channel, bell-shaped profiles are produced (**Figure 3B**). In addition, an equal increase from 1 mm/s to 100 mm/s in all input flow rates sharpens the profile peak (**Figure 3C,D**). In order to produce more intricate profiles, the contribution of each input flow can be varied. For example, linear gradients can be generated while stopping the left flow, and keeping the

middle flow at 50% of the right flow rate (**Figure 3E**). Any combination can be used to create varying parabolic profiles (**Figure 3F,G**).

Based on this concept, adding parallel mixing regions gives a higher resolution in the output channel and permits the generation of more complex shapes, such as triangular or bimodal profiles⁴². While these active approaches to engineer gradients are interesting in terms of control, they possess two main disadvantages. First, the produced gradients are not purely continuous, but could be considered more accurately as “digital”, since each contributing branch has a single, specific concentration. Secondly, high shear stresses induced by high flow rates tend to become deleterious for cells.

An alternative to using active flows is the use of free diffusion from a source to a sink compartment. To avoid convective flow between the two compartments and isolate the fluid of the gradient forming region, microchannels with high fluidic resistance⁴³⁻⁴⁵, porous semipermeable membranes⁴⁶⁻⁴⁸ and hydrogels, typically composed of collagen or agarose^{49,50}, have been used to form gradients. Here, the concentration gradient evolves over time as the molecules are transported through the convection barrier until a steady-state is reached, when the diffusive influx and outflux are balanced. To describe in details these convection-free cases, we will focus on hydrogel barriers, which are more relevant for live cell or organism culture.

Hydrogels as a barrier to generate concentration gradients

Hydrogels are porous natural or synthetic polymer networks with high water content. Their porosity allows molecules sized up to a few hundred kilodaltons to freely diffuse through the network while preventing convective flows. This characteristic renders hydrogels the ideal candidates for forming convection-free gradients. Saadi *et al.* first demonstrated hydrogel-mediated gradient generators. They developed a simple ladder-shaped device, called the “Ladder Chamber”, which could generate stable gradients across two-dimensional (2D) cell culturing microchannels or three-dimensional (3D) hydrogels. The device is composed of two parallel but separated channels, the source channel and the sink channel, connected with small, perpendicular, rectangular microchannels containing the cells or the hydrogel, which may or may not harbor cells⁴³.

Since only diffusion is involved and the device geometry is symmetric, this design is limited in the variety of gradients that can be generated. Mosadegh *et al.* achieved greater versatility of the ladder chamber by modifying the geometry of the flow-free chambers (**Figure 4**).

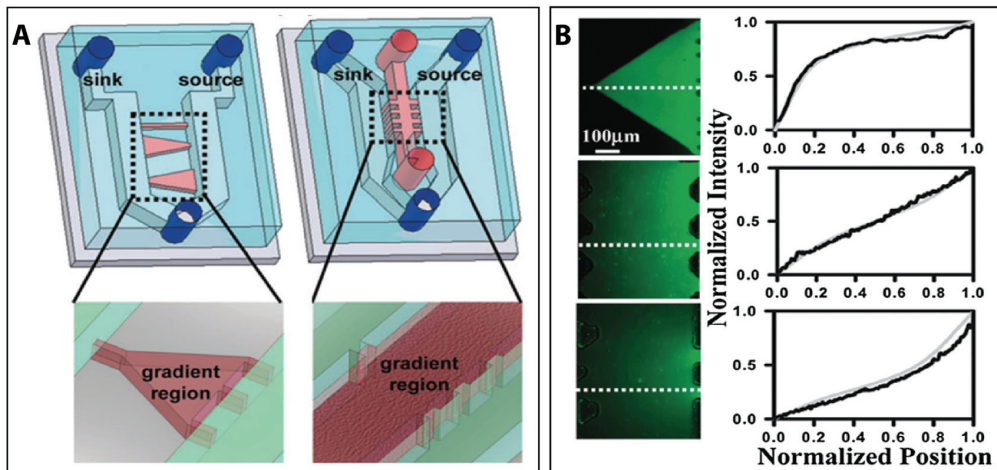


Figure 4: (A) Graphical representation of hydrogel barrier-induced gradients. The left panel shows the insertion of the hydrogel from the side channels. The right panel shows the insertion of the hydrogel from a specific hydrogel loading channel. In both cases, the number of microgrooves on the sink and the source side will define the gradient shape. (B) Different gradient shapes. Left, wide-field fluorescent micrographs of the forming gradients. Right, expected theoretical gradient are shown with a grey solid line, experimental analysis are shown with a black solid line. Figure reproduced from (42).

Indeed, varying the area of the interface between the source or sink and the hydrogel modifies the influx and outflux of molecules within the gel. This results in local accumulations or depletions of molecules and thus modifies the concentration gradient profile⁵¹. For example, a triangular-shaped chamber with its tip at the sink side allows the formation of a square root-shaped gradient (**Figure 4A**). Differentially varying the number of microgrooves touching the hydrogel on the source and the sink side generates different types of profiles, including linear and sigmoidal shapes (**Figure 4B**). Variations of this concept can give rise to a broad range of 2D and 3D gradient generators suited for different applications, from conventional cell culture to complex 3D cellular constructs.

Finally, it is noteworthy to point out here that using hydrogels in gradient-generating devices is of high interest as it has been shown extensively over the past decade that, in many cases, cells display completely different phenotypes when cultured in 3D as opposed to 2D. In particular, certain cell types, such as cancer cells⁵², appear to lose their aberrant characteristics in 2D, which may pose fundamental issues for drug screening accuracy, while they maintain the tumorigenic phenotype in 3D⁵³. Thus, assessing the behavior of cells in 3D, notably under a specific molecular gradient, is critical to observe reactions closest to *in-vivo*.

GENERATING MICRO-ENGINEERED GRADIENTS TO CONTROL STEM CELL FATE

Conventional microfluidics to spatially control stem cell fate

T/Y-shaped gradient generators have been primarily used to locally control stem cell differentiation. Their ease of use as well as their high predictability permits sensitive cells such as pluripotent stem cells and mesenchymal stem cells (MSCs) to be

cultured in microfluidic devices for limited time periods. At first, phenotypic changes were induced using growth factor or morphogen gradients in such devices. For example, Park *et al.* could locally manipulate the number of neuronal cell bodies as well as the density of the neurite bundle networks upon exposure of counter-gradients of SHH and FGF8 as well as SHH and BMP4⁵⁴. Similarly, multiple studies show gradient-induced migration or differentiation of MSCs into the three main lineages (*i.e.* adipogenesis, osteogenesis, chondrogenesis)^{55,56}.

Moreover, it was recently demonstrated that the spatial control of early differentiation of mouse embryonic stem cells (mESC) through gradient generators can mimic *in vivo* processes to a certain extent⁵⁷. It is well known that during the early organization of the inner cell mass, Nanog-positive and -negative cells segregate into, respectively, the epiblast that will later differentiate into all of the embryonic tissues, the extraembryonic mesoderm, and the primitive endoderm that will differentiate into extraembryonic tissues, namely the visceral and parietal endoderm⁵⁸ (**Figure 5A**). Furthermore, it has been shown that the heterogeneity of Nanog is also found in ESC cultures⁵⁹. Zhang and colleagues developed a microfluidic model (**Figure 5B**) of this early segregation by locally differentiating mESCs into Nanog-negative cells while keeping the neighboring cells Nanog-positive. Using doxycycline (Dox)-inducible Nanog-expressing cells, they demonstrate that upon exposure of Dox plus Leukemia Induced Factor (LIF) on one side and retinoic acid (RA) minus LIF on the other side, the cells located on the right half of the culture chamber stay pluripotent while the cells on the left half of the chamber lose their pluripotency and, therefore, expression of Nanog (**Figure 5C,D**).

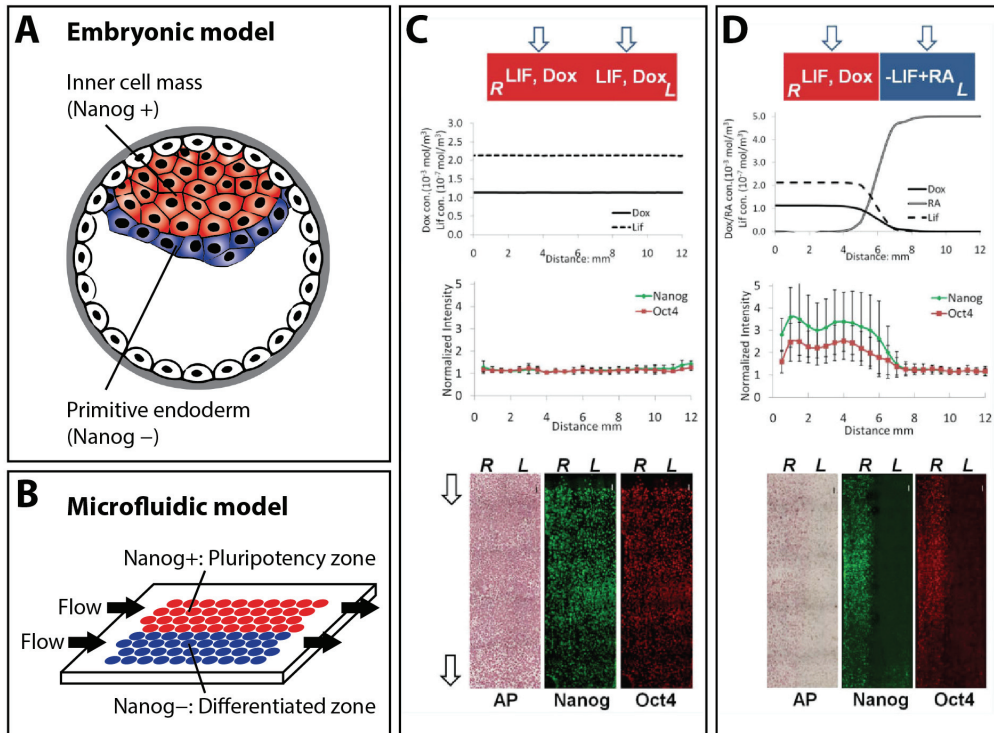


Figure 5: (A) Schematic representation of a mammalian blastocyst. The Nanog positive and negative cells segregate into distinct regions of the inner cell mass. (B) Microfluidic model of this natural organization. (C) Control condition. Constant LIF exposure as well as constant Nanog expression (Dox inducible) leads to a homogenous population of Nanog positive cells. (D) Counter gradients of LIF+Dox and RA allow the generation of distinct and neighboring populations of Nanog+ and Nanog- cells. Figure reproduced from (57).

This study highlights the ability of microfluidic approaches to recapitulate, *in-vitro*, important events of early development. Similarly, microfluidic bioreactors for the gradient-induced differentiation of human ESC (hESC)-based embryoid bodies (EB) have been developed. These systems typically possess two side channels, which act as source/sink for each other, and the EB culture chamber in the middle⁶⁰ (Figure 6). Even though such system could be interesting for screening applications, in this configuration, within the same connecting channel, the aggregates are not only exposed to the molecule of interest but also to the signaling activity of the neighboring aggregates. This has been suggested to increase the variability of the response of aggregates and, thus, of the results.

Overall, the deviations from nature in these systems are still profound as the cells reside on hard, glass or poly(dimethylsiloxane) (PDMS) surfaces, which is far from their *in-vivo* microenvironment.

Due to these differences, cell behavior can be dramatically altered in multiple ways. First, it is suggested that differentiation of mESCs is influenced by the stiffness of their substrate⁶¹. Therefore, glass, plastic or PDMS surfaces have limited biologically relevant adaptations as they cover a restricted range of stiffness. Second, conventional microfluidic devices are primarily made of PDMS. Despite its sufficient biocompatibility, ease-of-use, optical transparency and gas permeability, the cross-linking agent of this silicon-based polymer can display some toxicity. The uncross-linked oligomers can diffuse into the culture chambers, particularly when the surface to volume ratio is high. In addition, technical issues can arise due to the adsorption of molecules at the surface of PDMS, which causes local changes in molecular concentration, and osmolarity changes that can result from the evaporation of water⁶²⁻⁶⁴.

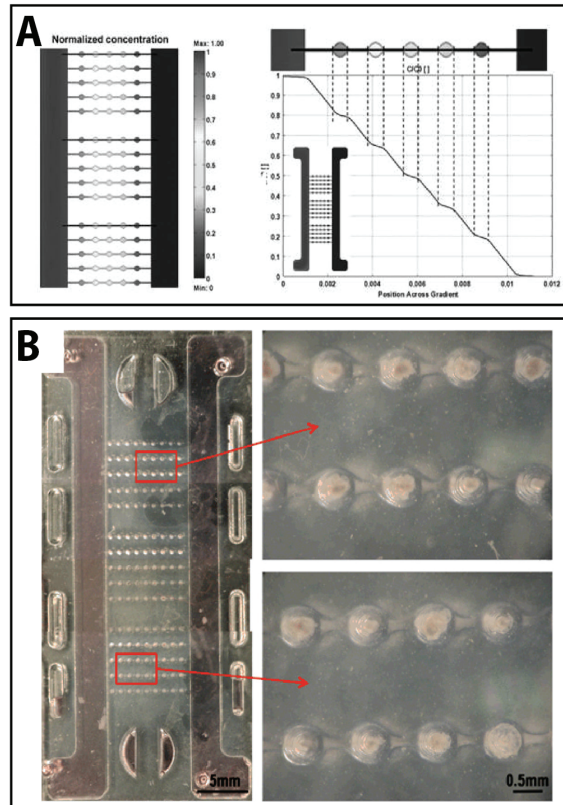


Figure 6: (A) Schematic representation of the microbioreactor including representative results of the computational modeling of mass transport within the bioreactor using a 70 kDa fluorescent molecule. The right panel shows the theoretical concentration profile across the microwells. (B) Photograph showing the entire microbioreactor seeded with EBs. Figure reproduced from (60).

Combining hydrogel and microfluidic technology to manipulate stem cell fate in near-physiological settings

In addition to their excellent mass transport properties, which allows molecular gradients to form, both naturally derived hydrogels, such as Matrigel™ or collagen, and synthetic hydrogels can be engineered to elicit physiologically highly relevant multicellular phenomena⁶⁵. In particular, synthetic hydrogels such as those composed of poly(ethylene glycol) (PEG) are attractive due to their highly controllable physicochemical and biological properties⁶⁶⁻⁶⁸. With these biomaterials, many parameters can be tested on cells or cellular constructs in two and three dimensions. As stated before, the stiffness of the microenvironment may play an important role in cellular processes⁶⁹⁻⁷², and it can be tuned extremely precisely⁷³ in

synthetic hydrogels to probe cellular behavior at a higher resolution than conventionally used biomaterials. Secondly, synthetic hydrogels can employ “cell-friendly” and highly selective chemistry to attach biochemical cues that direct both the behavior and fate of cells^{74,75}. Finally, the polymer backbone can also be modified to allow cell-mediated remodeling of the substrate, notably through the addition of matrix metalloproteinase-sensitive sites⁶⁶⁻⁶⁸, which permits cells to remodel their environment and deposit their own matrix. The combination of these parameters in cellular assays can lead to a complex analysis scheme^{8,74}, which can be addressed either by formulating educated guesses from *in-vivo* studies to find the accurate microenvironments for the cell types of interest⁷⁶ or developing 3D extracellular matrix (ECM) screening systems using robotic liquid dispensers in order to elucidate functionally relevant conditions⁸.

Despite the high versatility of these emerging biomaterials, cells in these culture systems are still exposed to homogenous mixtures of signaling cues, which do not mimic the dynamic nature of developmental and adult regeneration processes. To begin to trigger the organization of cells into more relevant tissue models, dynamic conditions must be interfaced with these model matrices. Thus, coupling microfluidic technologies with synthetic ECMs may be an attractive approach to probe yet unexplored, more complex biological processes *in vitro*⁷⁷.

As one of the first proof-of-concepts, Lutolf and co-workers developed a method that allows the attachment of biomolecular cues in a graded manner onto synthetic PEG hydrogel surfaces^{78,79}. By incorporating protein A- and/or NeutrAvidine-maleimide molecules in PEG-based hydrogels, the surface of these natively inert substrates can be functionalized with Fc-tagged and/or biotinylated biomolecules. They could for example interface microfabricated Y-shaped gradient generators (**Figure 7A**) and biofunctionalized surfaces to flow fluorescently labeled Fc-tagged bovine serum albumin (BSA) at the surface of the hydrogel (**Figure 7B**), generating a variety of gradient shapes, including linear, exponential or Gaussian⁷⁸. Perhaps more interestingly, they could show that, upon the formation of a graded, tethered LIF signal, the pluripotency of Rex1::GFP reporter mESCs could be spatially influenced following the gradient of the molecular effector. Cells forming colonies on the highest tethered area were maintaining Rex1 expression while colonies on the other end of the gradient were exiting pluripotency (**Figure 7C**). This system may also be explored to screen concentrations of biomolecules on adherent stem cells.

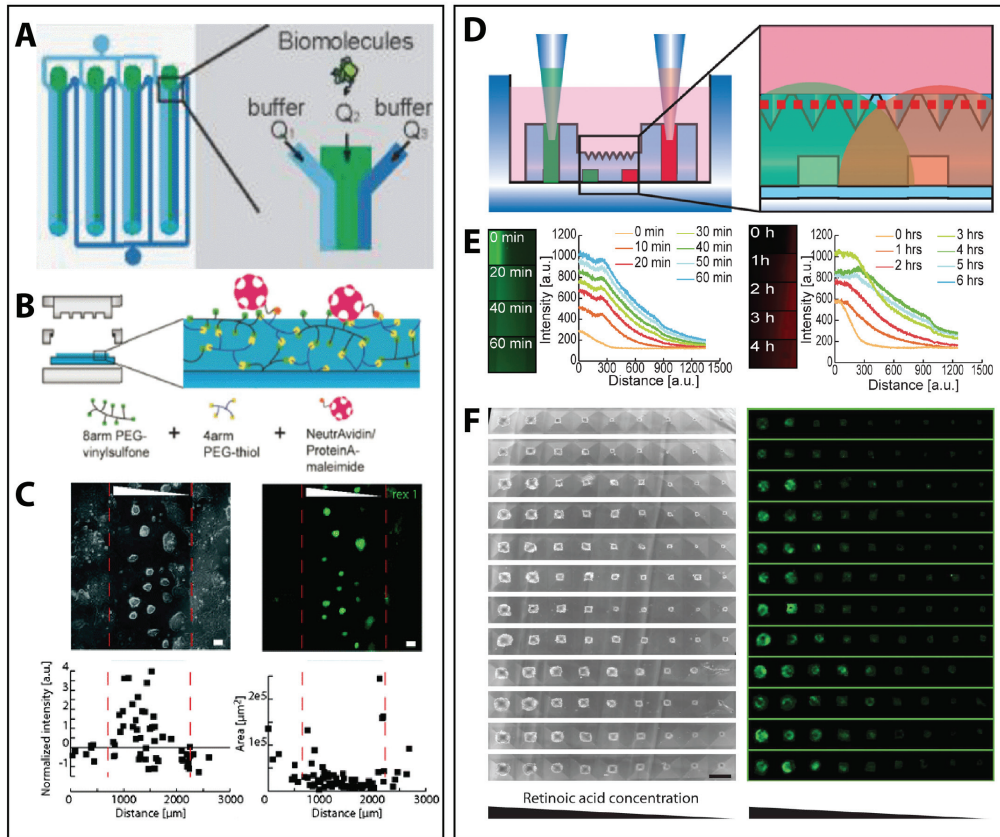


Figure 7: (A) Schematic representation of the gradient-generating microfluidic design. (B) Left, device holding the microfluidic chip onto the hydrogel surface, allowing the formation of the gradient and the attachment of the molecules onto the hydrogel. Right, chemistry used to attach the flowed molecules to the non-crosslinked polymer arms. (C) Bright-field and fluorescence micrographs showing Rex1::GFP reporter cells responding to the tethered LIF gradient. The GFP intensity of the colonies decreases along the gradient and the colony area increases inversely to the gradient, indicating differentiation. Figures reproduced from (79). (D) Conceptual scheme of the combination of aggregate culture with microfluidic-induced gradients. (E) Profile of the gradient forming over the first hour, *right*, and over the following 6 hours, *left*, upon active perfusion. (F) Bright-field and fluorescent micrographs showing sox1::GFP reporter ESCs derived EBs as a response to graded RA signaling. Expression of sox1 and the size of the colony increase with higher concentrations of RA. Figures reproduced from (80).

Yet, thus far these innovative microchip-based hydrogel culture platforms have been explored exclusively in 2D setting, while the culture of cells in three dimensions is arguably more physiological. What is more, existing 3D culture systems are still mostly static, enabling morphogens delivered in a rather unspecific manner. Thus, it is of high interest to merge microfluidic technology with 3D biomatrices affording precise delivery of specific biomolecules to cells in space and in time.

Perhaps one of the first demonstration for such a combination of hydrogel and microfluidic technology with 3D cell culture was described by Cosson and Lutolf⁸⁰. Using patterns made with soft-lithography and plastic supports, they molded agarose gels with pyramidal-shaped microwells on the upper part of device and microchannels in the lower part of the device to allow perfusion of molecules of

interest (**Figure 7D**). They show that green and red fluorescent BSA molecules diffuse across the aggregate culture upon active perfusion (**Figure 7E**). The left panel shows a higher resolution of the gradient behavior in the initial phase, and the right panel indicates that the gradient stabilizes after three hours. To demonstrate the advantage of the system to analyze the interaction of molecules of interest with the aggregates, retinoic acid (RA) was delivered to mESCs in a graded manner. With the green fluorescent reporter indicating SOX1 expression and, therefore, cell fate commitment into the neural lineage, they could observe that below a certain threshold of concentration, SOX1 was not expressed anymore, implying the cells were not committed towards the neural lineage (**Figure 7F**). Exposing cells to graded signals provides the elegant ability to analyze their behavior under continuous concentration changes in which the effective concentration can be discerned immediately. Finally, gradients in hydrogels in three dimensions have been recently shown in an elegant study by Ehrbar and co-workers to influence MSCs morphogenesis⁸¹. These authors aimed at mimicking native gradients of PDGF-BB that may exist in the perivascular niche to probe MSC behavior. They could observe that cells residing closer to the source were more elongated and displayed a higher migratory activity compared to the cells residing further away.

These early studies highlight the exciting potential in combining engineering of microfluidics and extracellular matrices to impact cell biology and tissue engineering.

RECAPITULATING TISSUE FUNCTION IN MICROENGINEERED SYSTEMS

“Organs”-on-a-chip

Thanks to these advances in microscale engineering technologies, researchers could develop intricate tools to miniaturize and compartmentalize our conventionally heterogeneous and large 2D cells culture systems. Microsystems have been recently combined with mammalian cells as an attempt to recapitulate some tissue level functions “on chip”. By depositing high number of cells into PDMS microchambers or onto semipermeable membranes, basic tissue functions could be recapitulated. Ingber and colleagues provided the first proof-of-concept of a biomimetic microsystem by fabricating a device termed “lung-on-a-chip”, recapitulating a few specific lung functions at the organ level⁸². In this study, they show an elegant method to create a micro-air-liquid interface and co-culture primary human alveolar epithelial cells and microvascular endothelial cells that sandwich a semi-permeable PDMS membrane (see **Figure 8A**). This microsystem format is a valuable tool for extracting organs specific tasks such as transepithelial transport and has been adapted for a multitude of epithelial cell types, such as Caco-2 intestinal cells (see **Figure 8B**, Gut-on-a-chip)⁸³ or primary human adult proximal tubular epithelial cells (see **Figure 8C**, Kidney-on-a-chip)⁸⁴. In addition to epithelial microchips, researchers also sought to mimic organs with widespread associated diseases. For example, cardiac muscles caught much attention, as heart failure remains one of the prevalent death causes in our societies⁸⁵. Recently, human iPS cells were differentiated into cardiomyocytes with nearly 90% efficiency⁸⁶ and seeded in an elongated microchamber.

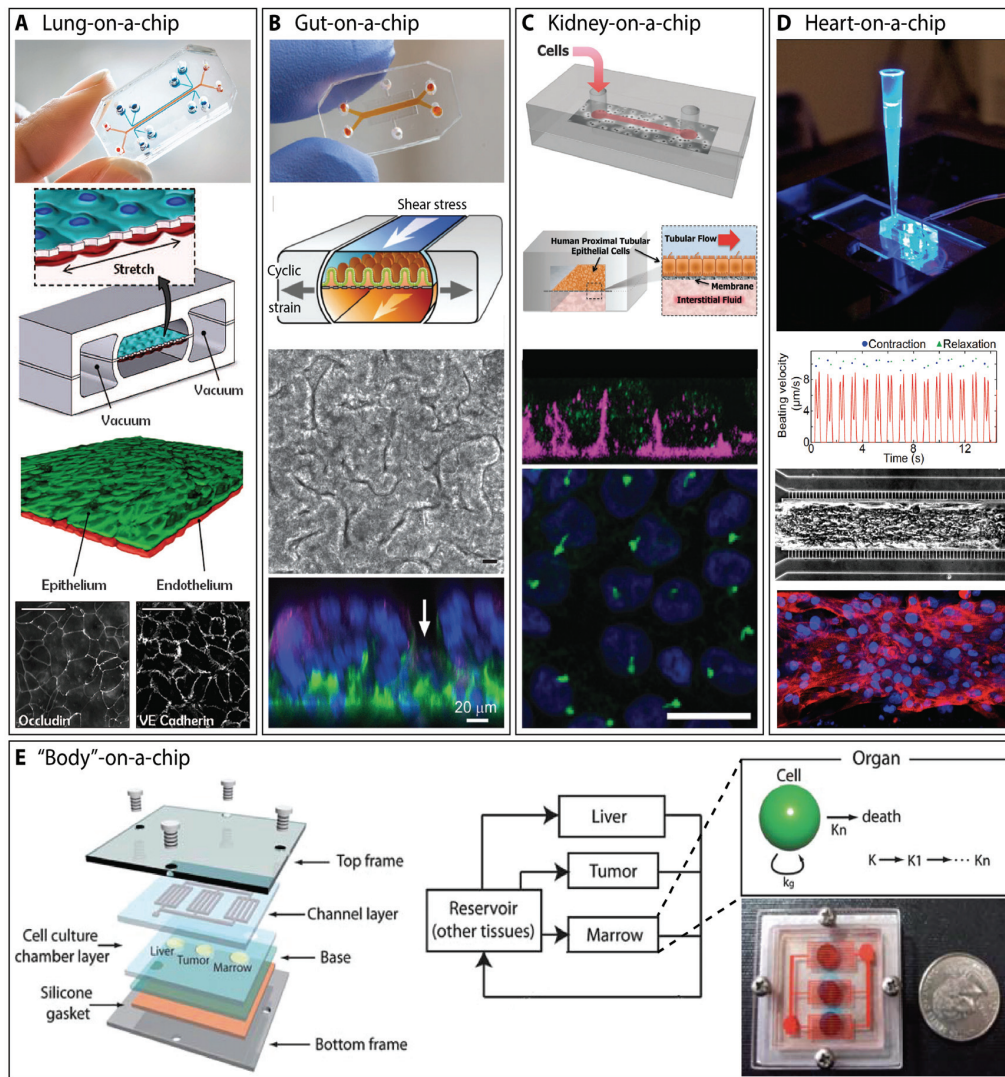


Figure 8: (A) Representative picture and schematic of a Lung-on-a-chip microdevice. The chip is composed of two culture chambers separated with a semipermeable PDMS membrane. The two cell types are separately cultured on each side of the membrane to mimic the lung epithelium architecture. Both cell types express tissue specific markers, such as Occludin for the alveolar epithelium and VE-cadherin for the endothelium. Figures reproduced from (82). (B) Gut-on-a-chip microdevice. The same concept was adapted to culture an intestinal cell line (Caco-2). The cells reach confluence and form villi-like structures. Figures reproduced from (83). (C) Kidney-on-a-chip microdevice. The same concept was adapted for the culture of primary human adult proximal tubular epithelial cells. They could show that Na/K-ATPase enzymes are distributed basolaterally and they visualized primary cilia with acetylated tubulin. Figures reproduced from (84). (D) Heart-on-a-chip microdevice. The chip is composed of an elongated microchamber connected to side channels with a vertical semi permeable membrane. iPS derived cardiomyoblasts are seeded in the microchamber and form a compact cardiac muscle-like structure, marked with characteristic sarcomeric alpha actinin (red). Figures reproduced from (87). (E) Body-on-a-chip concept. This microchip concept lies in multiplexing a multitude of “tissues-on-a-chip” to analyze the systemic effects of drugs and interactions between different tissues under disease conditions. Figures reproduced from (88).

The specificities of this microchip, termed by Mathur and colleagues, “microphysiological device” or MPS, lies in isolating the cells from flow-induced shear stress while still providing the required nutrients through a thin vertical PDMS semipermeable membranes (see **Figure 8D**). They could demonstrate that the muscle fibers of their on chip artificial cardiac muscle were aligned and were beating similarly to physiologic conditions⁸⁷. More strikingly, they could demonstrate that their heart-on-a-chip system performed more closely to tissue scale references, such as large animal testing, in comparison with studies at the cellular scale. These preliminary demonstrations lead the field dream of creating micro-versions of the human body, which would serve as personalized micro-testing platforms for drugs and pharmacological compounds. Conceptually, every tissue-on-a-chip would be multiplexed to create a physiologically consistent construct where systemic effects and organ interactions could be analyzed precisely (see **Figure 8E**)⁸⁸. However, these tissues-on-a-chip still lack most of the physiological relevance of native organs and the cultures will have to be highly improved to generate accurate and exploitable tissue models.

OPEN CHALLENGES

As reviewed in this introduction, tissue engineering is currently undergoing an extraordinary change in paradigm, where new fields such as stem cell biology and microengineering are growing in importance. We know now that both adult and pluripotent stem cells are able to form organoids. Yet, organoid systems can thus far only be obtained in rather ill-defined 3D culture systems in which the cells are flooded with morphogen proteins that induce *in vitro* organogenesis. Unsurprisingly, *in vitro* self-organization is thus far only very difficult to control and also mechanistically poorly understood.

Therefore, a major challenge is to replace current 3D culture systems with smarter biomaterials and micro-engineering systems that are able to deliver developmental signals in a spatiotemporally controlled manner *in vitro*. To address this formidable challenge, one has to take into consideration the final size of the developing tissues which can be up to several millimeters (e.g. 1-5 millimeters for neural organoids and 500 micrometers for epithelial organoids), as well as the often very long time scales of organogenesis, particularly in humans, which may be lasting for several months. This implies that common microfabrication techniques will have to be adaptable over this extended culture time to accommodate the size and allow sufficient access to nutrients for defined culture windows.

OBJECTIVES

Considering the above-described limitations, the overarching goal of this thesis is to establish new technologies offering the possibility to begin to control *in vitro* stem cell-based morphogenesis and organogenesis. The application of these technologies will enable the generation of more reliable and functional organoid models, opening up new avenues in the pharmaceutical drug discovery and personalized medicine.

Aim 1: To fabricate *in situ* microfluidic networks in hydrogels to control stem cell behavior in a spatio-temporal fashion

Focalized short-pulsed lasers have sufficient power to break even covalent bonds in various hydrogels. Using this specificity, I will fabricate intricate microfluidic networks in cell-containing gels in order to influence the behavior of 3D cultured cells directly *in situ*.

Aim 2: To microengineer hydrogel substrates for controlling stem cell-d basemorphogenesis in organoid cultures

We will establish a new concept to produce ultra-reproducible U-bottom microcavities of any shape or dimension in various cell culture substrates, including biologically relevant hydrogels that are normally difficult to micropattern. I will apply this technology to optimize the formation of 3D stem cell-derived microtissues and organoids.

Aim 3: To model cystic fibrosis for the first time in a culture format that is amenable to high-throughput pharmacological drug screening

We will interface the above-developed technologies with a label-free method to screen pharmacological compounds on intestinal organoids bearing a mutation on the cystic fibrosis transmembrane conductance regulator (CFTR).

REFERENCES

- 1 Good, R. A. Bone marrow transplantation for immunodeficiency diseases. *The American journal of the medical sciences* **294**, 68-74 (1987).
- 2 Lancaster, M. A. & Knoblich, J. A. Organogenesis in a dish: modeling development and disease using organoid technologies. *Science* **345**, 1247125, doi:10.1126/science.1247125 (2014).
- 3 Sato, T. *et al.* Single Lgr5 stem cells build crypt-villus structures in vitro without a mesenchymal niche. *Nature* **459**, 262-265, doi:10.1038/nature07935 (2009).
- 4 Fatehullah, A., Tan, S. H. & Barker, N. Organoids as an in vitro model of human development and disease. *Nature cell biology* **18**, 246-254, doi:10.1038/ncb3312 (2016).
- 5 Eiraku, M. *et al.* Self-organizing optic-cup morphogenesis in three-dimensional culture. *Nature* **472**, 51-56, doi:10.1038/nature09941 (2011).
- 6 Woodford, C. & Zandstra, P. W. Tissue engineering 2.0: guiding self-organization during pluripotent stem cell differentiation. *Current opinion in biotechnology* **23**, 810-819, doi:10.1016/j.copbio.2012.03.003 (2012).
- 7 Sato, T. & Clevers, H. Growing self-organizing mini-guts from a single intestinal stem cell: mechanism and applications. *Science* **340**, 1190-1194, doi:10.1126/science.1234852 (2013).
- 8 Ranga, A. *et al.* 3D niche microarrays for systems-level analyses of cell fate. *Nature communications* **5**, 4324, doi:10.1038/ncomms5324 (2014).
- 9 Huch, M. & Koo, B. K. Modeling mouse and human development using organoid cultures. *Development* **142**, 3113-3125, doi:10.1242/dev.118570 (2015).
- 10 Meinhardt, A. *et al.* 3D reconstitution of the patterned neural tube from embryonic stem cells. *Stem cell reports* **3**, 987-999, doi:10.1016/j.stemcr.2014.09.020 (2014).
- 11 Locke, M. The Cuticular Pattern in an Insect - the Intersegmental Membranes. *J Exp Biol* **37**, 398-& (1960).
- 12 Turing, A. M. The chemical basis of morphogenesis. 1953. *Bulletin of mathematical biology* **52**, 153-197; discussion 119-152 (1990).
- 13 Crick, F. Diffusion in embryogenesis. *Nature* **225**, 420-422 (1970).
- 14 Gerhardt, H. VEGF and endothelial guidance in angiogenic sprouting. *Organogenesis* **4**, 241-246 (2008).
- 15 Davis, G. E., Stratman, A. N., Sacharidou, A. & Koh, W. Molecular basis for endothelial lumen formation and tubulogenesis during vasculogenesis and angiogenic sprouting. *International review of cell and molecular biology* **288**, 101-165, doi:10.1016/B978-0-12-386041-5.00003-0 (2011).
- 16 Geudens, I. & Gerhardt, H. Coordinating cell behaviour during blood vessel formation. *Development* **138**, 4569-4583, doi:10.1242/dev.062323 (2011).
- 17 Hanoun, M. & Frenette, P. S. This Niche Is a Maze; An Amazing Niche. *Cell Stem Cell* **12**, 391-392, doi:10.1016/j.stem.2013.03.012 (2013).

- 18 Mohyeldin, A., Garzon-Muvdi, T. & Quinones-Hinojosa, A. Oxygen in Stem Cell Biology: A Critical Component of the Stem Cell Niche. *Cell Stem Cell* **7**, 150-161, doi:10.1016/j.stem.2010.07.007 (2010).
- 19 Crosnier, C., Stamatakis, D. & Lewis, J. Organizing cell renewal in the intestine: stem cells, signals and combinatorial control. *Nature reviews. Genetics* **7**, 349-359, doi:10.1038/nrg1840 (2006).
- 20 Davis, H. *et al.* Aberrant epithelial GREM1 expression initiates colonic tumorigenesis from cells outside the stem cell niche. *Nature medicine* **21**, 62-70, doi:10.1038/nm.3750 (2015).
- 21 Reeves, G. T., Muratov, C. B., Schupbach, T. & Shvartsman, S. Y. Quantitative models of developmental pattern formation. *Developmental cell* **11**, 289-300, doi:10.1016/j.devcel.2006.08.006 (2006).
- 22 Wartlick, O., Kicheva, A. & Gonzalez-Gaitan, M. Morphogen gradient formation. *Cold Spring Harbor perspectives in biology* **1**, a001255, doi:10.1101/cshperspect.a001255 (2009).
- 23 Kicheva, A. *et al.* Kinetics of morphogen gradient formation. *Science* **315**, 521-525, doi:10.1126/science.1135774 (2007).
- 24 Reinitz, J. Developmental biology: a ten per cent solution. *Nature* **448**, 420-421, doi:10.1038/448420a (2007).
- 25 Cheung, D., Miles, C., Kreitman, M. & Ma, J. Adaptation of the length scale and amplitude of the Bicoid gradient profile to achieve robust patterning in abnormally large *Drosophila melanogaster* embryos. *Development* **141**, 124-135, doi:10.1242/dev.098640 (2014).
- 26 Briscoe, J. & Novitch, B. G. Regulatory pathways linking progenitor patterning, cell fates and neurogenesis in the ventral neural tube. *Philosophical transactions of the Royal Society of London. Series B, Biological sciences* **363**, 57-70, doi:10.1098/rstb.2006.2012 (2008).
- 27 Cohen, M. *et al.* Ptch1 and Gli regulate Shh signalling dynamics via multiple mechanisms. *Nature communications* **6**, 6709, doi:10.1038/ncomms7709 (2015).
- 28 Kicheva, A. & Briscoe, J. Developmental Pattern Formation in Phases. *Trends in cell biology* **25**, 579-591, doi:10.1016/j.tcb.2015.07.006 (2015).
- 29 Sia, S. K. & Whitesides, G. M. Microfluidic devices fabricated in poly(dimethylsiloxane) for biological studies. *Electrophoresis* **24**, 3563-3576, doi:10.1002/elps.200305584 (2003).
- 30 Whitesides, G. M. The origins and the future of microfluidics. *Nature* **442**, 368-373, doi:10.1038/nature05058 (2006).
- 31 Chung, K. *et al.* A microfluidic array for large-scale ordering and orientation of embryos. *Nature methods* **8**, 171-176, doi:10.1038/nmeth.1548 (2011).
- 32 Dai, J., Suh, S. J., Hamon, M. & Hong, J. W. Determination of antibiotic EC using a zero-flow microfluidic chip based growth phenotype assay. *Biotechnology journal*, doi:10.1002/biot.201500037 (2015).
- 33 Hung, P. J., Lee, P. J., Sabounchi, P., Lin, R. & Lee, L. P. Continuous perfusion microfluidic cell culture array for high-throughput cell-based assays. *Biotechnology and bioengineering* **89**, 1-8, doi:10.1002/bit.20289 (2005).
- 34 Du, G., Fang, Q. & den Toonder, J. M. Microfluidics for cell-based high throughput screening platforms-A review. *Analytica chimica acta* **903**, 36-50, doi:10.1016/j.aca.2015.11.023 (2016).

- 35 Stone, H. A., Stroock, A. D. & Ajdari, A. Engineering flows in small devices: Microfluidics toward a lab-on-a-chip. *Annu Rev Fluid Mech* **36**, 381-411, doi:10.1146/annurev.fluid.36.050802.122124 (2004).
- 36 Stone, H. A. *CMOS Biotechnology*. pp. 5-30 (Springer, 2007).
- 37 Hatch, A. *et al.* A rapid diffusion immunoassay in a T-sensor. *Nature biotechnology* **19**, 461-465, doi:10.1038/88135 (2001).
- 38 Kamholz, A. E. & Yager, P. Theoretical analysis of molecular diffusion in pressure-driven laminar flow in microfluidic channels. *Biophysical journal* **80**, 155-160, doi:10.1016/S0006-3495(01)76003-1 (2001).
- 39 Ismagilov, R. F., Stroock, A. D., Kenis, P. J. A., Whitesides, G. & Stone, H. A. Experimental and theoretical scaling laws for transverse diffusive broadening in two-phase laminar flows in microchannels. *Appl Phys Lett* **76**, 2376-2378, doi:10.1063/1.126351 (2000).
- 40 Jeon, N. L. *et al.* Generation of solution and surface gradients using microfluidic systems. *Langmuir* **16**, 8311-8316, doi:10.1021/La000600b (2000).
- 41 Dertinger, S. K. W., Chiu, D. T., Jeon, N. L. & Whitesides, G. M. Generation of gradients having complex shapes using microfluidic networks. *Anal Chem* **73**, 1240-1246, doi:10.1021/Ac001132d (2001).
- 42 Kim, S., Kim, H. J. & Jeon, N. L. Biological applications of microfluidic gradient devices. *Integrative biology : quantitative biosciences from nano to macro* **2**, 584-603, doi:10.1039/c0ib00055h (2010).
- 43 Saadi, W. *et al.* Generation of stable concentration gradients in 2D and 3D environments using a microfluidic ladder chamber. *Biomedical microdevices* **9**, 627-635, doi:10.1007/s10544-007-9051-9 (2007).
- 44 Atencia, J., Morrow, J. & Locascio, L. E. The microfluidic palette: a diffusive gradient generator with spatio-temporal control. *Lab on a chip* **9**, 2707-2714, doi:10.1039/b902113b (2009).
- 45 Shamloo, A., Ma, N., Poo, M. M., Sohn, L. L. & Heilshorn, S. C. Endothelial cell polarization and chemotaxis in a microfluidic device. *Lab on a chip* **8**, 1292-1299, doi:10.1039/b719788h (2008).
- 46 Diao, J. *et al.* A three-channel microfluidic device for generating static linear gradients and its application to the quantitative analysis of bacterial chemotaxis. *Lab on a chip* **6**, 381-388, doi:10.1039/b511958h (2006).
- 47 Abhyankar, V. V., Lokuta, M. A., Huttenlocher, A. & Beebe, D. J. Characterization of a membrane-based gradient generator for use in cell-signaling studies. *Lab on a chip* **6**, 389-393, doi:10.1039/b514133h (2006).
- 48 Kim, D., Lokuta, M. A., Huttenlocher, A. & Beebe, D. J. Selective and tunable gradient device for cell culture and chemotaxis study. *Lab on a chip* **9**, 1797-1800, doi:10.1039/b901613a (2009).
- 49 Cheng, S. Y. *et al.* A hydrogel-based microfluidic device for the studies of directed cell migration. *Lab on a chip* **7**, 763-769, doi:10.1039/b618463d (2007).
- 50 Haessler, U., Kalinin, Y., Swartz, M. A. & Wu, M. An agarose-based microfluidic platform with a gradient buffer for 3D chemotaxis studies. *Biomedical microdevices* **11**, 827-835, doi:10.1007/s10544-009-9299-3 (2009).

- 51 Mosadegh, B. *et al.* Generation of stable complex gradients across two-dimensional surfaces and three-dimensional gels. *Langmuir* **23**, 10910-10912, doi:10.1021/la7026835 (2007).
- 52 Kenny, P. A. *et al.* The morphologies of breast cancer cell lines in three-dimensional assays correlate with their profiles of gene expression. *Molecular oncology* **1**, 84-96, doi:10.1016/j.molonc.2007.02.004 (2007).
- 53 Edmondson, R., Broglie, J. J., Adcock, A. F. & Yang, L. Three-dimensional cell culture systems and their applications in drug discovery and cell-based biosensors. *Assay and drug development technologies* **12**, 207-218, doi:10.1089/adt.2014.573 (2014).
- 54 Park, J. Y. *et al.* Differentiation of neural progenitor cells in a microfluidic chip-generated cytokine gradient. *Stem cells* **27**, 2646-2654, doi:10.1002/stem.202 (2009).
- 55 Lai, N., Sims, J. K., Jeon, N. L. & Lee, K. Adipocyte induction of preadipocyte differentiation in a gradient chamber. *Tissue engineering. Part C, Methods* **18**, 958-967, doi:10.1089/ten.TEC.2012.0168 (2012).
- 56 Zhang, Y., Gazit, Z., Pelled, G., Gazit, D. & Vunjak-Novakovic, G. Patterning osteogenesis by inducible gene expression in microfluidic culture systems. *Integrative biology : quantitative biosciences from nano to macro* **3**, 39-47, doi:10.1039/c0ib00053a (2011).
- 57 Zhang, Y. S., Sevilla, A., Wan, L. Q., Lemischka, I. R. & Vunjak-Novakovic, G. Patterning pluripotency in embryonic stem cells. *Stem cells* **31**, 1806-1815, doi:10.1002/stem.1468 (2013).
- 58 Mitsui, K. *et al.* The homeoprotein Nanog is required for maintenance of pluripotency in mouse epiblast and ES cells. *Cell* **113**, 631-642, doi:Doi 10.1016/S0092-8674(03)00393-3 (2003).
- 59 Singh, A. M., Hamazaki, T., Hankowski, K. E. & Terada, N. A heterogeneous expression pattern for nanog in embryonic stem cells. *Stem cells* **25**, 2534-2542, doi:10.1634/stemcells.2007-0126 (2007).
- 60 Cimetta, E. *et al.* Microfluidic bioreactor for dynamic regulation of early mesodermal commitment in human pluripotent stem cells. *Lab on a chip* **13**, 355-364, doi:10.1039/c2lc40836h (2013).
- 61 Poh, Y. C. *et al.* Generation of organized germ layers from a single mouse embryonic stem cell. *Nature communications* **5**, 4000, doi:10.1038/ncomms5000 (2014).
- 62 Regehr, K. J. *et al.* Biological implications of polydimethylsiloxane-based microfluidic cell culture. *Lab on a chip* **9**, 2132-2139, doi:10.1039/b903043c (2009).
- 63 Berthier, E., Young, E. W. & Beebe, D. Engineers are from PDMS-land, Biologists are from Polystyrenia. *Lab on a chip* **12**, 1224-1237, doi:10.1039/c2lc20982a (2012).
- 64 Halldorsson, S., Lucumi, E., Gomez-Sjoberg, R. & Fleming, R. M. Advantages and challenges of microfluidic cell culture in polydimethylsiloxane devices. *Biosensors & bioelectronics* **63**, 218-231, doi:10.1016/j.bios.2014.07.029 (2015).
- 65 Gjorevski, N., Ranga, A. & Lutolf, M. P. Bioengineering approaches to guide stem cell-based organogenesis. *Development* **141**, 1794-1804, doi:10.1242/dev.101048 (2014).

- 66 Ehrbar, M. *et al.* Enzymatic formation of modular cell-instructive fibrin analogs for tissue engineering. *Biomaterials* **28**, 3856-3866, doi:10.1016/j.biomaterials.2007.03.027 (2007).
- 67 Ehrbar, M. *et al.* Biomolecular hydrogels formed and degraded via site-specific enzymatic reactions. *Biomacromolecules* **8**, 3000-3007, doi:10.1021/bm070228f (2007).
- 68 Ehrbar, M. *et al.* Elucidating the role of matrix stiffness in 3D cell migration and remodeling. *Biophysical journal* **100**, 284-293, doi:10.1016/j.bpj.2010.11.082 (2011).
- 69 Charras, G. & Sahai, E. Physical influences of the extracellular environment on cell migration. *Nature reviews. Molecular cell biology* **15**, 813-824, doi:10.1038/nrm3897 (2014).
- 70 Engler, A. J., Sen, S., Sweeney, H. L. & Discher, D. E. Matrix elasticity directs stem cell lineage specification. *Cell* **126**, 677-689, doi:10.1016/j.cell.2006.06.044 (2006).
- 71 Gilbert, P. M. *et al.* Substrate elasticity regulates skeletal muscle stem cell self-renewal in culture. *Science* **329**, 1078-1081, doi:10.1126/science.1191035 (2010).
- 72 Lutolf, M. P. & Hubbell, J. A. Synthetic biomaterials as instructive extracellular microenvironments for morphogenesis in tissue engineering. *Nature biotechnology* **23**, 47-55, doi:10.1038/nbt1055 (2005).
- 73 Lutolf, M. P. & Hubbell, J. A. Synthesis and physicochemical characterization of end-linked poly(ethylene glycol)-co-peptide hydrogels formed by Michael-type addition. *Biomacromolecules* **4**, 713-722, doi:10.1021/bm025744e (2003).
- 74 Gobaa, S. *et al.* Artificial niche microarrays for probing single stem cell fate in high throughput. *Nature methods* **8**, 949-955, doi:10.1038/nmeth.1732 (2011).
- 75 Mosiewicz, K. A. *et al.* In situ cell manipulation through enzymatic hydrogel photopatterning. *Nature materials* **12**, 1072-1078, doi:10.1038/nmat3766 (2013).
- 76 Gobaa, S., Hoehnel, S. & Lutolf, M. P. Substrate elasticity modulates the responsiveness of mesenchymal stem cells to commitment cues. *Integrative biology : quantitative biosciences from nano to macro* **7**, 1135-1142, doi:10.1039/c4ib00176a (2015).
- 77 Kobel, S. & Lutolf, M. P. Biomaterials meet microfluidics: building the next generation of artificial niches. *Current opinion in biotechnology* **22**, 690-697, doi:10.1016/j.copbio.2011.07.001 (2011).
- 78 Allazetta, S., Cosson, S. & Lutolf, M. P. Programmable microfluidic patterning of protein gradients on hydrogels. *Chemical communications* **47**, 191-193, doi:10.1039/c0cc02377a (2011).
- 79 Cosson, S., Allazetta, S. & Lutolf, M. P. Patterning of cell-instructive hydrogels by hydrodynamic flow focusing. *Lab on a chip* **13**, 2099-2105, doi:10.1039/c3lc50219h (2013).
- 80 Cosson, S. & Lutolf, M. P. Hydrogel microfluidics for the patterning of pluripotent stem cells. *Scientific reports* **4**, 4462, doi:10.1038/srep04462 (2014).

- 81 Lienemann, P. S. *et al.* Locally controlling mesenchymal stem cell morphogenesis by 3D PDGF-BB gradients towards the establishment of an in vitro perivascular niche. *Integrative biology : quantitative biosciences from nano to macro* **7**, 101-111, doi:10.1039/c4ib00152d (2015).
- 82 Huh, D. *et al.* Reconstituting organ-level lung functions on a chip. *Science* **328**, 1662-1668, doi:10.1126/science.1188302 (2010).
- 83 Kim, H. J. & Ingber, D. E. Gut-on-a-Chip microenvironment induces human intestinal cells to undergo villus differentiation. *Integrative biology : quantitative biosciences from nano to macro* **5**, 1130-1140, doi:10.1039/c3ib40126j (2013).
- 84 Jang, K. J. *et al.* Human kidney proximal tubule-on-a-chip for drug transport and nephrotoxicity assessment. *Integrative biology : quantitative biosciences from nano to macro* **5**, 1119-1129, doi:10.1039/c3ib40049b (2013).
- 85 Mathur, A., Ma, Z., Loskill, P., Jeeawoody, S. & Healy, K. E. In vitro cardiac tissue models: Current status and future prospects. *Advanced drug delivery reviews* **96**, 203-213, doi:10.1016/j.addr.2015.09.011 (2016).
- 86 Lian, X. *et al.* Robust cardiomyocyte differentiation from human pluripotent stem cells via temporal modulation of canonical Wnt signaling. *Proceedings of the National Academy of Sciences of the United States of America* **109**, E1848-1857, doi:10.1073/pnas.1200250109 (2012).
- 87 Mathur, A. *et al.* Human iPSC-based cardiac microphysiological system for drug screening applications. *Scientific reports* **5**, 8883, doi:10.1038/srep08883 (2015).
- 88 Bhatia, S. N. & Ingber, D. E. Microfluidic organs-on-chips. *Nature biotechnology* **32**, 760-772, doi:10.1038/nbt.2989 (2014).

CHAPTER II

IN SITU PATTERNING OF MICROFLUIDIC NETWORKS IN 3D CELL-LADEN HYDROGELS

In Situ Patterning of Microfluidic Networks in 3D Cell-Laden Hydrogels

Published in Advanced Materials

Accepted June 23rd, 2016

Brandenberg N¹, Lutolf MP^{1,2}

¹Laboratory of Stem Cell Bioengineering, Institute of Bioengineering, School of Life Sciences, Ecole Polytechnique Fédérale de Lausanne (EPFL), 1015 Lausanne, Switzerland.

²Institute of Chemical Sciences and Engineering, School of Basic Sciences, EPFL, 1015 Lausanne, Switzerland.

Keywords: Short-pulsed laser, microfabrication, microfluidics, hydrogel, tissue engineering

Corresponding Author:

Prof. Matthias Lutolf

Laboratory of Stem Cell Bioengineering

Institute of Bioengineering

School of Life Sciences

Ecole Polytechnique Fédérale de Lausanne

CH-1015 Lausanne, Switzerland

Tel: +41216931876, E-mail: matthias.lutolf@epfl.ch

Abstract

Short-pulsed laser ablation is used to fabricate geometrically complex, functional microfluidic networks directly inside biological 3D hydrogels. The approach can be applied at any given time or location, enabling the manipulation of living cells *in situ*, for example to stimulate them to undergo desirable behavioural changes, or influence their self-assembly into tissue-mimetic structures.

Introduction

Cells in the body reside in complex, tissue-specific 3D microenvironments, termed extracellular matrices (ECM), that control their behaviour and orchestrate their interaction with other tissue components to facilitate tissue development, function and repair¹. These microenvironments are highly dynamic since cell behaviour often needs to rapidly respond to the changing physiological needs of the tissue and organism. A key mechanism to robustly control cellular dynamics is the tightly regulated presentation of cell signalling molecules in space and time. For example, during the development or regeneration of an organ, specific signalling molecules termed morphogens are secreted by cells from a restricted region of the tissue ('source') from where they diffuse to form concentration gradients^{2,3}. Cells respond differentially to concentrations of these signals, resulting in distinct patterns of development and behaviour.

Microfluidic technology offers unprecedented means to control exceptionally small amounts of fluids, making it ideally suited to build *in vitro* systems emulating the spatiotemporally complex signalling dynamics found in nature⁴⁻⁶. However, microfluidic technology has been largely limited to two-dimensional cell culture applications and is inadequate for long-term cell culture in biologically relevant extracellular environments^{7,8}. Moreover, most microfluidic systems are either fabricated from relatively non-biological materials such as poly(dimethylsiloxane) (PDMS) or they are static, *i.e.* their architecture is predefined and thus not adaptable to dynamic biological signalling within a native tissue.

Efforts have been made to engineer microfluidic networks directly within cell friendly 3D hydrogels, but existing platforms are based on laborious processes that require several post-processing steps and offer little flexibility in design⁹⁻¹⁴. Alternatively, advanced biomaterials approaches are being explored to generate spatiotemporally complex signalling microenvironments for 3D cell culture. To this end, synthetic polymer hydrogels have been interfaced with innovative photochemistry to precisely modulate their characteristics in space and time through the controlled application of a light beam (e.g.¹⁵⁻¹⁸). However, this approach limits itself to biomolecule patterns that are static, unlike those in native tissues.

Results and discussion

We surmised that laser photo-ablation could be exploited to fabricate, if desired *during* cell culture, functional 3D microfluidic networks within hydrogels. Indeed, nano- or femto-second pulsed lasers provide enough energy (approximately 80-150mW and 500-900mW, respectively) to break down covalent bonds and have been used for micromachining of hard materials such as glass and silicon^{19,20}. Furthermore, previous studies reported the laser-based generation of cavities in non-permissive hydrogels to promote 3D cell growth and migration²¹⁻²³. Taking advantage of the ablative properties of focalized pulsed lasers, we report a new paradigm for creating functional 3D microfluidic networks at any time and location during a cell or tissue culture experiment. The concept is shown in **Figure 1a-b**: By scanning the area of a specified pattern, a custom-made network of channels can be fabricated and connected to a perfusion system, such as to generate functional microfluidic systems without any post-processing steps. In addition, the networks can be modified on demand during the culture in order to respond to needs of an evolving biological system (Figure 1b). As we demonstrate below, constructing microfluidic networks by direct laser writing offers a wide range of material possibilities, geometrical freedom and the ability to introduce or modify existing microfluidic networks during the course of an experiment to manipulate cell behaviour *in situ* in an unprecedented manner.

To build functional microfluidic networks in hydrogels, we first designed simple custom-made PDMS mounts that can harbour a gel sample and interface the sample with inlets and outlets that enable perfusion (Figure 1c). The upper part of the hydrogel is covered with media, exhibiting an open cell culture configuration akin to standard 3D culture in multiwell plates. The hydrogel is cast in the centre chamber, and media, as well as factors of interest, can be flowed through the fabricated microfluidic networks by hydrostatic pressure differences¹², on-chip peristaltic valve-based systems, or conventional syringe pump-based systems.

To demonstrate the feasibility of our approach, we used the nanosecond-pulsed laser of a micro-dissection microscope (PALM MicroBeam system) to create various simple, planar patterns such as undulating (Figure S1a, Supporting Information) or ladder-shaped microfluidic channels in covalently cross-linked poly(ethylene glycol) (PEG) hydrogels (Figure 1d,e). An evaluation of channel stability by microscopy showed that geometries remain unchanged for at least 48 hours, both with and without flow (~ 1 mL/min; Figure S1b,c, Supporting Information). Importantly, microfluidic networks can be designed in numerous hydrogel types, including those made from natural ECM-derived proteins (gelatin, collagen type I, or fibrin) or polysaccharides (agarose, alginate), as well as various formulations of semi-synthetic or fully synthetic hydrogels. The latter can span a wide range of mechanical properties, including approximately 300 Pa in shear modulus (Figure S1d-f, Supporting Information), a particularly interesting range for 3D cell culture. To the best of our knowledge, such soft hydrogels cannot be micro-patterned with previously reported methods, such as those based on micromoulding^{12,13}.

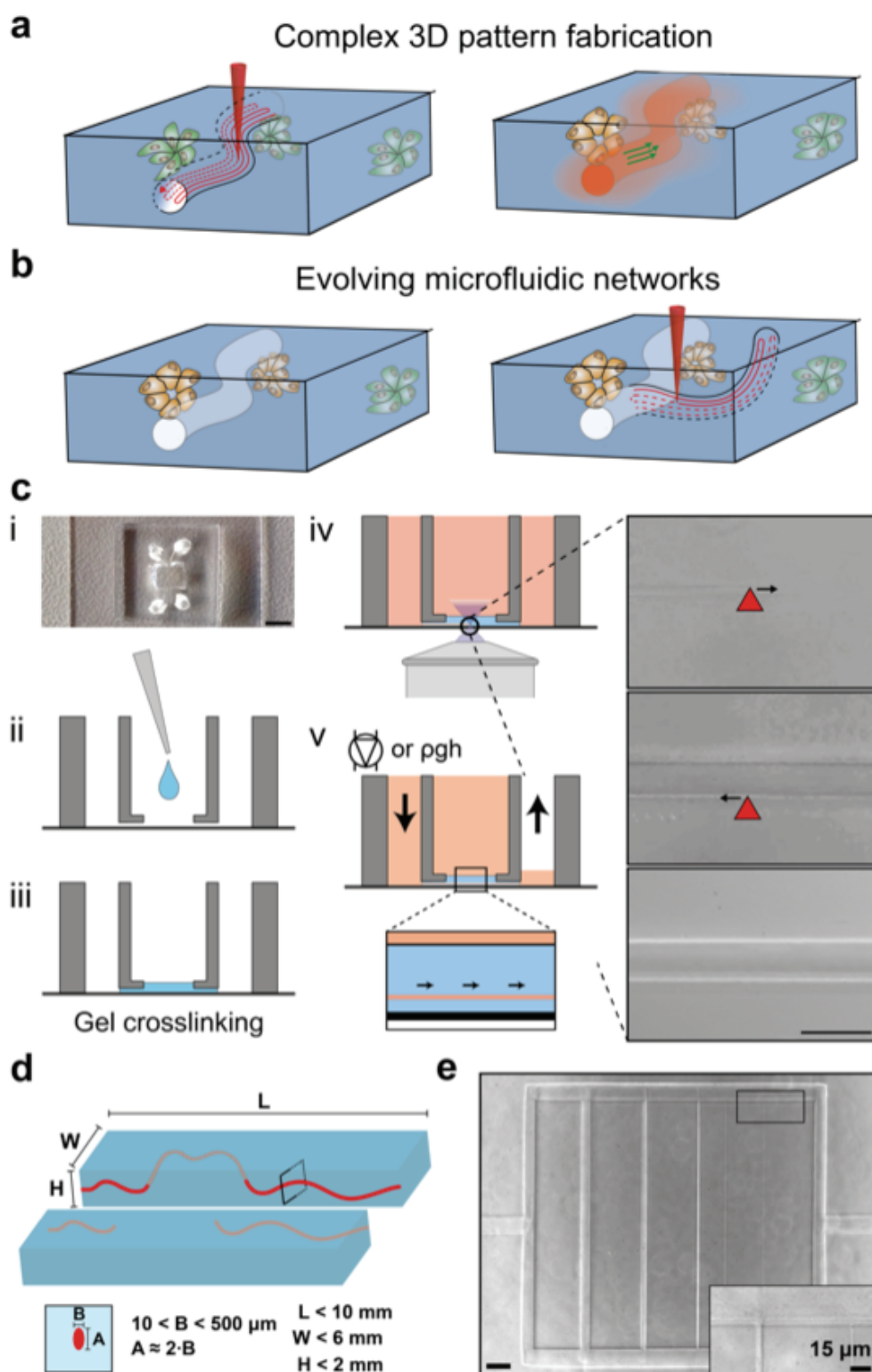


Figure 1. Overview of the fabrication process. (a) Schematic representation of laser-based *in situ* fabrication of biomicrofluidic networks. Using the ablative properties of focalized nano-

or femto-pulsed lasers, microfluidic channels are fabricated by scanning the area of desired patterns. The microchannels are directly functional after the fabrication process. (b) Additional microfluidic networks can be added on demand during at any location and time during culture. (c) Schematic overview of the fabrication process. (i) Representative image of the PDMS mount. Scale bar: 2mm. (ii) The final hydrogel mixture is moulded into the PDMS mounts and incubated at 37°C, 5% CO₂ for 20 minutes for crosslinking (iii). The gel is then immersed with the appropriate medium and (iv) microfluidic networks are fabricated by scanning the area of the pattern with the laser. (v) Flow can be induced using hydrostatic pressure-based or active flow-based pumping systems. (d) Schematic representation of the gel size range that can be processed as well as the resulting microfluidic network geometry. Any shape and curvature can be achieved with this method, such as ladder-like (e). Scale bars: 100 μ m, unless specified.

We then attempted to construct more complex microfluidic networks as a basis for fabricating sophisticated *in vitro* tissue models or permitting systematic studies of 3D cellular microenvironments. With the high resolution and reproducibility of controlling the coordinates of the automated microscope stage and the Z-position of a custom-made focus controller, we successfully fabricated perfusable microfluidic networks emulating blood flow through a flat capillary bed (**Figure 2**). Starting from a capillary bed photograph (Figure 2a), we generated a path file (Figure 2b) that the laser could read to generate the corresponding microchannel structure (Figure 2c). When connected to a pumping system, we could demonstrate for the first time that very complex networks in hydrogels can be fully perfused (Figure 2d).

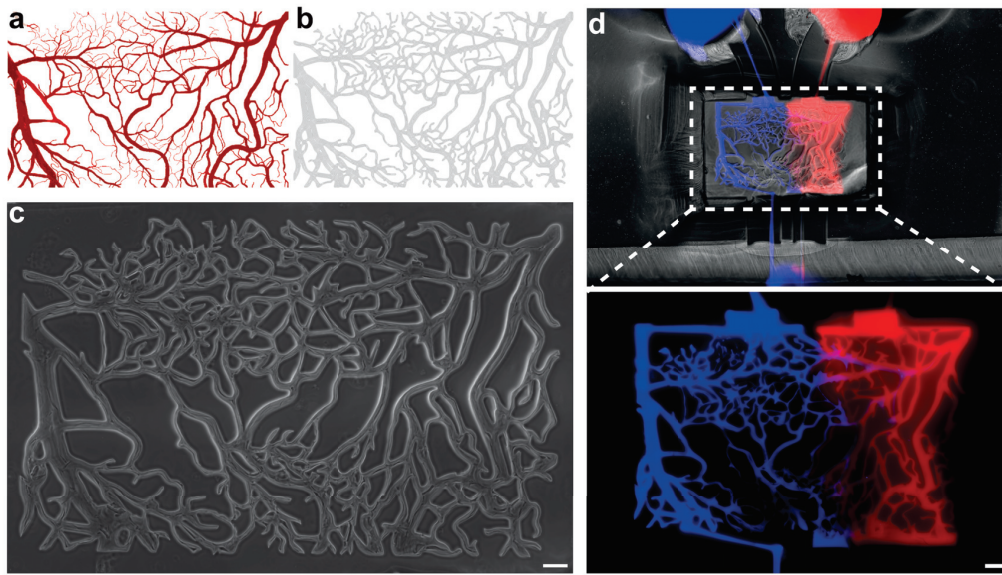


Figure 2. Complexity of the fabricated networks. (a) Capillary bed photograph (source: www.alamy.com/). (b) Path file derived from the photograph that the laser follows to fabricate the network. (c) Resulting capillary bed-mimicking microfluidic network prior to perfusion. (d) These networks can be connected and perfused with different fluorescent molecules (e.g. alexa-647 labelled PEG and 2000 kDa fluorescein isothiocyanate (FITC)-Dextrane), mimicking arteriovenous circulation. Scale bars: 100 μ m.

Furthermore, we could also form intricate 3D structures such as ramps, spirals and other irregular shapes (**Figure 3a,b**, Movie S1, S2, Supporting Information). Notably, the fidelity in 3D microfluidic patterning allowed us to superimpose different microfluidic networks without any tedious manual handling steps (Figure 3c). Flow experiments demonstrate the functionality of these microfluidic networks by efficiently transporting fluorescent molecules and polystyrene beads from the inlet to the outlet of the networks (Figure 3d, Movie S3, Supporting Information). Perhaps most interestingly, this strategy offers the possibility to readily modify microfluidic networks *in situ*, that is, during the time course of an experiment (Figure 3e,f). To the best of our knowledge, this aspect makes our approach unique among all hydrogel microfluidic strategies.

A thorough characterisation of the mass transport phenomena in our hydrogel microfluidic networks is essential for developing useful *in vitro* cell culture and tissue models. As a tractable model system, we first analysed the diffusion of fluorescent dextran (molecular weight ≈ 70 kDa) from a single source through covalently crosslinked PEG hydrogels (Figure S2, Supporting Information). Using curve fitting of the forming gradients (Figure S2a,c, Supporting Information), we estimated an effective diffusion coefficient (D_{eff}) for dextran of $1.8 \times 10^{-7} \text{ cm}^2/\text{s}$, which was then used to calculate the theoretical diffusion behaviour based on convection-diffusion equations. Indeed, employing a finite element approach, the theoretical diffusion patterns corresponded very well with experimental data (Figure S2c-d, Supporting Information). This provided the basis for employing more complex perfusion patterns such as those based on a non-linear delivery of factors such as a pulsed delivery (Figure S3, Supporting Information).

Given the importance of biomolecule gradients in controlling tissue development, we then aimed to construct a more physiological gradient system based on a source-sink mechanism (Figure S2e, Supporting Information). Indeed, by laser-etching and perfusing two parallel microfluidic channels in close proximity, one to deliver a biomolecule and the other to deplete it, we built highly stable source-sink gradient systems (Figure S2f,g, Supporting Information). Again, a strong correlation between theoretical and experimental diffusion properties was found in this delivery paradigm (Figure S2g,h, Supporting Information).

Finally, using a reactive fluorescent model compound (Alexa-546), we explored the possibility of establishing gradients of biomolecules which are tethered to the hydrogel matrix (Figure S2i, Supporting Information), a mode of biomolecule presentation that is physiologically relevant because ECM-binding *in vivo* can be beneficial for biomolecule activity²⁴. By perfusing reactive maleimide-Alexa-546 for two hours, we show that tethered gradients are established within synthetic PEG-based hydrogels bearing free thiol groups, and that these gradients remain stable over at least one week (Figure S2j-l, Supporting Information). Taken together, these experiments show that laser-based photo-ablation can be exploited to generate microfluidic networks with highly predictable mass transport behaviour.

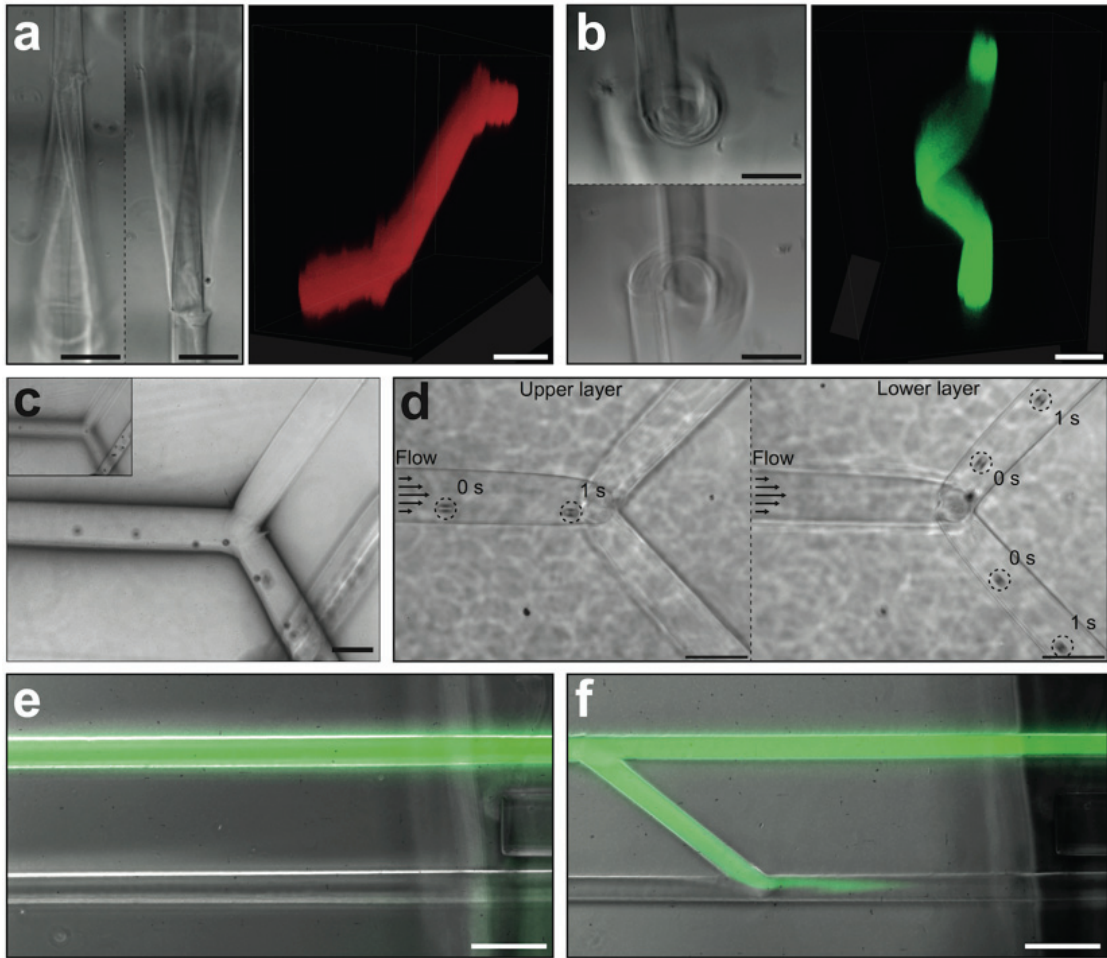


Figure 3. Three-dimensional and evolving microfluidics. (a,b) Confocal 3D reconstruction of fully three-dimensional microfluidic networks such as ramps or spirals. (c) Representation of superimposed and aligned microfluidic networks. (d) Composite image generated from **Movie S3** (Supporting Information) showing polystyrene microbeads flowing through a laser-ablated microchannel. The position of microbeads in the upper and lower layer of the microfluidic network is shown at 0 and 1 s in the composite image. (e) Proof-of-principle demonstration of evolving microfluidic systems. We merged a bright-field and a fluorescent image of parallel microfluidic channels. Initially, the upper channel is perfused with high molecular weight (2000 kDa) green fluorescent dextran. (f) The parallel channels are then connected by laser-ablation during the perfusion. The fluorescent solution is now being directed in the lower channel. Scale bars: 100 μm .

To demonstrate the relevance of our approach in biomedical research, we next sought to develop two *in vitro* models of biologically relevant processes (**Figure 4a**), namely, the induction of 3D chemotaxis and the establishment of an artificial blood vessel network. To do so, we first assessed the compatibility of live cell culture with laser photo-ablation (Figure 4b). Importantly, the viability of 3D-encapsulated cells in bioactive PEG hydrogels one hour after channel fabrication was not significantly different than the cell viability in standard 3D culture in multi-well plates, or in the PDMS mounts in which microfluidic networks were not fabricated. Even a one to two

cell diameters away (ca. 20 μm) from the laser-etched channels, we did not observe dying cells (Figure 4c). Mesenchymal stem cells (MSCs) play key roles in tissue dynamics due to their ability to differentiate into cells of the mesodermal lineage, such as adipocytes, osteocytes and chondrocytes, and also through modulation of the immune system²⁵. However, MSC biology is still poorly understood, in part because physiologically relevant *in vitro* models to capture tissue-level MSC functionality are inadequate. Having demonstrated that laser-based microchannel etching is compatible with 3D cell culture, we next sought to establish 3D human MSC invasion and chemotaxis assays based on the transient, localized perfusion of the chemoattractant platelet derived growth factor-BB (PDGF-BB). Indeed, time-lapse microscopy analyses showed that directional 3D MSC migration could be selectively induced in PEG-based hydrogels upon delivery of a short pulse of PDGF-BB through a laser-ablated microfluidic channel (Figure 4d,e; Movie S4,S5, Supporting Information). A more refined analysis of the single cell migration behaviour by image analysis provided clear evidence of 3D chemotactic behaviour of MSCs (Figure 4f,i).

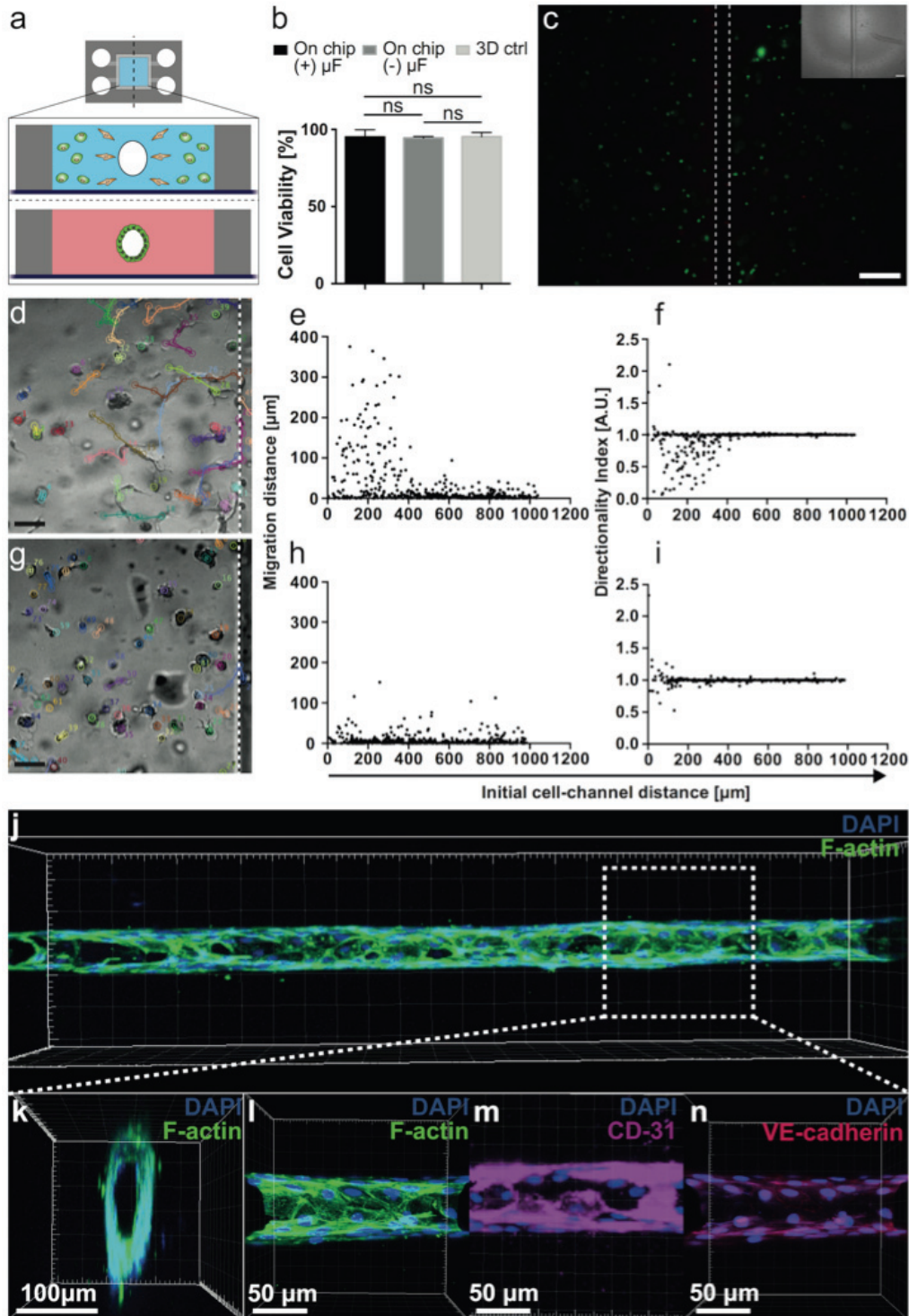


Figure 4. Applications of in-situ biomicrofluidics. (a) Schematic representation of the two *in vitro* models (3D invasion assays and blood vessel-like structures) generated here by laser-based fabrication of biomicrofluidic networks in hydrogels. (b) Cell viability was assessed by live/dead staining (green fluorescence: live cells, red: dead cells) one hour after the fabrication process (N=3, variation represented using

standard deviation). Conventional 3D cultures on a 24-well plate (3D ctrl), 3D culture in the PDMS mounts without the fabricated network ((-) μ F) and with the fabricated network ((+) μ F) were compared. (c) Wide-field fluorescent image of a representative, live/dead stained mouse myoblast (C₂C₁₂) culture. (d) A representative bright-field image overlapped with the cell tracks of pre-starved hMSCs perfused with PDGF-BB for 30 minutes. Analysis of the migration distance (e) and the directionality index (f) of hMSCs perfused with PDGF-BB for 30 minutes. (g) Representative bright-field image overlapped with the cell tracks of pre-starved hMSCs perfused with medium only. Analysis of the migration distance (h) and the directionality index (i) of hMSCs perfused with medium only. (j) Confocal 3D reconstruction of a hollow endothelial cell tube (HUVECs) formed in collagen type I. Transversal (k) and frontal (l) plane of the structure. Frontal planes showing endothelial markers immunostainings, *i.e.* CD-31 (m) and VE-cadherin (n).

Following, we attempted to establish a 3D MSC chemotaxis model in the context of a cell culture format that would necessitate an *in situ* formation of a microfluidic network, *i.e.* one in which the microchannel positioning is not pre-determined but rather dependent on the emergence of specific cellular behaviours (Figure S4, Supporting Information). As a proof-of-principle, we chose to grow MSCs as pre-formed 'microtissue' aggregates composed of ca. 400 cells, a format that may more faithfully mimic the physiological situation²⁶. MSC microtissues were randomly encapsulated at a low density in 3D PEG hydrogels and, depending on the specific location of a microtissue of interest, we programmed the laser to ablate a microchannel in close proximity to that microtissue. Indeed, a similar 3D chemotactic behaviour was observed in this experimental paradigm (Figure S4 and Movie S6,S7, Supporting Information). Taken together, these data show that the behaviour of live cells can be readily modulated by microfluidic delivery of diffusible signalling molecules. Therefore, our strategy permits the construction of functional microfluidic systems in a fully user-defined manner, based on cellular processes that are observed during a specific experiment. As such, the blueprint for the microfluidic chip is not determined *a priori*, but rather *a posteriori*, dependent on the biological question and cellular state investigated by an experimenter.

Finally, we sought to utilize laser-based photo-ablation to fabricate *in vitro* tissues. As a first model system, we decided to build user-defined, perfusable vascular networks within 3D collagen networks. A variety of such systems have already been described^{12,13}, yet the state-of-the-art is based on rather complicated and time-consuming methods that possess a paucity of design flexibility and no adaptability. Here, we laser-etched micro-channels into collagen type I hydrogels and seeded the channels with human umbilical vein endothelial cells (HUVEC) by microfluidic perfusion. Within five days, a confluent, perfusable layer of HUVEC expressing the phenotypic markers CD31 and VE-cadherin was established (Figure 4j-n). This approach could provide an elegant means to model complex phenomena in vascular or cancer biology and may also facilitate the fabrication of sophisticated 3D stem cell microenvironments containing a microvasculature.

Conclusions

Fabricating physiologically relevant cell culture and tissue models *in vitro* holds tremendous promise for applications in basic biology, drug discovery, toxicology and regenerative medicine. However, generating *in vitro* models that capture even a modicum of natural tissue functionality is a formidable effort that requires sophisticated tools to control many aspects of the complex cellular microenvironment. While significant advances have been made in the development of 3D matrices that mimic key biochemical and biophysical properties of native cellular microenvironments^{27,28}, it has not yet been possible to build *in vitro* systems that allow the physiological, spatiotemporally complex delivery of biomolecules in these microenvironments in an adaptable manner, that is, based on the biology that 'unfolds' in the cell culture dish. In this report, we provide the first demonstration of microfluidic networks that are fully adaptable and can be designed and fabricated *in situ*, according to cellular and multicellular events observed during an experiment.

Compared to existing strategies based on micromoulding and sacrificial layer elimination (e.g. ^{10,13}), our approach shows several distinct advantages. First, no complex steps are involved in the fabrication of microfluidic networks. Hydrogels of choice can be formed in a perfusion chamber, fluid networks fabricated by laser etching and perfusion directly performed by connecting to a tubing system integrated in a world-to-chip interface. As the process can be performed without the need of an operator, this method significantly decreases the tedious aspect of microfluidic chip fabrication, requiring only equipment that is readily available at most research institutes. Second, since light is used for the fabrication, the sterility of the cell cultures is guaranteed. Finally, the fabrication of microfluidic networks is not restricted in geometry and complexity. We think that the presented strategy represents an important step forward in the implementation of miniaturized, near-physiological cell and tissue culture platforms to answer currently unresolved questions in biomedical research as well as the ability to guide cellular self-organisation to form functional tissues *in vitro*.

Experimental methods

Preparation of hydrogels: PEG hydrogels crosslinked via Michael-type addition reaction (termed 'MT-gel' in this work) were prepared as described,²⁹ mixing aqueous solutions containing thiol- and vinylsulfone- functionalized 4arm- and 8arm-PEG macromers (mol. weight 10 kDa and 40kDa, respectively) at various concentrations to adjust stiffness and stoichiometric ratio.

PEG hydrogels crosslinked via the transglutaminase factor XIIIa (FXIIIa) (termed 'TG-gel' in this work) were prepared as previously described³⁰⁻³². Briefly, 8arm-PEG macromers (40 kDa) bearing lysine-containing or glutamine-containing FXIIIa substrate peptides were mixed at various concentrations to adjust stiffness and stoichiometric ratio. For 3D cell culture experiments, FXIIIa-based PEG hydrogels were synthesized containing matrix metalloprotease (MMP)-sensitive as well as arginylglycylaspartic acid (RGD) integrin-binding peptides³². Hydrogel precursor solutions were moulded into the hydrogel chamber of the PDMS mounts. After hydrogel crosslinking, buffer or appropriate medium was added to allow equilibration of the hydrogel.

Native bovine dermis collagen type I (5mg/mL stock concentration, Kouken, Japan) was reconstituted according to the manufacturer's protocol. The water content was adjusted to obtain the appropriate concentration and variable mechanical properties.

Fabrication of microfluidic networks via laser ablation: A nanosecond laser system was used for the fabrication of microfluidic networks in hydrogels: a PALM MicroBeam system (1 ns pulses, 100 Hz frequency, 355 nm) from Carl Zeiss Microscopy (Göttingen, Germany) set with a 10X objective (NA = 0.25) and a constant stage speed, $95 \mu\text{m s}^{-1}$, was used in all experiments. To fabricate planar microfluidic networks, the built-in interface, including software connected with the laser as well as an automated stage to control the laser position, was used. The patterns were drawn as vectorial designs of the shape of interest, which can be created in any vectorial drawing software (here Adobe® Illustrator® CS6). The designs were then converted to the microscope specific format using a custom-made converter before being imported onto the PALM MicroBeam system's interface. The laser was then started and the network was fabricated similarly to previously described work by Sarig-Nadir and colleagues²¹.

To fabricate 3D microfluidic networks, the same strategy was adopted. In addition, a custom-made z-controller was fabricated using a bipolar stepper motor interfaced with Arduino™ microcontrollers (Arduino Uno™ & Arduino Motor Shield™). The laser's host system and x-y stage were coordinated with the stepper motor to achieve a coherent 3D network fabrication. Finally, the size of the microfluidic network could be varied by increasing the volume scanned by the laser. The 2D and 3D microfluidic networks were imaged by wide-field microscopy as well as confocal microscopy.

Acknowledgements

We thank Tunvez Boulic and Marie-Laure Naudin for help with the characterization of biomolecule diffusion through hydrogels and the characterization of the artificial vasculature network, respectively. We thank Michael Snyder, Nikolce Gjorevski and Andrea Manfrin for helpful discussions and critical reading of the manuscript, and Sylke Höhnel for contributions to the figure design. This work was funded by the EU framework 7 HEALTH research programme PluriMes (<http://www.plurimes.eu/>), the SystemsX.ch RTD project StoNets, an ERC grant (StG_311422) and a Swiss National Science Foundation Singergia grant (CRSII3_147684).

Authorship

M.P.L. and N.B. conceived the study, interpreted results and wrote the manuscript; N.B. performed all experimental and computational work as well as statistical analyses.

REFERENCES

- 1 Frantz, C., Stewart, K. M. & Weaver, V. M. The extracellular matrix at a glance. *J Cell Sci* **123**, 4195-4200, doi:10.1242/jcs.023820 (2010).
- 2 Crick, F. Diffusion in embryogenesis. *Nature* **225**, 420-422 (1970).
- 3 Gurdon, J. B. & Bourillot, P. Y. Morphogen gradient interpretation. *Nature* **413**, 797-803, doi:10.1038/35101500 (2001).
- 4 Bhatia, S. N. & Ingber, D. E. Microfluidic organs-on-chips. *Nat Biotechnol* **32**, 760-772, doi:10.1038/nbt.2989 (2014).
- 5 Sackmann, E. K., Fulton, A. L. & Beebe, D. J. The present and future role of microfluidics in biomedical research. *Nature* **507**, 181-189, doi:10.1038/nature13118 (2014).
- 6 Dvir, T., Timko, B. P., Kohane, D. S. & Langer, R. Nanotechnological strategies for engineering complex tissues. *Nature nanotechnology* **6**, 13-22, doi:10.1038/nnano.2010.246 (2011).
- 7 Regehr, K. J. *et al.* Biological implications of polydimethylsiloxane-based microfluidic cell culture. *Lab on a chip* **9**, 2132-2139, doi:10.1039/b903043c (2009).
- 8 Berthier, E., Young, E. W. & Beebe, D. Engineers are from PDMS-land, Biologists are from Polystyrenia. *Lab on a chip* **12**, 1224-1237, doi:10.1039/c2lc20982a (2012).
- 9 Nguyen, D. H. *et al.* Biomimetic model to reconstitute angiogenic sprouting morphogenesis in vitro. *Proceedings of the National Academy of Sciences of the United States of America* **110**, 6712-6717, doi:10.1073/pnas.1221526110 (2013).
- 10 Choi, N. W. *et al.* Microfluidic scaffolds for tissue engineering. *Nature materials* **6**, 908-915, doi:10.1038/nmat2022 (2007).
- 11 Golden, A. P. & Tien, J. Fabrication of microfluidic hydrogels using molded gelatin as a sacrificial element. *Lab on a chip* **7**, 720-725, doi:10.1039/b618409j (2007).
- 12 Morgan, J. P. *et al.* Formation of microvascular networks in vitro. *Nature protocols* **8**, 1820-1836, doi:10.1038/nprot.2013.110 (2013).
- 13 Miller, J. S. *et al.* Rapid casting of patterned vascular networks for perfusable engineered three-dimensional tissues. *Nature materials* **11**, 768-774, doi:10.1038/nmat3357 (2012).
- 14 Isern, J. *et al.* Self-renewing human bone marrow mesospheres promote hematopoietic stem cell expansion. *Cell reports* **3**, 1714-1724, doi:10.1016/j.celrep.2013.03.041 (2013).
- 15 Kloxin, A., Kasko, A. M., Salinas, C. N. & Anseth, K. Photodegradable Hydrogels for Dynamic Tuning of Physical and Chemical Properties. *Science* **324**, 59-63 (2009).
- 16 Wylie, R. G. *et al.* Spatially controlled simultaneous patterning of multiple growth factors in three-dimensional hydrogels. *Nature materials* **10**, 799-806, doi:10.1038/NMAT3101 (2011).

- 17 Mosiewicz, K. A. *et al.* In situ cell manipulation through enzymatic hydrogel photopatterning. *Nature materials* **12**, 1072-1078, doi:10.1038/nmat3766 (2013).
- 18 DeForest, C. A. & Tirrell, D. A. A photoreversible protein-patterning approach for guiding stem cell fate in three-dimensional gels. *Nature materials* **14**, 523-531, doi:10.1038/NMAT4219 (2015).
- 19 Gittard, S. D. & Narayan, R. J. Laser direct writing of micro- and nano-scale medical devices. *Expert review of medical devices* **7**, 343-356, doi:10.1586/erd.10.14 (2010).
- 20 Liu, C. *et al.* Fabrication of three-dimensional microfluidic channels inside glass using nanosecond laser direct writing. *Optics express* **20**, 4291-4296, doi:10.1364/OE.20.004291 (2012).
- 21 Sarig-Nadir, O., Livnat, N., Zajdman, R., Shoham, S. & Seliktar, D. Laser photoablation of guidance microchannels into hydrogels directs cell growth in three dimensions. *Biophysical journal* **96**, 4743-4752, doi:10.1016/j.bpj.2009.03.019 (2009).
- 22 Iliina, O., Bakker, G.-J., Vasaturo, A., Hoffman, R. M. & Friedl, P. Two-photon laser-generated microtracks in 3D collagen lattices: principles of MMP-dependent and -independent collective cancer cell invasion. *Physical Biology* **8**, 029501-029501, doi:10.1088/1478-3975/8/2/029501 (2011).
- 23 Applegate, M. B. *et al.* Laser-based three-dimensional multiscale micropatterning of biocompatible hydrogels for customized tissue engineering scaffolds. *Proceedings of the National Academy of Sciences of the United States of America*, doi:10.1073/pnas.1509405112 (2015).
- 24 Ramirez, F. & Rifkin, D. B. Cell signaling events: a view from the matrix. *Matrix Biol* **22**, 101-107, doi:10.1016/S0945-053X(03)00002-7 (2003).
- 25 Bianco, P. *et al.* The meaning, the sense and the significance: translating the science of mesenchymal stem cells into medicine. *Nature medicine* **19**, 35-42, doi:10.1038/nm.3028 (2013).
- 26 Saleh, F. A. & Genever, P. G. Turning round: multipotent stromal cells, a three-dimensional revolution? *Cytotherapy* **13**, 903-912, doi:10.3109/14653249.2011.586998 (2011).
- 27 DeForest, C. A. & Anseth, K. S. Advances in bioactive hydrogels to probe and direct cell fate. *Annual review of chemical and biomolecular engineering* **3**, 421-444, doi:10.1146/annurev-chembioeng-062011-080945 (2012).
- 28 Gjorevski, N., Ranga, A. & Lutolf, M. P. Bioengineering approaches to guide stem cell-based organogenesis. *Development* **141**, 1794-1804, doi:10.1242/dev.101048 (2014).
- 29 Gobaa, S. *et al.* Artificial niche microarrays for probing single stem cell fate in high throughput. *Nature methods* **8**, 949-955, doi:10.1038/nmeth.1732 (2011).
- 30 Ehrbar, M. *et al.* Enzymatic formation of modular cell-instructive fibrin analogs for tissue engineering. *Biomaterials* **28**, 3856-3866, doi:10.1016/j.biomaterials.2007.03.027 (2007).
- 31 Ehrbar, M. *et al.* Biomolecular hydrogels formed and degraded via site-specific enzymatic reactions. *Biomacromolecules* **8**, 3000-3007, doi:10.1021/bm070228f (2007).

- 32 Ehrbar, M. *et al.* Elucidating the role of matrix stiffness in 3D cell migration and remodeling. *Biophysical journal* **100**, 284-293, doi:10.1016/j.bpj.2010.11.082 (2011).

CHAPTER III

STANDARDIZING COMPLEX ORGANOID CULTURES THROUGH MICROENGINEERED SUBSTRATES

Standardizing complex organoid cultures through microengineered substrates

Manuscript in preparation

Patent pending

Brandenberg N^{1*}, Hoehnel S^{1*}, Decembrini S³, Gjorevski N¹, Arsenijevic Y³, Lutolf
MP^{1,2}

¹Laboratory of Stem Cell Bioengineering, Institute of Bioengineering, School of Life
Sciences, Ecole Polytechnique Fédérale de Lausanne (EPFL), 1015 Lausanne,
Switzerland.

²Institute of Chemical Sciences and Engineering, School of Basic Sciences, EPFL, 1015
Lausanne, Switzerland.

³ Department of Ophthalmology, University of Lausanne, Jules-Gonin Eye Hospital,
FAA, Unit of Gene Therapy & Stem Cell Biology, Avenue de France 15,
1004 Lausanne, Switzerland

* The authors contributed equally to the presented work

Keywords: Microfabrication, micropatterning, hydrogel, organoid, high-throughput,
standardization, U-shaped microwell, array

Corresponding Author:

Prof. Matthias Lutolf

Laboratory of Stem Cell Bioengineering

Institute of Bioengineering

School of Life Sciences

Ecole Polytechnique Federale de Lausanne

CH-1015 Lausanne, Switzerland

Tel: +41216931876, E-mail: matthias.lutolf@epfl.ch

Abstract

Organoids have emerged as powerful models of organ development, function and disease. A key hurdle to move organoid application from basic science into pharmaceutical drug discovery is the lack of reproducibility, standardization and scalability found in existing organoid cultures. Organoid systems are mainly generated, either in heterogeneous floating cultures or in variable three-dimensional naturally derived matrices that hampers their controlled morphogenesis and their traceability. To address this problem, we here report micro-engineered culture substrates which render organoid cultures significantly more reproducible by *i*) aggregating defined (stem) cell numbers at the onset of an experiment, *ii*) precisely controlling the distance between individual developing organoids, and *iii*) exposing developing organoids to microenvironmental signals influencing stem cell fate and self-organization. To validate our platform, we generated arrays of optic cup organoids and intestinal organoids. We demonstrate that combining specific mechanical properties of the substrate with additional soluble cues increases cellular differentiation in retinal tissue within the culture. Moreover, keeping the organoids within the microwells allows to track precisely each developing retina during the entire culture time. In addition, intestinal organoids grown in our controlled microenvironments were highly monodisperse and were located all in a single focal plane. Our approach offers key advantages to standardize and control organoid growth as it provides a modular but controlled microenvironment. Also, it allows to confer complex 3D cultures a two dimensional organization that adapts better to standard analysis procedures. Our technology opens the door for high-resolution screenings of tissue-level function in organoid cultures.

Introduction

Cellular self-organization is the founding principle of organ development, homeostasis and regeneration. This extraordinary process gives rise to complex three-dimensional (3D) entities composed of specialized cells, adjacent support cells, extra-cellular matrix (ECM) components and other structural and dimensional elements that interact continuously to ensure organ function¹. Although developmental biologists extensively studied tissue and organ morphogenesis in animal models, isolated cells or tissue units do not seem to retain this capability *in vitro* when cultured using conventional two-dimensional (2D) cell culture techniques because they simply lack dimensionality as well as other essential physiological properties².

Only relatively recently, experimental designs in biological *in vitro* research have shifted towards more relevant 3D models, such as those based on cell-containing hydrogel matrices or cellular aggregate cultures³⁻⁵. Over the last few years, two landmark studies have revealed that the extraordinary capacity of stem cell to self-organize is also conserved *in vitro*, provided that the cells receive the appropriate signaling input and can grow within a near-physiological, permissive 3D microenvironment. In 2009, Clevers and colleagues isolated mouse adult intestinal stem cells (ISC) to grow intestinal organ-like structures when cultured in a naturally derived matrix termed MatrigelTM ⁶. ISCs give rise to their adjacent supporting cells,

required for their maintenance, and to multiple differentiated cells of the intestine such as enterocytes or enteroendocrine cells. Around the same time, Sasai and colleagues showed that retinal as well as photoreceptor progenitor cells can be differentiated from aggregates of pluripotent stem cells *in vitro*⁷.

Organoids represent a crucial technological advance and are becoming an essential tool for understanding a wide range of complex physiological and pathophysiological processes such as tissue renewal, stem cell niche functions and tissue responses to drug, mutation or damage. For example, Cystic Fibrosis is accurately modeled with mutated murine or patient-derived intestinal organoids. Transepithelial fluid transport can be assessed and the effect of drugs rescuing the function of mutated *cftr* (cystic fibrosis transmembrane conductance regulator) proteins is clearly observable⁸. Another key example is retinal organoids that display, *in vitro*, the architecture of the retina. Retinoblastoma disease models are currently being established to enable, for the first time, drug testings on this adverse disease that usually results in an eye enucleation.

However, by and large, organoid cultures are still in their infancy as they remain highly variable, hampering their standardized use in pharmaceutical drug screening and therapy development. We believe that first generation organoid systems suffer from three main limitations: *(i)* existing culture conditions fails to mimic the native microenvironment, i.e. biomechanical forces, growth factors/signaling gradients, which strongly limits the control over organoids development, *(ii)* MatrigelTM and similar naturally derived 3D matrices induced artifacts and due to their complex composition may influence cell fate in ways that are undesirable, and *(iii)* organoids are highly heterogeneous in terms of size and shape, making phenotypic assay development very complex⁹.

Here, we present a hydrogel-based microwell array platform that allows the reproducible aggregation any type of cell within naturally derived or synthetic hydrogel substrates. We show that this platform is highly modular and is adaptable to virtually any desired 3D cellular and organoid model. Moreover, we expect our technology to allow, for the first time, large-scale production of organoids in order to develop standardized assays for pharmaceutical screenings and fabricate synchronized, phenotype-matched cells in numbers relevant to clinical applications.

Results and discussion

Heterogeneity in organoid cultures

It is widely known that organoids cultures are inherently variable in terms of differentiation capacity, morphology and size⁹, hampering their successful translation towards a wealth of applications. Surprisingly, no study has yet quantified the variability of current organoid cultures. Therefore, we first measured organoid heterogeneity in terms of fusion, size and traceability over time (**Figure 1**). Organoids grown in the same culture compartment, whether in 3D Matrigel drops (**Fig. 1A**) or in floating cultures (**Fig. 1B**), fuse most of the time to create “multi-organoid” structures (**Fig. 1C,E**, red arrows). As a result, the size distribution of these organoids is extremely broad (**Fig. 1E**). After Gaussian fitting, we could observe that the standard deviation (SD) of the distribution was of about 24000 μm^2 or approximatively three times more than organoids grown in microwell arrays. Moreover, the long-term traceability of organoids is a major challenge in the development of robust assays. As shown by the blue arrows in **Figure 1C**, organoids are in different foci and move within the culture compartment, making a long-term analysis of organoid cultures challenging.

To address these challenges, we reasoned that next-generation organoid cultures should fulfill the following criteria: First, the substrate needs to evenly separate individual organoids, ideally arranging them on equal foci (**Fig. 1F,G**). This would offer the possibility to automate the analysis of single organoids (**Fig. 1H**). Secondly, cells need to be cultured in three dimensions, implying that the culture substrate should be inert to prevent non-specific cell adhesion. Thirdly, the culture system should provide the possibility to be interfaced various 3D matrices (**Fig. 1F-H**).

Microstructuring hydrogels

To fulfill these requirements, we conceived a hydrogel-based microwell array platform that is adaptable to virtually any organoid system (**Fig. 2**). By using conventional soft-lithography and deep reactive ion etching (DRIE), we produced silicon masters harboring U-shaped cavities of any geometry. This master was counter-molded in poly(dimethylsiloxane) (PDMS) serving as mold for imprinting the desired cavities into natural and synthetic hydrogel substrates (**Fig. 2A**).

The geometry of our U-shaped microwells can be adapted to organoid systems of highly variable size and geometry (**Fig. 2B-F**, **Supplementary Fig. 1A,B**). For example, microwells with a diameter of 10 μm , suitable for single cell analysis (**Supplementary Fig. 1C**) can be produced, as well as microwells with a diameter of 1.5 mm for retinal organoids (**Fig. 2G**). Notably, U-shaped microwells can be fabricated from numerous biologically relevant materials including PDMS, naturally derived hydrogels composed of alginate, agarose, gelatin and collagen type I (**Supplementary Fig. 1D**), or synthetic hydrogels such as those composed of poly(ethylene glycol) (PEG)¹⁰⁻¹³. The latter are particularly interesting for organoid cultures because they are chemically defined and their physical and biochemical properties are highly controllable. Indeed, hydrogels of a wide range of mechanical properties, from 150

Pa up to 30kPa in stiffness, can be micropatterned with arrays of U-shaped microwells (**Fig. 2H**).

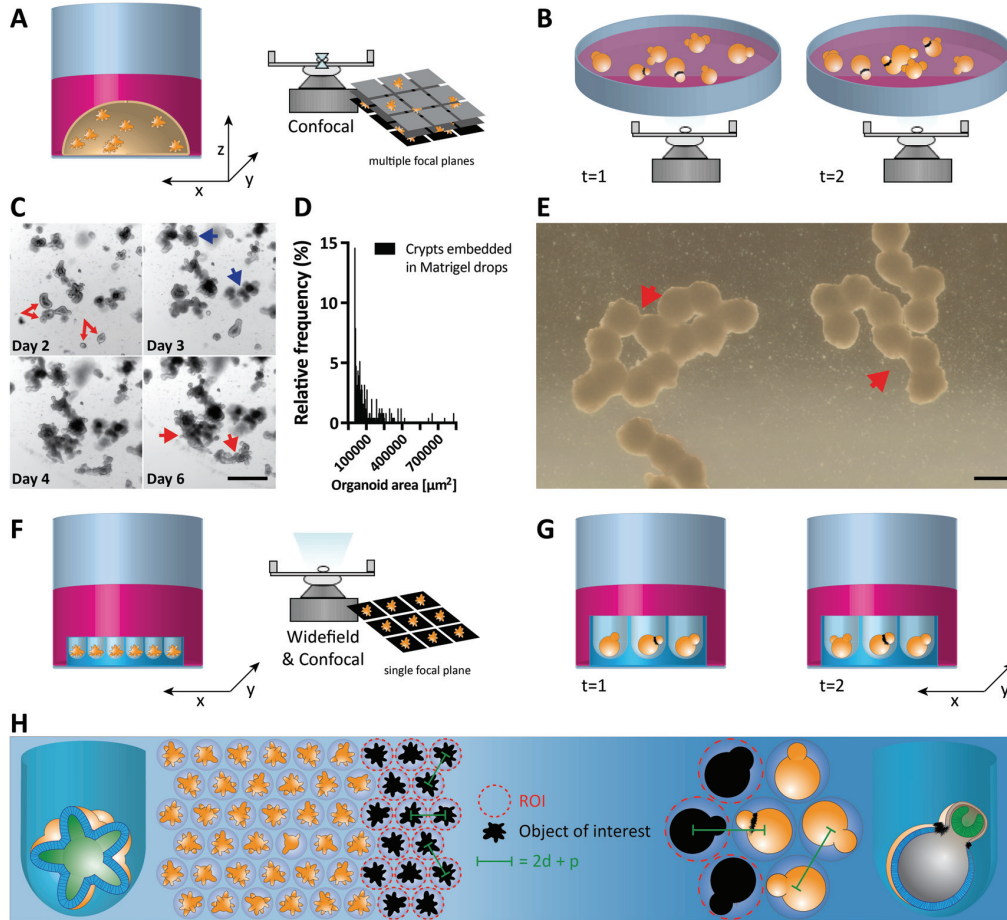


Figure 1: (A) Schematic description of conventional cultures of intestinal organoids in 3D hydrogel drops. (B) Schematic description of conventional cultures of retinal organoids in floating conditions. (C) Widefield microscopy representative images of intestinal organoids fusing in four days. Long tailed red arrows: organoids before fusion. Short tailed red arrows: the same organoids after fusion. Blue arrows: organoids out of focus. Scale bar: 500 μm . (D) Heterodisperse size distribution of intestinal organoids grown from crypts. After Gaussian fit: Mean: 37500 μm^2 , standard deviation: 23735 μm^2 . (E) Widefield microscopy representative images of fused retinal organoids in floating culture. Short tailed red arrows: organoids after fusion. Scale bar: 500 μm . (F) Ideal culture configuration to grow homogenous intestinal organoids. (G) Ideal culture configuration to grow homogenous retinal organoids. This concept would allow each tissue to be equally spaced in x and y together with being all in the same focus. (H) Conceptual schematic on the ease to analyze 3D cultures when placed at equidistant interval and placed in the same focus. ROI: region of interest. D: distance between microwells. p: distance in between microwells.

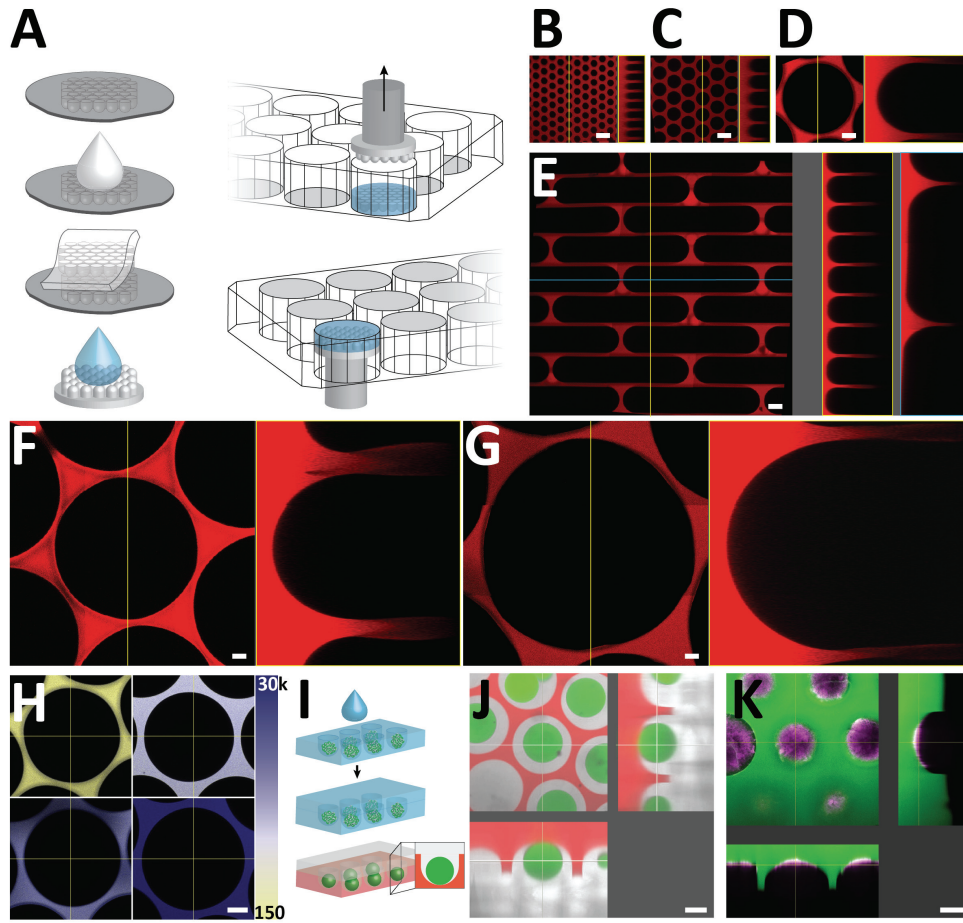


Figure 2: **A)** Fabrication process flow. U-shaped microcavities were fabricated into silicon master using conventional soft-lithography and deep ion reactive etching (DRIE). The master was then counter-molded in PDMS and the cavities were imprinted from the latter into various naturally derived and synthetic hydrogels. **(B)-(G)** U-shaped hydrogel microwells of different geometry. As exemplified here, microwells with 50 **(B)**, 100 **(C)**, 500 **(D)** μm in diameter, rod-shaped microwells **(E)**, and 1 **(F)** or 1,5 **(G)** mm in diameter. **(H)** The stiffness of the microwell substrate can be varied at will from 150 Pa to 30 kPa (shear modulus, G'). **(I)** The microwells are compatible with sandwich culture, which offers the possibility to perform controlled full 3D culture. **(J)** Confocal scan of green (488)-labeled hydrogel microbeads seeded in microwells, labeled with red fluorophore (alexa-546) and encapsulated within an upper layer of far-red labeled hydrogel. **(K)** The bottom of U-shaped microwells (green, 488-labeled) can be functionalized with specific proteins (far-red (647) labeled bovine serum albumin (BSA)).

Our microwell array platform is fully compatible with conventional 3D organoid culture methods. That is, cells can be seeded at the bottom of micro-cavities and then overlaid with a 3D gels such as MatrigelTM, Collagen type I or synthetic PEG-based matrices (**Fig. 2I-J**). Importantly, microwells fabricated from inert synthetic hydrogels can be readily bioconjugated¹⁴ to allow cellular interaction with specific ECM signals (**Fig. 2K**).

Generation of cellular aggregates in U-shaped microwell arrays

After designing the U-shaped microwell platform according to the above-mentioned requirements, we validated and characterized its compatibility with stem cell culture using PEG hydrogel-based culture substrates (**Fig. 3**). Thanks to a honeycomb arrangement and the ultra-high density of the microcavities, cells are seeded by simply placing a cell solution on the culture surface (**Fig. 3A**). By choosing the number of cells desired in each microwells, the appropriate density can be calculated according to the number of microwells present on the culture substrate.

We first analyzed whether R1 Oct4 eGFP (Oct4-GFP) mouse embryonic stem cells (mESC) could be grown as 3D aggregates over a period of five days. Thus, we settled five hundred cells in each microwell and let them grow for five consecutive days (**Fig. 3B**). We performed wide-field time-lapse microscopy to track cell compaction and growth. After compacting in less than six hours, the aggregate grew linearly for four days (**Fig. 3C**). More importantly, the generated aggregates are highly monodisperse over the entire culture period (**Fig. 3D,E**).

We next compared the performance of aggregation in our microengineered substrates with the most commonly used culture platform for cell aggregation, the low adherent 96 U-bottom. Spheroid formation of 100, 1000 and 3000 Oct4-GFP mESCs was compared in 500, 1500 μm microwells and 96 U-bottom well plates. Notably, cells that settled down in PEG microwells compacted faster (six hours or less) compared to those in 96 U-bottom plates (seven to eight hours) (**Fig. 3F**). Despite the similar initial cell number, cells in the PEG microwells tended to compact more for higher number of cells compared to those in the 96 U-bottom well plate (**Fig. 3G**). In addition, aggregates formed in microwell arrays were rounder and more homogenous than those formed in 96 U-bottom wells (**Fig. 3H**). Taken together, these data demonstrate that aggregates formed in our hydrogel-based microwells are more homogenous and compact faster. These characteristics are a first important step to assemble cells in a very consistent and controlled fashion.

Finally, thanks to the excellent biocompatibility of PEG hydrogels, we found that mESC could be expanded clonally in a scaffold-free environment for up five days. Interestingly, each single cell had a strikingly different growth capacity from apoptosis to growth nearly reaching the walls of the micro-cavities (**Fig. 3I**).

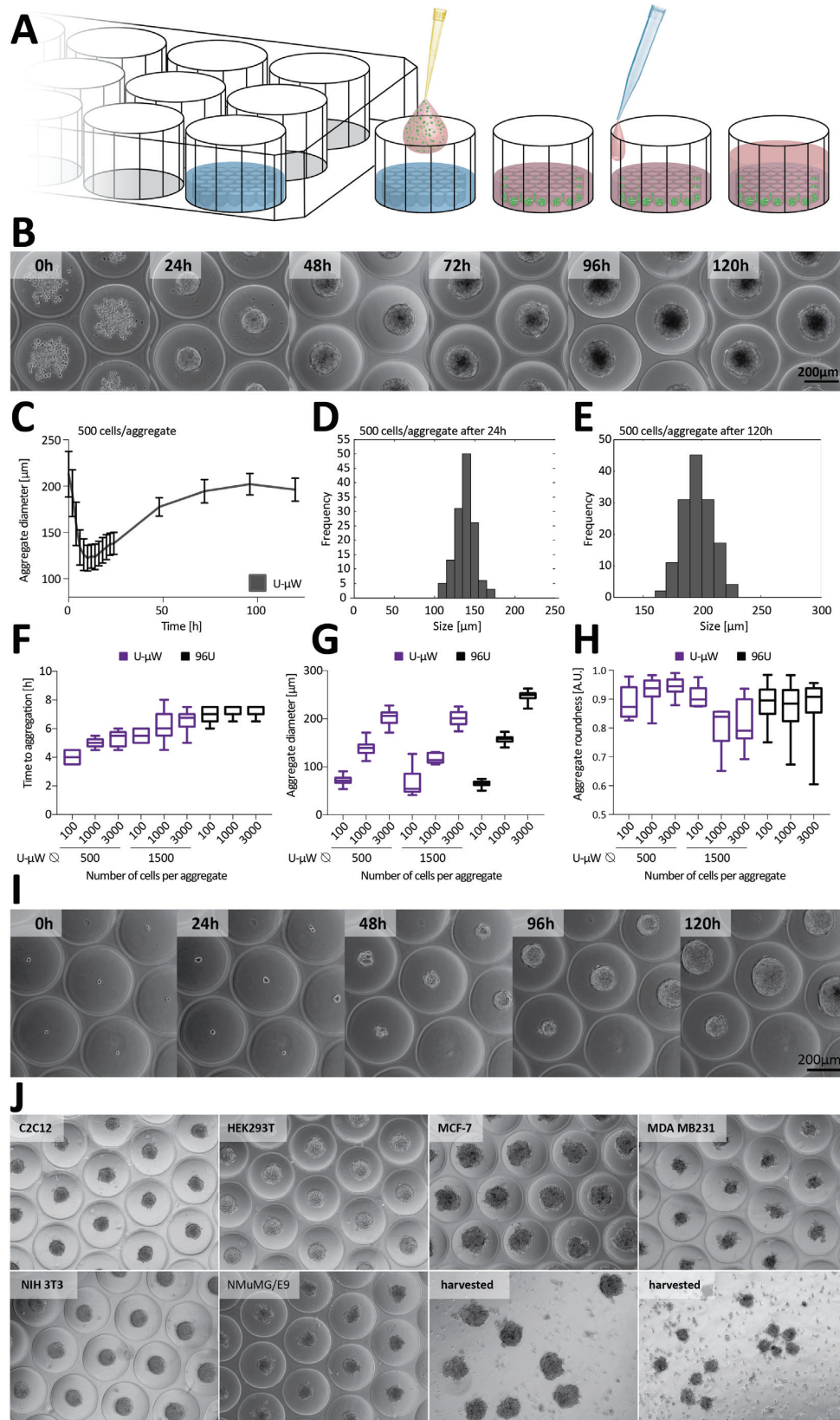


Figure 3: (A) Schematic description of cell seeding on hydrogel-based U-shaped microwell arrays. (B) Time lapse widefield microscopy of OCT4::GFP mES cells aggregation and growth over five days, or 120 hours, in 500 μ m diameter microwells. (C) Quantification of cell compaction and growth. (D) Size distribution of the population of aggregates after twenty-four hours. The spheroids are highly monodisperse. (E) Size distribution of the population of aggregates after 120 hours. The spheroids are still highly monodisperse. (F)-(H) Quantification of the performances of U-shaped PEG microwells (U- μ W) in comparison with 96 U-bottom (96U) plates. For the same initial cell numbers, the compaction time into aggregates is strikingly shorter in U- μ W than in 96U (F). Interestingly, the aggregate diameter, for the same initial cell numbers, is smaller in U- μ W than in 96U (G). Finally, the roundness of the aggregates in U- μ W is visibly more homogenous in U- μ W compared with 96U (H). (I) We show, for the first time, that mES cells can be clonally expanded from single cells on scaffold free substrates. We could observe that each single cell grows with different capabilities. (J) Numerous cell types form spheroids in our microwell arrays. We show conventional cell lines aggregates such as C2C12, HEK293T, NIH3T3, and NMuMG/E9 for human muscle and kidney together with mouse fibroblasts, and mammary glands cells, respectively. In addition, we show that two human breast cancer cell lines, MCF-7 and MDA-MB231 can also form spheroids efficiently, even though MDA-MB231 cells are reported to not form cell clusters without the addition of external ECM components.

We next produced aggregates of numerous human and mouse cell types, including muscle, kidney, fibroblasts and mammary gland cells (**Fig. 3J**). All of the tested cell lines successfully aggregated in our PEG-based microwells. Notably, the human breast cancer cell lines MCF-7 and MDA MB231 both formed *in vitro* tumor microtissues. This is expected for MCF-7 that are well known to form aggregates¹⁵. In contrast, MDA MB231 are difficult to aggregate without using specific ECM components¹⁶.

Interestingly, we found a correlation between cell compaction time and the size of aggregates after twenty-four hours (**Fig. 3F,G**). We suppose that the higher slope in terms of curvature radius, to which the cells are exposed to in the microwells, may boost cell-cell interactions. In hydrogel-based microwells, cells may start interacting with each other before undergoing a first cellular division, whereas in 96 U-bottom well plates that are less curved, some cells might undergo cell divisions before interacting with other cells in the well.

We next tested whether our hydrogel-based microwells would support stem cell self-organisation into organoids. To this end, we optimized published methods^{6,7} to grow the two most widely studied organoid systems, retinal and intestinal organoids.

Improving the induction of mouse retinal organoids using hydrogel substrates

First, we seeded cone-rod homeobox (CRX) GFP reporter mESC¹⁷ in 1.5 millimeters microwells (**Fig. 4A**). The aggregation speed was considerably faster than in conventional 96 U-bottom plates (data not shown). Among different mESC reporter lines, the same behavior was observed.

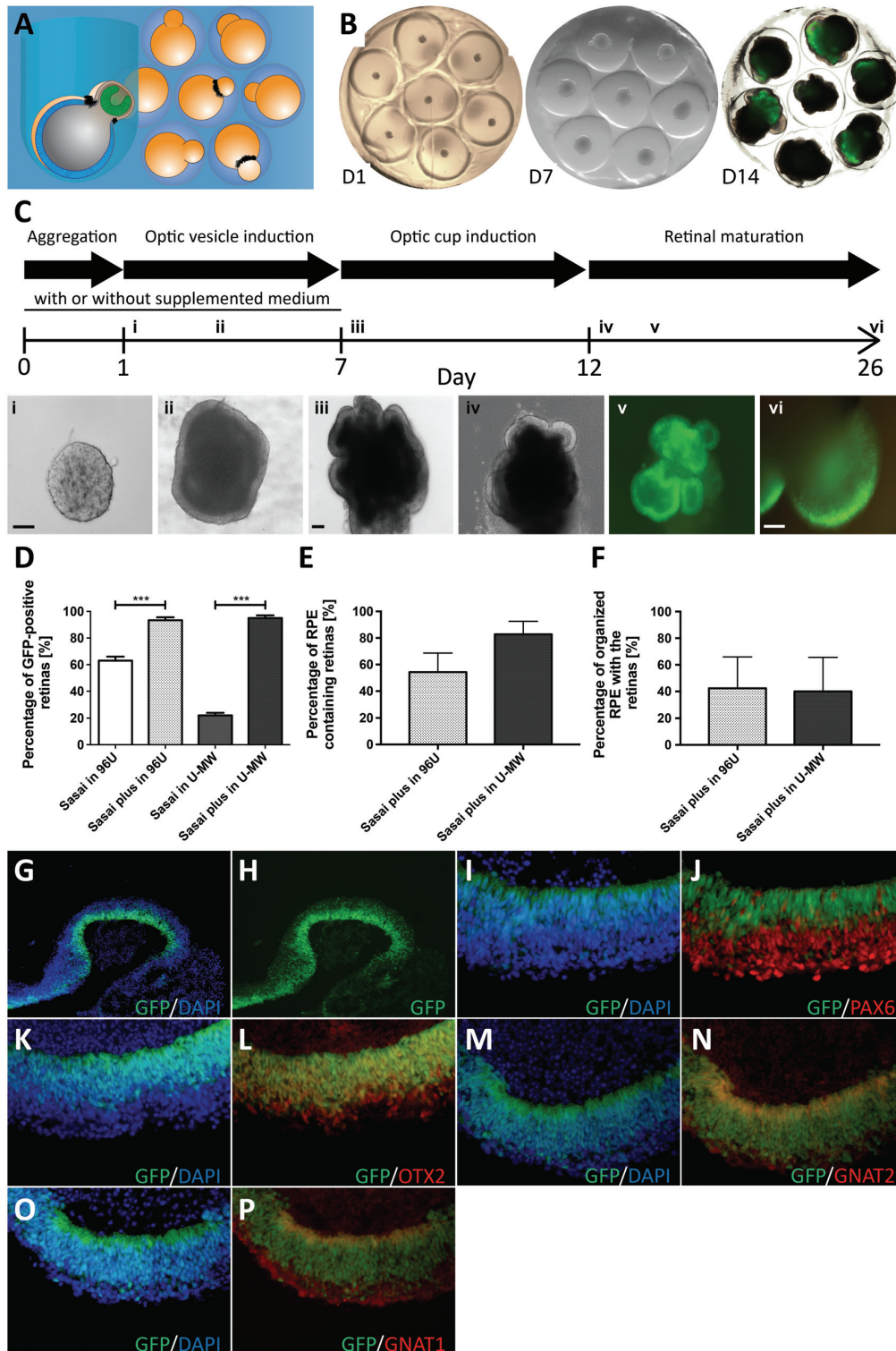


Figure 4: (A) Schematic representation of retinal organoids in microwells of 1.5 millimeters in diameter. (B) Time course tile scans of retinal organoids at different stages; 1, 7 and 14 days old cultures. (C) Optimized protocol to generate retinal organoid and improve their differentiation in microwell arrays using supplemented medium. (i) Cone-rod homeobox (CRX) GFP reporter mES form homogenous aggregates after 20 hours. Matrigel is added to the culture at a final concentration of 2%. (ii) After three days in culture, a neuroepithelium forms at the surface of the aggregate. The cells are committed to the neural lineage. (iii) The neuroepithelium bulges to give rise to structures committed to the retinal lineage or optic vesicles. At this stage the medium is changed to optic cup induction medium. (iv) CRX expression is traceable and the medium is changed to retina maturation medium. (v) Retinal tissue of the organoid expressing CRX after fourteen days in culture. (vi) Matured retina after twenty-six days. The photoreceptors form an organized epithelium. Scale bars: 100 μ m. (D) Quantification of the percentage of CRX-positive organoids after fourteen days in culture. Three independent experiments are represented. Four conditions are compared; the conventional protocol described by Prof. Sasai & colleagues using 96 U plates, the same protocol with supplemented medium, the conventional protocol described by Sasai & colleagues using μ -MW plates, and the supplemented medium in μ -MW plates. Conditions using supplemented medium particularly increases differentiation efficiency as up to 90% of the organoids give rise to retinal tissues compared to 60% or less in the conventional protocol. (E) Quantification of the number of organoids containing retinal pigmented epithelium after fourteen days. (F) Quantification of the number of organoids containing retinal pigmented epithelium co-localized with the retinal tissue after fourteen days. (G) Characterization by immunofluorescence of the retinal tissue grown in supplemented medium in μ -MW plates. GFP marks the expression of endogenous CRX, a specific marker for cones and rods.

Notably, while differentiating aggregates towards retinal tissue in the PEG microwells, a combination of stiffer PEG substrates and a medium with neural cell-specific supplements, termed Sasai plus, was found to be optimal for in vitro eye cup formation (**Fig. 4B,C**). Indeed, by addition of neural cell-specific supplements in the optic vesicle induction medium (from day 0 to day 7), organoid differentiation can be enhanced dramatically.

In order to evaluate the differences between the different culture conditions, we next performed a comparative analysis between the four following conditions: (1) the conventional protocol using commercial 96-well U-bottom plates (i.e. Sasai in 96U), (2) the optimized protocol using commercial 96-well U-bottom plates (i.e. Sasai plus in 96U), (3) the conventional protocol using 1.5 mm microwells, and, (4) the optimized protocol using 1.5 mm microwells. The supplemented medium increased efficiency of differentiation of the neural aggregate into retinal tissue from approximately 60 to 90%. Likewise, even though the differentiation efficiency was found to be lower in the microwells using the conventional protocol, the combination of a stiffer substrate and supplemented medium strongly increased organoid differentiate towards the retinal lineage (**Fig. 4D**). Interestingly, we observed that in microwell cultures, RPE appeared more frequently, while the retinal tissue differentiates (**Fig. 4E**). However, enveloping of the neural retina by the RPE, the naturally occurring architecture of these two tissues, could only be observed at relatively low frequencies, and we could not conclude on differences between plastic and PEG hydrogel-based cultures (**Fig. 4F**). More experiments are necessary to

understand whether the microengineered substrate improves this co-localization (**Supplementary Fig. 2A** for a representative example).

Finally, to cellular organization and key marker expression, we produced histological sections of the retinal tissues obtained from organoids cultures in hydrogel microwells over twenty-six days. All the main neuronal cell types in the retina were found to be present (**Fig. 4G-P**). PAX6 positive cells, marking ganglion and amacrine neurons, were located at the opposite side of the cone and rod progenitor cells, marked by endogenous CRX::GFP (**Fig. I,J**). OTX2, which is known to trans-activate the *Crx* gene¹⁸ and shown to be a marker of both bipolar and photoreceptor cells, was also present (**Fig. K,L**) and we detected the GNAT1 and GNAT2, two proteins involved in the cone and rod phototransduction cascade, mostly at the inner surface of our *in vitro* retinal tissues (**Fig. M-P**).

These data show that retinal organoids can be obtained in microengineered substrates towards assay miniaturization and standardization. Adapting the medium with neural cell culture supplements significantly increased the differentiation efficiency of retinal tissues both on plastic and in hydrogel microwells. In addition, the stiffness of cell culture substrate has a surprising effect on the onset of differentiation, suggesting that further optimization of microenvironmental parameters might be a promising means in organoid development.

Standardizing intestinal organoids in circular U-shaped microwells

One of the major limitation of the widely used intestinal organoid system is its heterogeneity, particularly when starting from single ISCs but also in cultures of tissue fragments. We hypothesized that aggregates of defined numbers of intestinal stem cell could results in the highly reproducible formation of intestinal organoids (**Fig. 5A,B**).

Therefore, we developed a protocol to create small ISC colonies by aggregation, expand them for a short time and then differentiate them into intestinal organoids (**Fig. 5C**). We first seed low numbers of single ISCs in PEG microwells of 500 μ m in diameter and let the cells form a colony overnight in stem cell expansion medium supplemented with 2% of Matrigel, ENRCV¹⁹. After the cells form a small colony, the array is overlaid with a soft poly(ethylene glycol)-based gel containing 1mM RGD and 200 μ g/mL full length laminin. After gelation, expansion medium is added to this sandwich culture. After two days in expansion medium the colony harbored a thick columnar epithelium (**Fig. 5D**), we thus exchanged the medium to differentiate the colonies into organoids (**Fig. 5D**).

This method allows us to generate reproducibly sized organoids from ISCs in six days. Interestingly, when 50, 100, 200 and 500 cells are seeded per microwells, the percentage of organoids that do not bud after six days is lowest when the initial cell number per microwell is 100 (**Fig. 5E**). The colonies expanded during the first three days, but upon medium change towards differentiation, organoids stopped growing for two days to finally expand in size again from day five to day six (**Fig 5F**).

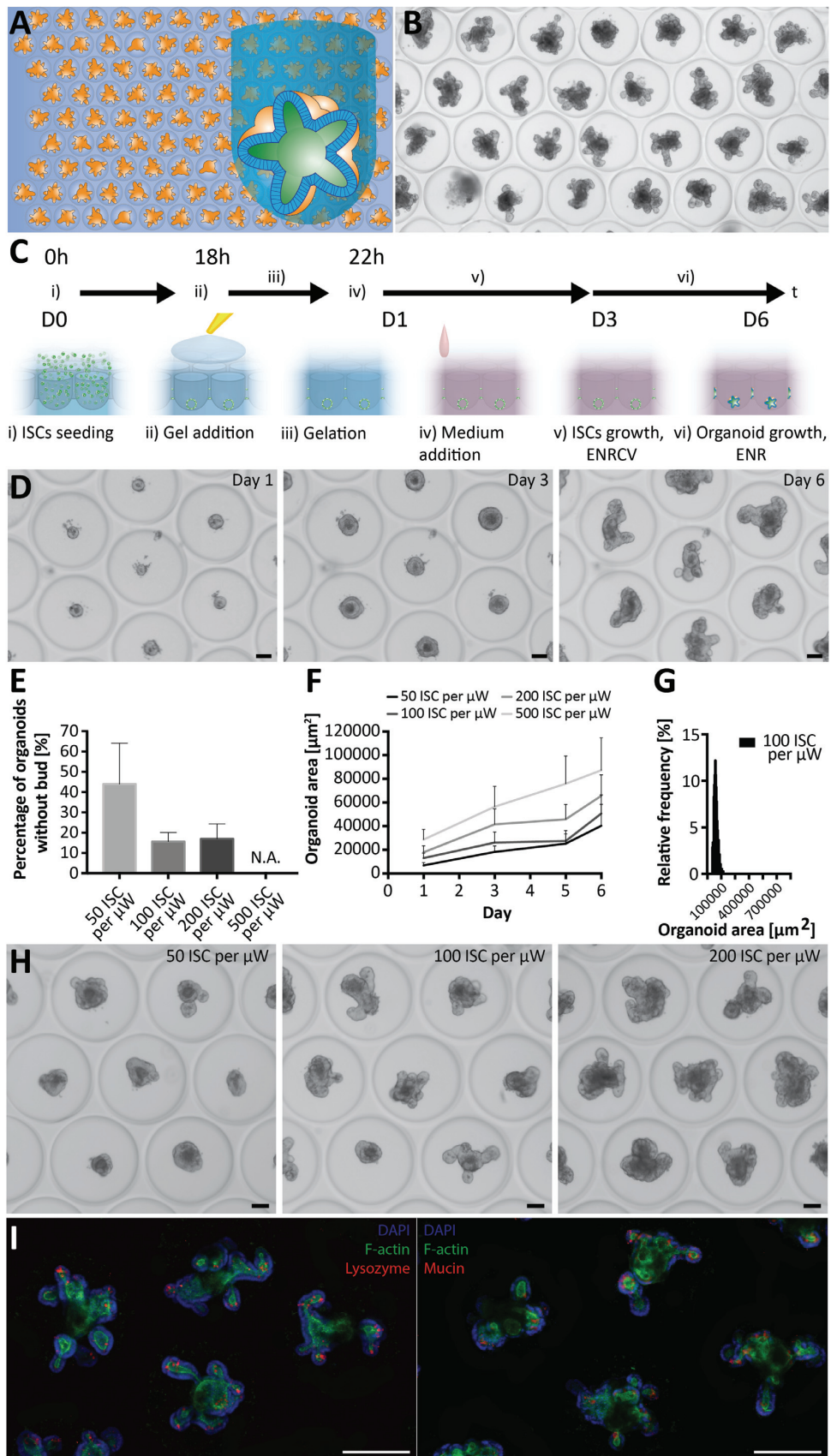


Figure 5: (A) Schematic representation of intestinal organoids in microwells of 500 μm in diameter. (B) Representative image of an intestinal organoid array in 500 μm diameter microwells. (C) Optimized protocol to grow intestinal organoids in U-shaped microwells. (i) Dissociated intestinal stem cells are seeded in low numbers in the microwells and let to form a colony over night in medium supplemented with 2% matrigel. (ii) An overlaying ECM is added at the surface of the culture to sandwich the formed colonies in a three dimensional matrix. After gelation of the upper layer (iii), expansion medium, ENRCV, is added to expand the colonies (iv). Once the colonies form a columnar epithelium (v), the medium is exchanged to differentiation medium (vi) to favor the budding and the differentiation of the stem cell colonies into organoids. (D) Representative images of the key steps of the protocol; IS cells after seeding (Day 1), expanded IS cells colonies (Day3) and differentiated organoids (Day6). (E) Quantification of the percentage of organoids without buds after six days following the above described optimized protocol. Colonies starting with 500 IS cells per microwells were not analyzed due to their multilumenization. (F) Differences in organoid growth when different initial IS cells are seeded. (G) Surface area distribution of organoids grown from 100 ISCs per microwell. After Gaussian fit: Mean: 29323 μm^2 , standard deviation: 7726 μm^2 . (H) Representative images of intestinal organoid arrays starting from 50, 100 and 200 cell per microwells. (I) Presence of different key markers of the intestinal niche and differentiated progeny. *Left.* Lysozyme reveals the presence of paneth cells, which maintain intestinal stem cells. *Right.* Mucin reveals the presence of goblet cells. Scale bars: 200 μm .

However, when 500 cells per microwells are seeded, the colonies grow continuously. Therefore, 100 cells per microwell appears to be the optimal number to generate very homogenous organoid arrays (**Fig. 3E-H**). A higher number aggregated ISCs gives rise to multi-lumen organoids that are irregular (**Supplementary Fig. 2B**), whereas a lower number of cells requires a longer stem cell expansion phase. Indeed, intestinal organoids formed from 100 ISCs are highly uniform in size (**Fig. 5G**).

Finally, we performed immunohistochemistry directly on top of the array. We found that paneth cells are present in the buds (**Fig. 5I, left**). Additionally, we also demonstrate that stem cells residing in the buds produce their differentiated progeny as described previously⁶, by revealing the presence of goblet cells (**Fig. 5I, right**) in the organoids.

These results demonstrate that we can generate reproducible and homogenous populations of organoids by gathering low numbers of single intestinal stem cells in U-shaped microwells. The power of this method lies in the generation of assay-ready intestinal organoids in only six days from a solution of dissociated stem cells. In contrast, Sato and colleagues show that single cells seeded in three-dimensional naturally-derived or synthetic ECM drops take up to two weeks to generate fully differentiated organoids⁶.

In addition to speeding up and simplifying the generation of organoids from dissociated cells, we show that organoids grown in microwell arrays display a convincing homogeneity in terms of size and shape. This is a critical requirement to standardize tissue models reliably for pharmacological screenings⁹. Unexpectedly, thanks to this homogeneity, we could observe the growth dynamic of the organoids more precisely. This suggests that the differentiation dynamic of intestinal stem cells can be tightly deconstructed and analyzed at the population level, while still

capturing the differences within the population. We hypothesize that, when gathered together, single intestinal stem cells reorganize and their individual growth potential is averaged at the colony level, while single stem cells have heterogeneous potential to expand, that in turns gives rise to colonies of significantly different sizes.

Conclusions

In this study, we present a novel platform that offers the possibility to generate any kind of 3D cultures, from cell lines spheroids to complex ESC/iPSC or adult stem cell-based organoids. Unlike previously described microwell technologies^{20,21}, our microwell platform offers several advantages including a tremendous design flexibility in the choice of geometry, substrate material and microenvironmental characteristics. Moreover, as the microcavities can be imprinted in a hydrogel phase, biomolecular gradients can be generated over single cavities. Here, we characterized the behavior of stem cell lines as well as primary stem cells in the microwells and could show that the generated 3D tissues are more homogenous than previously reported. More importantly, we standardized the culture of well-established organoid systems such as retinal and intestinal organoids. This standardization is a crucial step to use these novel tissue-mimicking cultures for pharmacological screenings and the clinical production of transplantable cells.

Experimental methods

Fabrication of poly(dimethylsiloxane) (PDMS) rings: PDMS rings that serve as microwell arrays containers were fabricated as follows: PDMS (ratio 1:10, crosslinking agent-elastomer, SYLGARD® 184 SILICONE ELASTOMER KIT, Dow Corning) was poured onto non-tissue culture treated 10cm petri dishes and cured overnight at 75°C. To control the height of the rings, the quantity of PDMS was carefully adjusted with respect to the surface of the petri dish. After crosslinking, PDMS was de-moulded, and punched twice with an inner diameter (ID) of 5.5, 6, 8 or 10mm and an outer diameter of 12 mm. The resulting PDMS rings were fixed at the bottom of standard 24 well plates (Falcon™) via unspecific interactions.

Fabrication of epoxy resin PDMS stamp holders: PDMS stamp holders were manually cut and counter molded to generate a master mold. Epoxy resin (SIKA Sikadur®-52 Injection) was then poured into the holder mold and cured overnight at room temperature. After crosslinking, the epoxy holders were de-moulded and used as such.

Fabrication of U-bottom microwell arrays PDMS molds: U-shaped microcavities of any size between 10 µm and 1.5 mm were generated onto standard 4 inches silicon wafers using standard Si Bosch in combination with soft lithography processes. PDMS (ratio 1:10) was poured onto the wafers and cured overnight at 75°C. After crosslinking, the PDMS stamps were de-moulded and punched with various diameters; 5.5, 6, 8, 10 or 12mm.

Imprinting the U-shaped microwells onto hydrogel substrates: The desired stamps were mounted on the epoxy holders using double-sided tape. As depicted in figure 2, the final uncrosslinked hydrogel mix was deposited onto the PDMS stamp, and the holder-stamp-hydrogel construct was placed into the PDMS ring at the bottom of wells of a 24 well plate. The hydrogels were incubated at 37°C and 5% CO₂ for 15 minutes to 1h, depending on the type of hydrogel used (see below). After crosslinking, aqueous buffer (e.g. 1X PBS) was pipetted into the wells and the holders-stamps were removed carefully. The resulting microwell arrays were sterilized thoroughly in buffer under UV light and stored at 4°C upon use.

Application	Microwells diameter [µm]	Microwells height [µm]	Distance between microwells [µm]	Microwell array diameter [mm]
Spheroid arrays	400	480	40	10
Intestinal organoid arrays	500	600	40	6
Retinal organoid arrays	1500	1800	100	5.5

Table 1: Summary of various applications with their corresponding microwell geometry.

Preparation of hydrogels: PEG hydrogels crosslinked via Michael-type addition reaction (termed ‘MT-gel’ in this work) were prepared as described,²² mixing aqueous solutions containing thiol- and vinylsulfone- functionalized 4arm- and 8arm-PEG macromers (mol. weight 10 kDa and 40kDa, respectively) at various concentrations to adjust stiffness and stoichiometric ratio. The solution was deposited and molded as explained above. The construct was crosslinked for 15 minutes at room temperature.

PEG hydrogels crosslinked via the transglutaminase factor XIIIa (FXIIIa) (termed ‘TG-gel’ in this work) were prepared as previously described¹¹⁻¹³. Briefly, 8arm-PEG macromers (40 kDa) bearing lysine-containing or glutamine-containing FXIIIa substrate peptides were mixed at various concentrations to adjust stiffness and stoichiometric ratio. Additionally, proteins or peptides were incorporated, covalently or non-covalently in the hydrogel network. The solution was deposited and molded as explained above. The construct was crosslinked for 30 minutes at at 37°C and 5% CO₂.

Native bovine dermis collagen type I (5mg/mL stock concentration, Kouken, Japan) was reconstituted according to the manufacturer’s protocol. The water content was adjusted to obtain the appropriate concentration and variable mechanical properties. The solution was deposited and molded as explained above. The construct was crosslinked for 30 minutes at at 37°C and 5% CO₂.

Gelatin (porcine high strength, Fluka) was solubilized at 10% w/v. The solution was deposited and molded as explained above. The construct was crosslinked for 2 hours at 37°C and 5% CO₂.

Agarose (agarose, standard molecular biology grade, EUROBIO, Brunswick) was solubilized at 2% w/v and heated to reach full solubility. . The solution was deposited and molded as explained above. The construct was crosslinked for 1 hours at 4°C.

Alginate (PRONOVATM, low viscosity sodium alginate, FMC biopolymer/Novamatrix) was solubilized at 2% w/v. The solution was deposited and molded as explained above. The construct was exposed to a solution of calcium chloride (CaCl₂) at 100mM for 4 hours at room temperature to ensure homogenous crosslinking.

Cell culture: OCT4::GFP Mouse Embryonic Stem Cells (mESCs) provided by Austin Smith (University of Cambridge) were routinely expanded without feeders in Dulbecco's Modified Eagle Medium (DMEM) supplemented with leukemia inhibitory factor (LIF), ESC screened fetal bovine serum (FBS, Gibco) (15%) medium, Non-essential amino acids (NEAA) sodium pyruvate (10mM) and b-mercaptoethanol (0.1 mM), hereafter referred as ES cell medium²³.

Human mesenchymal stem cells (hMSCs, PT-2501, Lonza) and OP9 murine stromal cells were routinely maintained in alpha-MEM supplemented with 10% FCS (Hyclone, batch AUA33984) and 1ng/mL human FGF-2 (Peprotech).

NIH3T3 fibroblasts, MCF-7 human breast cancer cells, MDA-MB231 human breast cancer cells, C2C12 mouse myoblast cells, NMuMG E9 mouse breast cancer cells and human embryonic kidney (HEK) 293 cells were routinely maintained in DMEM

supplemented with 10% fetal bovine serum (FBS), HEPES (10 mM) and sodium pyruvate (1 mM).

CRX::GFP Mouse Embryonic Stem Cells (mESCs) derived by Decembrini and colleagues were routinely maintained as reported previously¹⁷.

LGR5::GFP mouse Intestinal Stem Cells. Crypts were extracted from murine small intestine as reported previously⁶. The isolated crypts were maintained and expanded in MatrigelTM, in self-renewal medium, ENR-CV¹⁹.

Preparation of spheroids microwell arrays: Cells of interest were detached with trypsin (TrypLE, Life Technologies). Cell suspensions with specific densities were prepared (e.g. 4.68×10^6 cells/mL, 9.36×10^4 cells/mL, and 9360 cells/mL for achieving 500 cells/microwell, 100 cells/microwell and 1 cell/microwell, respectively) in the cell-type specific media. Subsequently, 50 μ L of the prepared cell solution was added in the inner ring containing the microwell arrays. Cells settled down by gravitational sedimentation for 30 minutes at 37°C and 5% CO₂ and 700 μ L of appropriate media were then added. All cell types were cultured for 5 days and their respective media was changed every other day.

Preparation of retinal organoids microwell arrays: CRX::GFP mESCs¹⁷ were washed with phosphate-buffered saline (1X PBS, Gibco) and detached with trypsin (Gibco, Cat. n° 25200-056). The cells were then resuspended in Optic Vesicle (OV) induction medium¹⁷ at a density of 525'000 cells/mL in order to seed 3000 cells per microwell. The cell suspension was then added on top of the arrays, in the inner ring, and the cells were left to sediment for 30 minutes at 37°C and 5% CO₂. Then, 660 μ L of OV induction medium was added. After an overnight incubation, the cells formed aggregates in each microwell and 140 μ L of a diluted growth factor reduced MatrigelTM solution (12%, Corning) was added in each 24 wells, where the final matrigel concentration was 2%. The aggregated cells were left in OV induction medium for 7 days. At day 7, the medium was changed to Optic Cup (OC) induction medium¹⁷ and left until day 12. At day 12, the medium was subsequently changed to Retina Maturation medium¹⁷ until day 30. In this case the medium was changed every other day. Additionally, the organoids were incubated in hyperoxic incubators from day 12 on, to promote the survival of newly born photoreceptors.

Preparation of intestinal organoids microwell arrays: LGR5::GFP intestinal organoids were released from MatrigelTM in cold basal medium (advanced DMEM/F-12 containing 1mM HEPES, GlutamaxTM and 1% P/S). The organoids were spun down at 800rpm, for 4 minutes, at 4°C and resuspended 1mL of cell dissociation solution (TrypLE, 2mg/mL DNase I, Gibco, 1mM N-acetylcysteine and 10 μ M Y27632). Cells were dissociated for 8 minutes at 37°C and subsequently washed with basal medium containing 10% foetal bovine serum (FBS, heat inactivated, Gibco). After centrifugation at 1000 rpm, for 4 minutes, at 4°C, the cells were resuspended at a density of 2.24×10^5 cells/mL in ENR-CV medium supplemented with 2.5 μ M Thiazovivin and different concentration of laminin of matrigel (see **Table 3.1**) in

order to deposit 100 cells per microwell. 50 μ L of the cell suspension was added in each microwell. The cells were aggregated overnight as such and sandwiched in 300Pa non-degradable TG-PEG, containing 200 μ g/mL full length laminin (Laminin Mouse Protein, Natural, ThermoFisher Scientific) and 1mM RGD tethered to the hydrogel network¹³. The hydrogel was left to crosslink 4h at 37°C and 5% CO₂. Finally, 750 μ L of self-renewal medium (ENR-CV) was added to each well. The aggregated mISCs were expanded in self-renewal for 2 days, and the organoids were differentiated for 4 days in differentiation medium (ENR)¹⁹. Growth factors were replenished every other day.

REFERENCES

- 1 Li, L. & Xie, T. Stem cell niche: structure and function. *Annual review of cell and developmental biology* **21**, 605-631, doi:10.1146/annurev.cellbio.21.012704.131525 (2005).
- 2 Griffith, L. G. & Swartz, M. A. Capturing complex 3D tissue physiology in vitro. *Nature reviews. Molecular cell biology* **7**, 211-224, doi:10.1038/nrm1858 (2006).
- 3 Zhang, S. Beyond the Petri dish. *Nature biotechnology* **22**, 151-152, doi:10.1038/nbt0204-151 (2004).
- 4 Abbott, A. Cell culture: biology's new dimension. *Nature* **424**, 870-872, doi:10.1038/424870a (2003).
- 5 Pampaloni, F., Reynaud, E. G. & Stelzer, E. H. K. The third dimension bridges the gap between cell culture and live tissue. *Nat Rev Mol Cell Bio* **8**, 839-845, doi:10.1038/Nrm2236 (2007).
- 6 Sato, T. *et al.* Single Lgr5 stem cells build crypt-villus structures in vitro without a mesenchymal niche. *Nature* **459**, 262-265, doi:10.1038/nature07935 (2009).
- 7 Eiraku, M. *et al.* Self-organizing optic-cup morphogenesis in three-dimensional culture. *Nature* **472**, 51-56, doi:10.1038/nature09941 (2011).
- 8 Dekkers, J. F. *et al.* A functional CFTR assay using primary cystic fibrosis intestinal organoids. *Nature medicine* **19**, 939-945, doi:10.1038/nm.3201 (2013).
- 9 Fatehullah, A., Tan, S. H. & Barker, N. Organoids as an in vitro model of human development and disease. *Nature cell biology* **18**, 246-254, doi:10.1038/ncb3312 (2016).
- 10 Lutolf, M. P. & Hubbell, J. A. Synthetic biomaterials as instructive extracellular microenvironments for morphogenesis in tissue engineering. *Nature biotechnology* **23**, 47-55, doi:10.1038/nbt1055 (2005).
- 11 Ehrbar, M. *et al.* Enzymatic formation of modular cell-instructive fibrin analogs for tissue engineering. *Biomaterials* **28**, 3856-3866, doi:10.1016/j.biomaterials.2007.03.027 (2007).
- 12 Ehrbar, M. *et al.* Biomolecular hydrogels formed and degraded via site-specific enzymatic reactions. *Biomacromolecules* **8**, 3000-3007, doi:10.1021/bm070228f (2007).
- 13 Ehrbar, M. *et al.* Elucidating the role of matrix stiffness in 3D cell migration and remodeling. *Biophysical journal* **100**, 284-293, doi:10.1016/j.bpj.2010.11.082 (2011).
- 14 Lutolf, M. P., Doyonnas, R., Havenstrite, K., Kolekar, K. & Blau, H. M. Perturbation of single hematopoietic stem cell fates in artificial niches. *Integrative biology : quantitative biosciences from nano to macro* **1**, 59-69, doi:10.1039/b815718a (2009).
- 15 Olea, N., Villalobos, M., Ruiz de Almodovar, J. M. & Pedraza, V. MCF-7 breast cancer cells grown as multicellular spheroids in vitro: effect of 17 beta-estradiol. *International journal of cancer* **50**, 112-117 (1992).

- 16 Ivascu, A. & Kubbies, M. Diversity of cell-mediated adhesions in breast cancer spheroids. *International journal of oncology* **31**, 1403-1413 (2007).
- 17 Decembrini, S., Koch, U., Radtke, F., Moulin, A. & Arsenijevic, Y. Derivation of traceable and transplantable photoreceptors from mouse embryonic stem cells. *Stem cell reports* **2**, 853-865, doi:10.1016/j.stemcr.2014.04.010 (2014).
- 18 Nishida, A. *et al.* Otx2 homeobox gene controls retinal photoreceptor cell fate and pineal gland development. *Nature neuroscience* **6**, 1255-1263, doi:10.1038/nn1155 (2003).
- 19 Yin, X. *et al.* Niche-independent high-purity cultures of Lgr5+ intestinal stem cells and their progeny. *Nature methods* **11**, 106-112, doi:10.1038/nmeth.2737 (2014).
- 20 Ungrin, M. D., Joshi, C., Nica, A., Bauwens, C. & Zandstra, P. W. Reproducible, ultra high-throughput formation of multicellular organization from single cell suspension-derived human embryonic stem cell aggregates. *PloS one* **3**, e1565, doi:10.1371/journal.pone.0001565 (2008).
- 21 Vrij, E. J. *et al.* 3D high throughput screening and profiling of embryoid bodies in thermoformed microwell plates. *Lab on a chip* **16**, 734-742, doi:10.1039/c5lc01499a (2016).
- 22 Gobaa, S. *et al.* Artificial niche microarrays for probing single stem cell fate in high throughput. *Nature methods* **8**, 949-955, doi:10.1038/nmeth.1732 (2011).
- 23 Smith, A. Culture and differentiation of embryonic stem cells. *J. Tiss. Cult. Meth.*, 89-94 (1991).

CHAPTER IV

ORGANOIDS IN DRUG SCREENING: THE EXAMPLE OF CYSTIC FIBROSIS INTESTINAL ORGANOIDS

Organoids in Drug Screening: The Example of Cystic Fibrosis Intestinal Organoids

Manuscript in preparation

Patent pending

Brandenberg N^{1*}, Hoehnel S^{1*}, Rappaz B^{3,4}, Gjorevski N¹, Turcatti G⁴, Lutolf MP^{1,2}

¹Laboratory of Stem Cell Bioengineering, Institute of Bioengineering, School of Life Sciences, Ecole Polytechnique Fédérale de Lausanne (EPFL), 1015 Lausanne, Switzerland.

²Institute of Chemical Sciences and Engineering, School of Basic Sciences, EPFL, 1015 Lausanne, Switzerland.

³Lyncée Tec SA, PSE-A, Lausanne, Switzerland.

⁴Biomolecular Screening Facility (BSF), EPFL, 1015 Lausanne, Switzerland.

* The authors contributed equally to the presented work

Keywords: Cystic fibrosis, intestinal organoids, U-bottom microwells, array, hydrogel, screening, digital holographic microscopy (DHM), label-free imaging

Corresponding Author:

Prof. Matthias Lutolf

Laboratory of Stem Cell Bioengineering

Institute of Bioengineering

School of Life Sciences

Ecole Polytechnique Fédérale de Lausanne

CH-1015 Lausanne, Switzerland

Tel: +41216931876, E-mail: matthias.lutolf@epfl.ch

Abstract

Organoids recapitulate organ physiology better than any previously described in-vitro tissue model. Their biological relevance raised high hopes in drug development and for their use in regenerative medicine. They are currently suggested to be ideal candidates to capture our increasingly complex diseases in vitro. Yet, organoid culture is still poorly controlled and developing tractable, deterministic and meaningful assays is of major interest. Cystic fibrosis is the most lethal autosomal recessive disease in Caucasian phenotypes. Recently, high throughput screenings revealed a family of small molecules capable of rescuing the function of mutated cystic fibrosis transmembrane conductance regulator (CFTR) proteins. However, the number of different mutations leading to severe diseased phenotypes is too high to determine what combination of drugs each patient needs using a HTS approach. Most recently, it was demonstrated that intestinal organoids can be used to screen specific combinations of drugs prior to patient treatment. However, the existing readouts are simplistic and provide limited information. In this study, we show that more phenotypically accurate measures can be extracted from intestinal organoids. We demonstrate that, by using interferometry, we can track precisely three critical parameters related to the behavior of the epithelium when exposed to compounds triggering transmembrane transport. We show that measures like the time lag between the addition of forskolin and the initiation of swelling, the total fluid uptake inside the organoid and the rate at which fluids are pumped in the lumen of the organoid can be evaluated precisely with this technique. Moreover, we could see that these parameters vary significantly between wild type and diseased organoids ($\Delta F508$ double mutants). Finally, we demonstrate that this interferometry-based technique using rectal organoids meets all the necessary requirements to be implemented drug screening.

Introduction

Cystic fibrosis is an autosomal recessive disease having the highest prevalence in Caucasian phenotypes particularly across Europe, North America and Australia (approx. 1 in 3000 births). In addition, this disease affects various organs as it is considered to be a mucosal immunodeficiency syndrome, which complicates the development of efficient targeted treatments. Mutations in the gene encoding for the cystic fibrosis conductance regulator (CFTR) protein is responsible for severe clinical manifestations, such as thick secretions that lead to obstruction of the airways or the intestinal tract to finally damage irreversibly the affected organs. Conventionally, symptoms have been treated in an organ-specific way, but patients' life improvements were poor.

Among 2000 mutations discovered in the *cftr* gene, about 242 are known to cause cystic fibrosis. CFTR, a protein member of the ATP binding cassette (ABC) family, has a higher degree of complexity in term of function as it harbors an additional regulatory domain that tightly modulates the opening and the closing of the channel. Thus, it is prone to more deleterious mutations. In order to understand the different effects of the numerous mutations, six different classes of protein dysfunction have been proposed (see **Figure 1A**)^{1,2}. Class I mutations, often associated with

premature stop codons, give rise to truncated messenger RNAs that get degraded before even being translated into proteins³. Class II mutations result in misfolded proteins that are poorly processed and that do not traffic properly. The amount of protein that reaches the cell membrane is extremely low and most of the proteins get prematurely degraded in the proteasomes like in the example of the most common mutation; $\Delta F508$ ⁴. Class III and class IV mutations refer strictly to protein dysfunction once integrated in the cellular membrane. Class III mutations impact directly CFTR activation, where the gating is disrupted and class IV mutations impact the conductivity of Cl^- ions through the channel itself⁵. Class V mutations are located on either promoter or splice regions of the gene, leading to low amounts of transcript and thus decreases the protein production. Finally, class VI mutations, that have been discovered only recently, impact the protein stability at the membrane surface and thus lead to a higher protein turnover⁶. Even though these classes give a comprehensive tool to understand the possible protein dysfunctions, studies still show that primary abnormalities, such as degradation in the proteasomes, of any mutation also leads to downstream effects in the core function of the protein^{5,7}.

Recently, owing to advances in gene sequencing and high throughput screening, selected families of molecules capable of recovering some CFTR dysfunctions were discovered^{8,9}. However, these molecules were discovered in high throughput screenings on genetically modified human cell lines, such as NIH3T3. Ion transport readouts based on fluorescence, such as fluorescent membrane soluble voltage sensitive dyes or yellow fluorescent (YFP) protein-based halide sensors, were used to measure Cl^- fluxes across cellular membranes^{10,11}. Yet, most of these methods rely on fluorescence, a readout that needs to be carefully calibrated. Moreover, these techniques measure precisely transmembrane ion potential or ion levels in the intracellular compartment, which are tightly linked to cystic fibrosis symptoms but do not represent these symptoms as a whole¹²⁻¹⁴.

In recent years, label-free imaging methods based on interferometry or, more precisely, digital holographic microscopy have emerged. This non-invasive method allows the measurement of refractive index changes into cells or organisms that directly correlates with cellular transmembrane water fluxes and cell viability¹⁵⁻¹⁷. Interestingly, it showed promising results for evaluating CFTR activity in genetically modified CHO cell lines. Using this unique method, the authors demonstrated that water fluxes accompanying CFTR activity were co-dependent on Aquaporin 3 transmembrane transport¹⁸.

Despite these significant advances at the cellular scale, representing accurately cystic fibrosis at the tissue level in vitro is still a major challenge. Mouse models have provided valuable insight into the molecular mechanisms of the disease¹² but these models are very hard to maintain and use routinely due to the extremely severe symptoms mice encounter. Most recently, Dekkers and colleagues showed that intestinal organoids were ideal candidates to study intestine-related diseases with a particular focus on cystic fibrosis¹⁹. In particular, they demonstrate that tracking organoid area during forskolin induced swelling (FIS) can be considered as an appropriate measure for CFTR activity^{19,20} (**Figure 2**). In particular, they show that mutated organoids are dysfunctional and do not undergo swelling. However, when treated with specific drugs, or their combination, this swelling defect can be rescued.

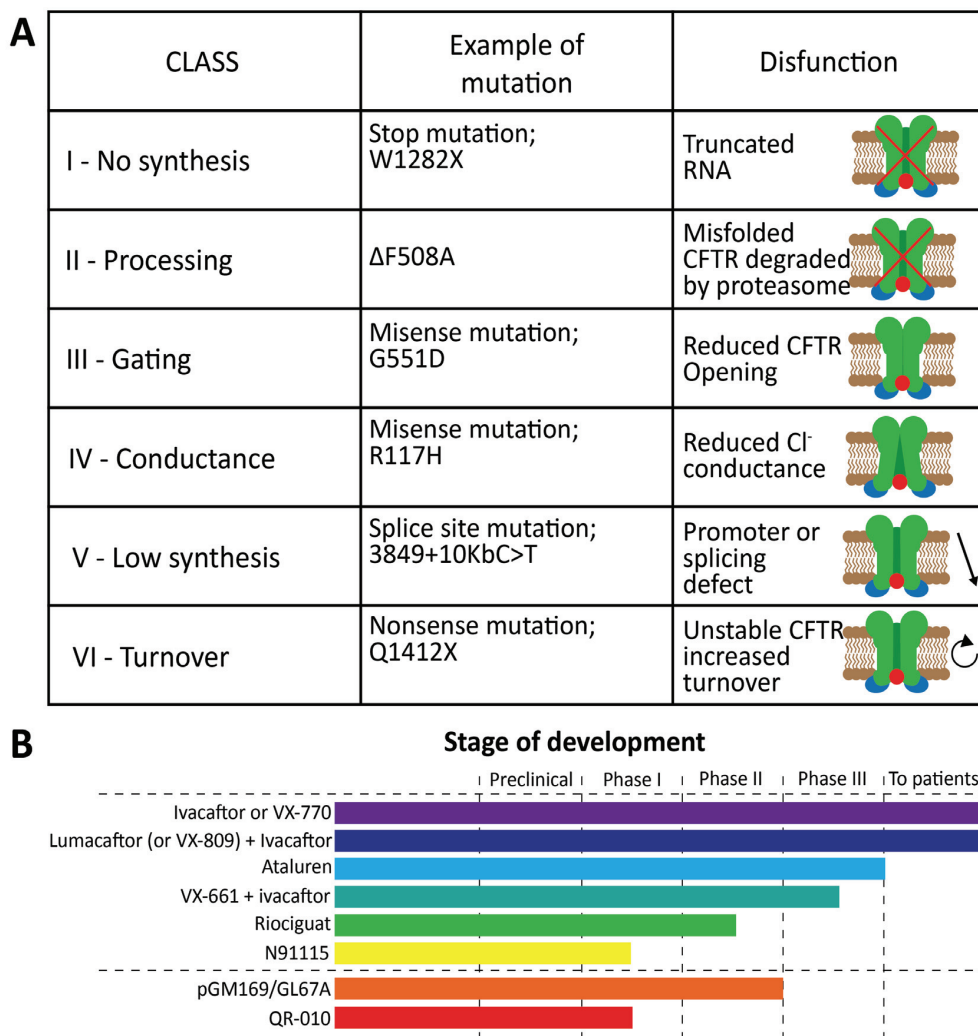


Figure 1: (A) Classification of the different types of mutation on the gene encoding the cystic fibrosis conductance regulator (CFTR) protein. These different mutations can lead to symptoms with varying severity and can now be corrected using small molecules via different modes of action. (B) In the upper category (from purple to yellow), small molecules capable of correcting or rescuing the function of CFTR are shown together with their respective stages in drug development. The lower category (orange and red) shows the current gene therapy approaches that are currently in clinical trials. Figure modified according to 5.

Using this assay, they screened combinations of molecules on patient-derived intestinal organoids. They could find in consistency with the preclinical trials that the combination of the two small molecules (i.e. Ivacaftor, VX-770, and Lumacaftor, VX-809) have a synergistic effects in rescuing CFTR function in organoids derived from $\Delta F508$ double mutant. This study exemplifies how organoids can be used to perform personalized drug screenings. However, this method is based on the analysis of a unique parameter averaged for an entire well of a 96 microtiter plate.

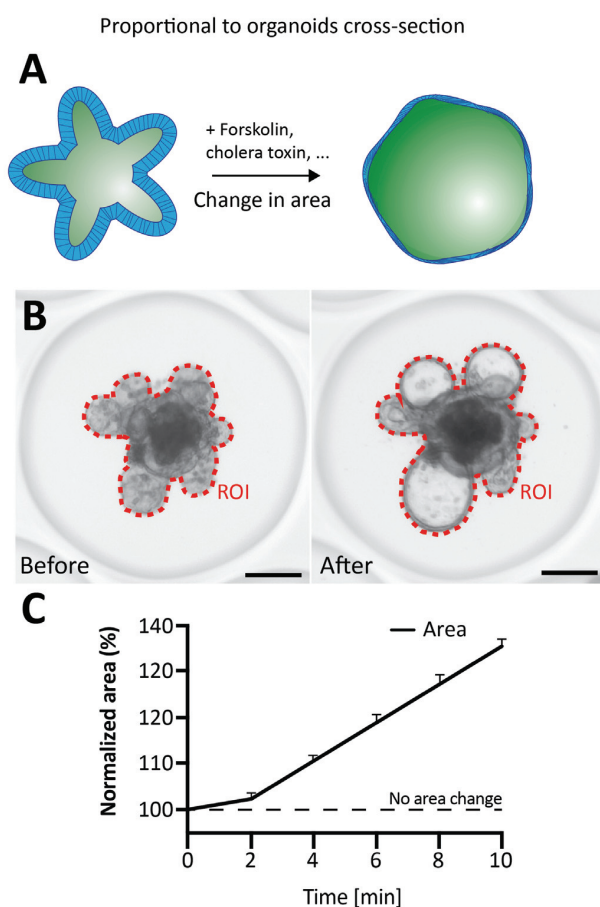


Figure 2: (A) Schematic representation of intestinal organoids swelling and two-dimensional surface changes analysis (i.e. Dekkers method). (B) Representative widefield microscopy images of swelling intestinal organoids before and 15 minutes after addition of 5 μ M Forskolin. The red dotted line represents the region of interest (ROI) where area was measured. Scale bar: 100 μ m. (C) Plot of the increasing surface area in control organoids over time as a percentage increase compared to t=0. The black dashed line represents non-swelling organoids as baseline.

We believe that changes in area are a relevant, but not highly sensitive readout of intestinal organoid function. Hence, we developed a more comprehensive assay for assessing organoid function and changes therein in response to pharmacological perturbations. In this work, we compare the two methods: the approach proposed by Dekkers and colleagues based on fluorescent area changes and our novel approach using interferometry to track changes in refractive index within the lumen of the organoids.

Results and discussion

We first performed calibration experiments to understand differences in read-out dynamics between the two methods. When analyzed in details, the method described by Dekkers et al relies on relatively simple, but numerous steps. First, the organoids are grown and differentiated in routinely used three-dimensional matrigel drops. After seven days, they are extracted from the drops and deposited at the surface of 96 flat bottom plates wells coated with a thin layer of matrigel. Finally, after settling down, the organoids can be treated with CFTR correctors and/or potentiators.

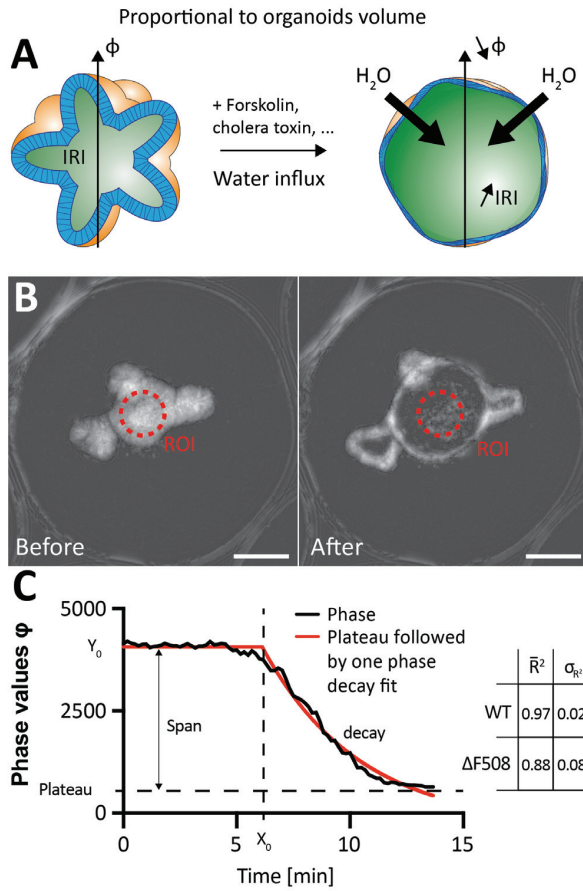


Figure 3: (A) Schematic representation of intestinal organoids swelling and analysis of the changes in refractive index within the organoid lumen. The arrows across the organoid represent the light path. Φ = Phase, IRI = Intraorganoid refractive index. (B) Phase intensity images of swelling intestinal organoids before and 15 minutes after addition of 5 μ M Forskolin. The red dotted line represents the region of interest (ROI) where the phase was monitored. Scale bar: 100 μ m. (C) Plot of phase change in control organoids over time in absolute value. The phase is fitted to a linear step followed by a one-phase decay to extract parameters of interest (description in the main text). R^2 represents the fitting quality. Both wild-type and diseased organoids phase curves fit to this pattern with high fidelity. Outliers displaying a R^2 lower than 0.75 were discarded (4 samples).

On the subsequent day, the organoids are washed, pretreated with a green fluorescent calcein, swollen using forskolin (see **Figure 2A,B**) and imaged using live-cell confocal microscopy¹⁹. This assay involves a significant amount of intermediate steps that are supplementary to the addition of the drugs acting on CFTR and the addition of forskolin. Moreover, here, fluorescence is key to homogeneously reveal the epithelium and thus being able to evaluate changes in area. In the case of wild type intestinal organoids, they demonstrated that the averaged surface area increase per well is 1.5 fold its initial area ten minutes after addition of forskolin (see **Figure 2C**), whereas diseased organoids showed an area increase of about 1.1 fold after 10 minutes.

Using digital holographic microscopy, we developed a novel procedure to track transepithelial water fluxes. When a coherent light beam passes through a specimen of interest, here intestinal organoids, its front phase delays with respect to the reference beam as a function of the different refractive indexes encountered in the optical path (see **Figure 3A**). This technique measures refractive index differences within samples, and, thus, is a direct measure of the local fluid density, considering that the local atomic composition is homogenous enough to assume it equal from

one organoid to the other. Hence, our phase measurement is inversely proportional to the local molecular density¹⁸. We first imaged wild-type intestinal organoids grown from dissociated cells in U-shaped PEG microwells. We observed that, after addition of forskolin, the phase intensity dropped critically within the lumen after fifteen minutes (see **Figure 3B,C**). While measuring every fifteen seconds, we could track the phase precisely and observe its behavior. Interestingly, we could see that, first, the phase stay stable to then drop in an exponential fashion (see **Figure 3C**). This behavior is easily fitted with an “initial plateau followed by an exponential decay”, which can be formalized by the following equation:

$$\text{Plateau} + (Y_0 - \text{Plateau})e^{-K(x-x_0)} \quad (1)$$

where x_0 is the time at which the exponential decay starts, the plateau is the Y value of the exponential decay at infinite times, Y_0 is the average value of the step before x_0 , K is the rate constant of the decay, the half-life represents time the organoid needs to uptake half of its final volume and is expressed as $\ln(2)/K$ and the span is the difference between the initial step, Y_0 , and the plateau. Moreover, we could demonstrate that this analytical fit is appropriate as the averaged R^2 values for wild type and diseased organoids are 0.97 and 0.88 and their respective standard deviation is less than 10%. Four samples in the category of mutated organoids showing a R^2 value lower than 0.75 were discarded. Finally, we set the x-axis origin to be the time of addition of forskolin. This normalization can allow us to evaluate how long organoids need to activate transepithelial flow.

We evaluated these parameters for wild type and $\Delta F508$ intestinal organoids in order to capture possible differences. Thus, we performed forskolin-induced phase shift (FIPS) experiments with an acquisition frequency of fifteen seconds on a set of about 30 individual organoids in each category. First, we analyzed individually the area increase for each sample. We found that the surface area increases about 1.6 and 1.2 fold after fifteen minutes for wild type and diseased organoids, respectively, which is consistent with what Dekkers and colleagues reported¹⁹ (see **Figure 4A**).

In addition to the sole size of the organoid, we could extract our parameters of interest. Although the differences were subtle, we showed that diseased organoids initiated swelling later than wild-type organoids (see **Figure 4B**).

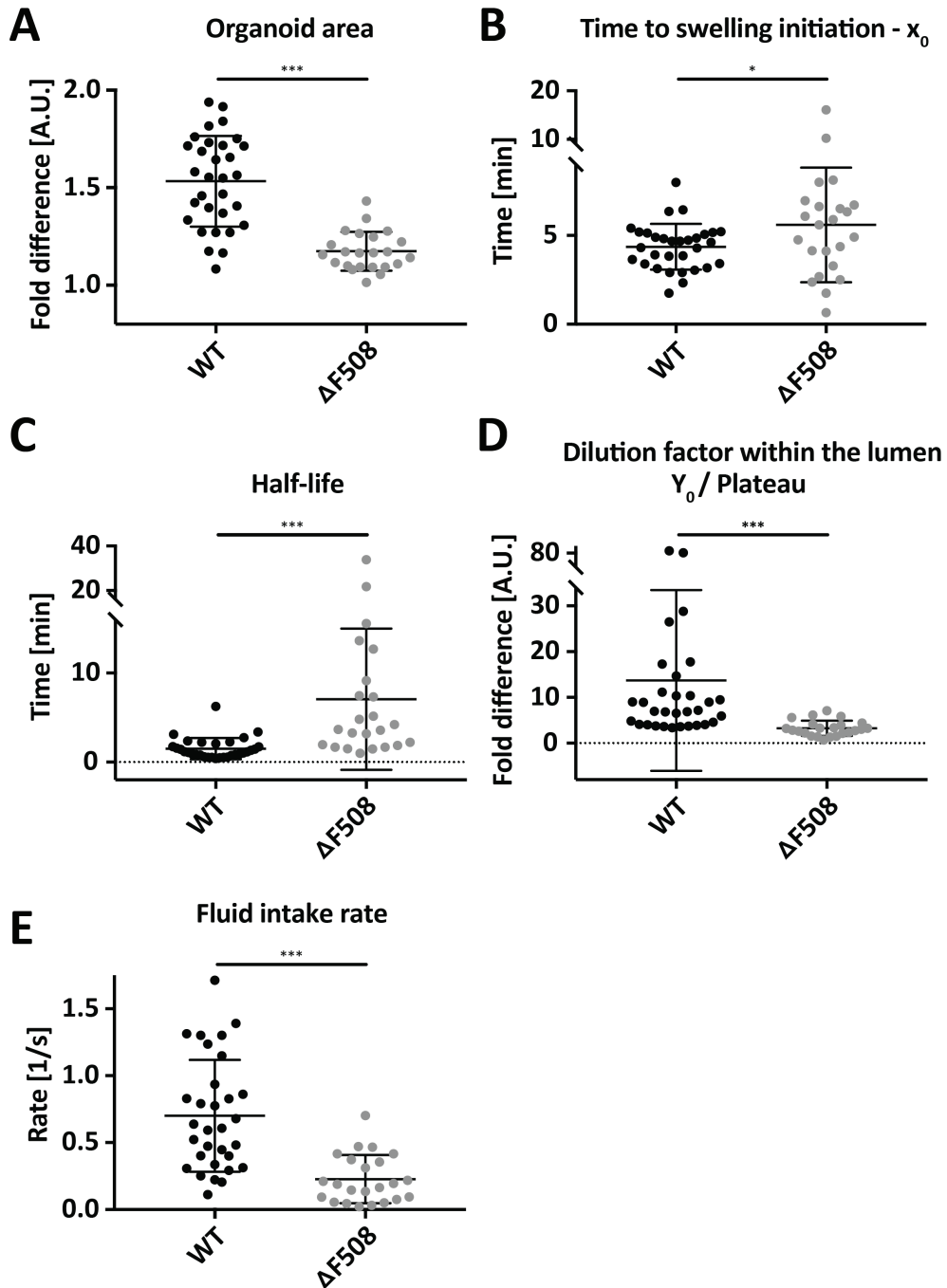


Figure 4: (A) Fold increase in surface area. (B) Time delay between the addition of forskolin and the initiation of the phase drop or x_0 . (C) Half-life of the phase exponential decay. This measure represents the time required for the phase to drop by half. (D) The initial linear value of the phase was normalized by the plateau to represent the drop in density within the lumen, i.e. the dilution factor. (E) The rate of the phase exponential decay representing the rate at which fluids are uptaken into the lumen. WT: $n=32$, $\Delta F508$: $n=24$. Statistical test between the two populations: Kolmogorov-Smirnov. *: $p < 0.05$, **: $p < 0.01$, ***: $p < 0.001$.

More interestingly, we observed that the influx rate and the dilution inside the organoid lumen were impacted severely. Indeed, whereas the swelling half-life of wild type organoids was very short and homogenous, the half-life of mutated organoids became at least twice longer and very heterodisperse (**Figure 4C**). Importantly, we could also measure the intralumen density and thus the dilution factor. We found that, within fifteen minutes, the lumen of the control samples had been diluted three times more than the diseased samples (**Figure 4D**). Finally, we directly measured the influx rate in the lumen, and found that wild type organoids uptake fluids faster than mutated organoids, in agreement with the other parameters we report (**Figure 4E**) that these rates correlate with the other parameters and show.

By measuring these parameters, we are now able to predict and understand the behavior of the organoid epithelium more precisely. As shown previously^{19,20} and by the above-described results, luminal fluid influx and the resulting swelling of wild-type organoids is fast, after which a plateau is reached. Thus, a linear approximation of this behavior in two dimensions is a poor representation of a complex three-dimensional process. Linear measurements cannot predict accurately when the influx starts, how much fluid will be uptaken and at which rate. We demonstrate here that interferometry can be used to quantitatively describe the swelling process using more than one parameter, thus enhancing the sensitivity and dynamic range of the measurement. These quantitative phase shift analyses correlate with samples local density, thus, reflecting volumetric changes.

After observing that FIPS offers a better characterization of the transepithelial transport in intestinal organoids, we analyzed whether this method is amenable to high throughput screening. As briefly introduced above, Dekkers et al's method relies on green fluorescent calcein to reveal the organoid epithelium (see **Figure 5A**). Using live-cell confocal microscopy they show that they can acquire images fast enough to be able to track increases in size. Even though commercial softwares have the capacity to segment calcein-labeled organoid with high fidelity, fluorescence based quantification is still prone to significant errors. The method we describe in the study, the FIPS method, is label free. By simply measuring phase shift differences on the culture surface, intestinal organoids can be revealed (see **Figure 5B**). We can see that after background subtraction, the organoids and especially their lumen show the highest phase shift compared to the surrounding. Interestingly, as the hydrogel thickness is higher at the sidewalls of the microwell compared their bottom, the phase shift is high as well. Object recognition using fluorescence is a standard procedure, where the intensity is thresholded from the background using a mask to allow for the segmentation of the objects of interest. In Dekkers et al's study, a mask is generated from the fluorescence to segment all the organoids from the background (see **Figure 5C**). They use total organoid area as a quantitative measurement considering that this image-based method does not allow for the segmentation of individual organoids. To measure differences, they quantify the total area that organoids cover before the addition of forskolin and set it as the baseline (100%) and evaluate the changes at specific times with respect to this baseline after forskolin addition.

When using phase shift measurements, we can plot two-dimensional or unidimensional maps of the intensity of the phase shift (see **Figure 5D**). This “intensity” represents how different the two beams phases are from one another. Strikingly, we observed that these phase shift intensity maps are very instructive and that different threshold accounts for different features of the culture. For better visualization purposes, we plotted the phase shift intensity in only one dimension and following the dotted lines shown in figure 5B (see **Figure 5F**). First, we could observe that the microwell edges are easily recognizable and show constant phase shift throughout the experimental procedure (see **Figure 5F**, blue dotted lines).

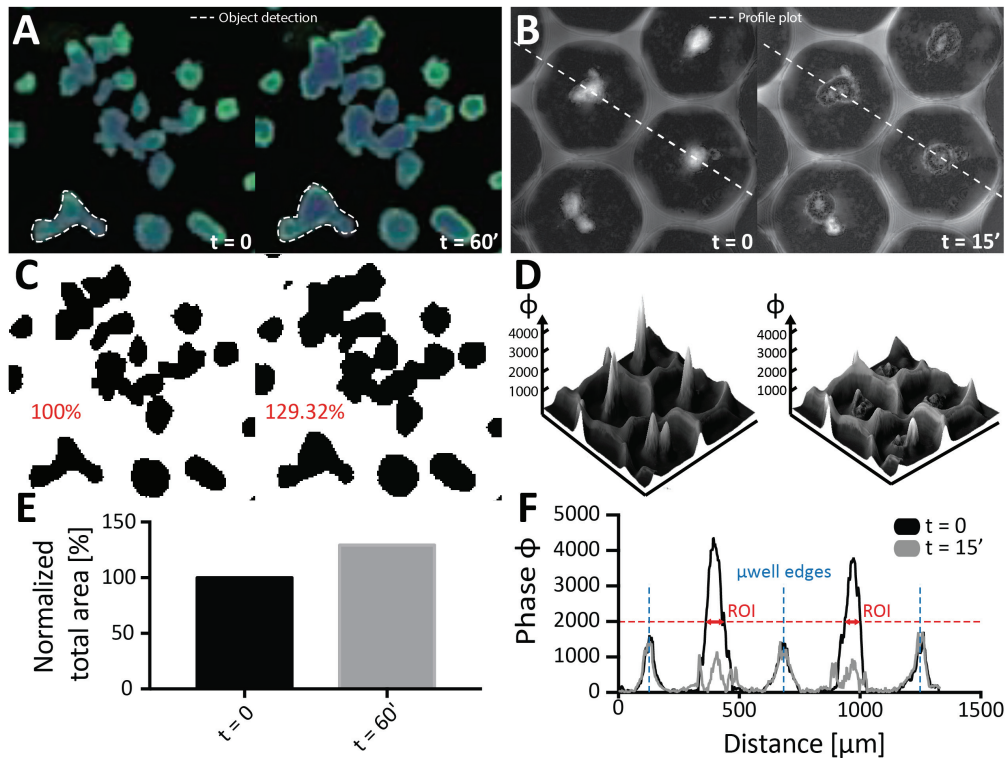


Figure 5: (A) Representative confocal microscopy image of intestinal organoids. The epithelium of the organoid is revealed using green fluorescent calcein. *Left*, organoids before swelling. *Right*, organoids 60 minutes after swelling. Object recognition is based on the calcein signal. Panel reproduced from 17. (B) Representative phase map of intestinal organoids. No label is necessary to reveal the epithelium and its lumen. *Left*, Organoids before swelling. *Right*, organoids 15 minutes after swelling. One dimensional or two dimensional profiles can be generated to recognize regions of interests. (C) Segmentation of the recognized objects. *Left*, the total area is set as 100%. *Right*, the normalized total area is calculated with respect to the reference total area. (D) Two-dimensional phase shift maps are generated. (E) Example of an area increase using $\Delta F508$ rectal organoids treated with VX-809. (F) One-dimensional phase plot before and after swelling, shown in black and gray, respectively. The edges of the microwells are nicely highlighted and the phase drop is easily observable. Moreover, thresholding the phase shift plot before swelling enables the automatic detection of the regions of interest.

Moreover, we could see that the plot was accurate as we can measure exactly 500 micrometers between these constant thresholds. This distance exactly reflects the microwells geometry used in these experiments. Using these thresholds, we can extract precisely the pattern of microwells and thus subtract it to the map using filters cancelling appropriate frequencies. More interestingly, we observed that the organoids can be easily thresholded from these intensity plots as, before water uptake, the phase shift in the lumen is the highest due to the high density of particles present in this region of the organoid. Thus, using appropriate thresholds we can segment the organoids and define regions of interest where phase measurements are relevant (see **Figure 5F**, red dotted lines). This allows for the development of an automatic segmentation pipeline to determine appropriate ROIs used to track the changes in phase.

These results demonstrate that complex physiological parameters can be extracted from three dimensional organotypic cultures using simple technologies such as interferometry. We show that we can measure three interesting characteristics specific to transmembrane transport, without requiring the use of patch clamp-based methods or fluorescent membrane potential reporters²¹. First, the delay between the addition of a swelling compound and the initiation of swelling can be assessed. This measure is interesting per se as we could hypothesize its potential correlation with the activation of the protein once exposed to forskolin, which can be in turn correlated with gating mechanisms. Secondly, phase shift tracking over time and fitting to an exponential decay allowed to extract two other parameters; rate of fluid uptake and the total amount of fluid uptaken in the organoid lumen. The intake rate is an interesting measure, despite its correlation with the total amount of proteins present at the apical side of the epithelium, it also correlates with the direct activity of the protein. Hence, patch clamp experiments could be performed in order to relate the organoid-scale transepithelial fluxes with the local transmembrane ion movement. Finally, these measures can be analyzed precisely to characterize how drugs or their combination rescue CFTR function.

In addition, we show that FIPS can be implemented in high throughput drug screening as we can detect the specific regions of interest automatically using thresholding techniques. We show here that complex cultures, such as intestinal organoids, can be accurately recognized without the use of fluorescent markers. Finally, we performed a short analysis that consisted in sampling the phase every two minutes considering that 96well plate can be scanned in 2 minutes using our interferometer. We could see that the phase shift could still be fitted to the same Plateau followed by an exponential decay with R^2 values that were ranging around 0.9. In addition, the extracted parameters of the fitted curved were found to show a coefficient of variation lower than 10% compared to the parameters extracted from curves fitted to phase measurements made every fifteen seconds. This guarantees that entire 96 microtiter plates can be used using this method while still extracting the same information from the assay.

Conclusions

In this work we present a novel method to precisely analyze transepithelial fluid transports in mouse intestinal organoids. In comparison with previously reported methods such as the one described in the study of Dekkers et al¹⁹, our strategy allows for a stringent analysis of the epithelium's behavior. Instead of relying on the sole analysis of size changes, we describe key metrics, such as the time to induce swelling, the intralumen dilution factor and the fluid uptake rate, to characterize our intestinal organoids and to establish correlations with transmembrane transporters such as CFTR. We were able to observe significant differences of these new metrics between mouse wild type and $\Delta F508$ double mutant intestinal organoids. We believe that these parameters can be used in the future to characterize in a stringent way the different types of mutations affecting the protein behavior. Analyzing precisely the behavior of the epithelium will provide more insights about the effects that CFTR correctors or potentiators have on the whole epithelium and can be correlated to specific symptoms found in different populations of patients. In conclusion, we demonstrate that functional assays can be developed using organoids. These proof-of-concept studies promise to pave the way to more accurate and reliable preclinical drug discovery, and will significantly lower the incredibly high amount of drugs failing at the different clinical phases.

Experimental methods

Crypts isolation: Mouse intestinal crypts were isolated from wild type and $\Delta F508$ double mutant small intestines, a kind gift from Mrs Katrine Maillard (TAAM, CNRS Orléans), following previously established protocols²². Briefly, the proximal part of the intestine was cut, opened longitudinally and washed with ice-cold PBS. The luminal side of the intestine was scraped with a glass slide to remove villi, and the intestine was cut into 4 mm pieces and washed with ice-cold PBS 5-10 times. To release the crypts, the intestinal fragments were incubated in 20 mM EDTA/PBS (20 min on ice). EDTA was removed, the fragments were resuspended in 10 ml of cold PBS was added, and shaken manually for 5 min to release the crypts into the suspension. The supernatant was collected and filtered through a 70 μ m cell strainer (BD Biosciences). The resulting crypt-enriched suspension was centrifuged at 800 rpm for 5 min. The pellet was resuspended in 10 ml cold Advanced DMEM/F12 (Invitrogen) and centrifuged at 700 rpm to remove single cells and tissue debris. The resulting pellet was enriched in crypts, which were subsequently dissociated or directly embedded in MatrigelTM (BD Biosciences; growth factor reduced, phenol red-free formulation).

Mouse intestinal stem cells culture: The isolated crypts were maintained and expanded in MatrigelTM, in self-renewal medium, ENR-CV²³. They were passaged every four days and the cultures were supplemented with growth factors every other day.

Preparation of intestinal organoids microwell arrays: LGR5::GFP intestinal organoids were released from MatrigelTM in cold basal medium (advanced DMEM/F-12 containing 1mM HEPES, GlutamaxTM and 1% P/S). The organoids were spun down at 800rpm, for 4 minutes, at 4°C and resuspended 1mL of cell dissociation solution (TrypLE, 2mg/mL DNase I, Gibco, 1mM N-acetylcysteine and 10 μ M Y27632). Cells were dissociated for 8 minutes at 37°C and subsequently washed with basal medium containing 10% foetal bovine serum (FBS, heat inactivated, Gibco). After centrifugation at 1000 rpm, for 4 minutes, at 4°C, the cells were resuspended at a density of 2.24×10^5 cells/mL in ENR-CV medium supplemented with 2.5 μ M Thiazovivin and different concentration of laminin of matrigel (see **Table 3.1**) in order to deposit 100 cells per microwell. 50 μ L of the cell suspension was added in each microwell. The cells were aggregated overnight as such and sandwiched in 300Pa non-degradable TG-PEG, containing 200 μ g/mL full length laminin (Laminin Mouse Protein, Natural, ThermoFisher Scientific) and 1mM RGD tethered to the hydrogel network²⁴. The hydrogel was left to crosslink 4h at 37°C and 5% CO₂. Finally, 750 μ L of self-renewal medium (ENR-CV) was added to each well. The aggregated mISCs were expanded in self-renewal for 2 days, and the organoids were differentiated for 4 days in differentiation medium (ENR)²³. Growth factors were replenished every other day.

Quantitative phase imaging using digital holographic microscopy (DHM) of intestinal organoids As described previously^{15,18}, DHM is an imaging technique based on interferometry. It measures the wave front phase retardation of a transmitted wave

induced by a transparent specimen, such as epithelialized organoids. We can consider that this “quantitative phase signal” or QPS depends on two parameters, the intracellular refractive index (RI) and the thickness of the observed specimen. Thus, phase shifts are highly sensitive to variation of intracellular RI. Consequently, transepithelial water fluxes, modifying the RI in the organoids lumen through a dilution or concentration process, drastically induces QPS variations¹⁵. As shown by Fig. 3, a decrease of phase will correspond to an inflow of water and an increase in phase would indicate an exit of water^{15,25-27}. The entire imaging system has been described elsewhere¹⁵. In our experimental procedure, holograms are acquired with a DHM T1000 instrument (Lyncée Tech SA, PSE-EPFL, Switzerland). A laser diode source (15683 nm) produces the coherent beam, which is divided by a beam splitter into a reference wave and an object wave. The object wave diffracted by the specimen is collected by a microscope objective and interferes with a reference beam to produce the hologram recorded by the CCD camera. In this study, holograms were acquired every fifteen second and their reconstruction was performed manually. According to Cuche et al.²⁸ and Colomb et al.²⁹ the reconstruction algorithm provides simultaneous amplitude and quantitative phase images of the cells (Koala software)^{28,29}. It is important to note that an extensive characterization of the DHM technology has been published³⁰.

Image processing and data analysis: Holograms were opened in Fiji (ImageJ). The background was subtracted using a rolling ball of 50 μm in radius. The luminal regions of interest of the organoids were selected by segmentation described in figure 5. The average intensity of the hologram was measured for each individual organoid and plotted using Prism7 software (GraphPad). The phase values were fitted to a “plateau followed by one phase decay” using the inbuilt curved fitting interface. The characteristic parameters were calculated for each organoids and statistically tested using an upaired, non-parameteric test: the Kolmogorov-Smirnov test. The following notation was used to indicate levels of significance; *: $p < 0.05$, **: $p < 0.01$, ***: $p < 0.001$.

Acknowledgements

We warmly thank Mrs Katrine Maillard from the unit of Transg n se et Archivage d’Animaux Mod les of the Centre National de la Recherche Scientifique (CNRS) in Orl ans for their kind gift of CFTR+/+, CFTR-/-, $\Delta\text{F508}/+$ and $\Delta\text{F508}/-$ mice small intestines.

REFERENCES

- 1 Zielenski, J. & Tsui, L. C. Cystic fibrosis: genotypic and phenotypic variations. *Annual review of genetics* **29**, 777-807, doi:10.1146/annurev.ge.29.120195.004021 (1995).
- 2 Welsh, M. J. & Smith, A. E. Molecular mechanisms of CFTR chloride channel dysfunction in cystic fibrosis. *Cell* **73**, 1251-1254 (1993).
- 3 Mendell, J. T. & Dietz, H. C. When the message goes awry: disease-producing mutations that influence mRNA content and performance. *Cell* **107**, 411-414 (2001).
- 4 Welch, W. J. Role of quality control pathways in human diseases involving protein misfolding. *Seminars in cell & developmental biology* **15**, 31-38, doi:10.1016/j.semcdb.2003.12.011 (2004).
- 5 Quon, B. S. & Rowe, S. M. New and emerging targeted therapies for cystic fibrosis. *Bmj* **352**, i859, doi:10.1136/bmj.i859 (2016).
- 6 Haardt, M., Benharouga, M., Lechardeur, D., Kartner, N. & Lukacs, G. L. C-terminal truncations destabilize the cystic fibrosis transmembrane conductance regulator without impairing its biogenesis. A novel class of mutation. *The Journal of biological chemistry* **274**, 21873-21877 (1999).
- 7 Castellani, C. *et al.* Consensus on the use and interpretation of cystic fibrosis mutation analysis in clinical practice. *Journal of cystic fibrosis : official journal of the European Cystic Fibrosis Society* **7**, 179-196, doi:10.1016/j.jcf.2008.03.009 (2008).
- 8 Van Goor, F. *et al.* Rescue of CF airway epithelial cell function in vitro by a CFTR potentiator, VX-770. *Proceedings of the National Academy of Sciences of the United States of America* **106**, 18825-18830, doi:10.1073/pnas.0904709106 (2009).
- 9 Van Goor, F. *et al.* Correction of the F508del-CFTR protein processing defect in vitro by the investigational drug VX-809. *Proceedings of the National Academy of Sciences of the United States of America* **108**, 18843-18848, doi:10.1073/pnas.1105787108 (2011).
- 10 Galletta, L. V., Jayaraman, S. & Verkman, A. S. Cell-based assay for high-throughput quantitative screening of CFTR chloride transport agonists. *American journal of physiology. Cell physiology* **281**, C1734-1742 (2001).
- 11 Van Goor, F. *et al.* Rescue of DeltaF508-CFTR trafficking and gating in human cystic fibrosis airway primary cultures by small molecules. *American journal of physiology. Lung cellular and molecular physiology* **290**, L1117-1130, doi:10.1152/ajplung.00169.2005 (2006).
- 12 De Lisle, R. C. & Borowitz, D. The cystic fibrosis intestine. *Cold Spring Harbor perspectives in medicine* **3**, a009753, doi:10.1101/cshperspect.a009753 (2013).
- 13 Kalin, N., Claass, A., Sommer, M., Puchelle, E. & Tummeler, B. DeltaF508 CFTR protein expression in tissues from patients with cystic fibrosis. *The Journal of clinical investigation* **103**, 1379-1389, doi:10.1172/JCI5731 (1999).
- 14 Frizzell, R. A. & Hanrahan, J. W. Physiology of epithelial chloride and fluid secretion. *Cold Spring Harbor perspectives in medicine* **2**, a009563, doi:10.1101/cshperspect.a009563 (2012).

- 15 Rappaz, B. *et al.* Measurement of the integral refractive index and dynamic cell morphometry of living cells with digital holographic microscopy. *Optics express* **13**, 9361-9373 (2005).
- 16 Rappaz, B. & Wiseman, P. W. Image correlation spectroscopy for measurements of particle densities and colocalization. *Current protocols in cell biology / editorial board, Juan S. Bonifacino ... [et al.] Chapter 4*, Unit 4 27 21-15, doi:10.1002/0471143030.cb0427s59 (2013).
- 17 Kuhn, J. *et al.* Label-free cytotoxicity screening assay by digital holographic microscopy. *Assay and drug development technologies* **11**, 101-107, doi:10.1089/adt.2012.476 (2013).
- 18 Jourdain, P. *et al.* The human CFTR protein expressed in CHO cells activates aquaporin-3 in a cAMP-dependent pathway: study by digital holographic microscopy. *Journal of cell science* **127**, 546-556, doi:10.1242/jcs.133629 (2014).
- 19 Dekkers, J. F. *et al.* A functional CFTR assay using primary cystic fibrosis intestinal organoids. *Nature medicine* **19**, 939-945, doi:10.1038/nm.3201 (2013).
- 20 Dekkers, J. F. *et al.* Characterizing responses to CFTR-modulating drugs using rectal organoids derived from subjects with cystic fibrosis. *Science translational medicine* **8**, 344ra384, doi:10.1126/scitranslmed.aad8278 (2016).
- 21 Moran, O. & Zegarra-Moran, O. On the measurement of the functional properties of the CFTR. *Journal of cystic fibrosis : official journal of the European Cystic Fibrosis Society* **7**, 483-494, doi:10.1016/j.jcf.2008.05.003 (2008).
- 22 Wang, F. *et al.* Isolation and characterization of intestinal stem cells based on surface marker combinations and colony-formation assay. *Gastroenterology* **145**, 383-395 e381-321, doi:10.1053/j.gastro.2013.04.050 (2013).
- 23 Yin, X. *et al.* Niche-independent high-purity cultures of Lgr5+ intestinal stem cells and their progeny. *Nature methods* **11**, 106-112, doi:10.1038/nmeth.2737 (2014).
- 24 Ehrbar, M. *et al.* Elucidating the role of matrix stiffness in 3D cell migration and remodeling. *Biophysical journal* **100**, 284-293, doi:10.1016/j.bpj.2010.11.082 (2011).
- 25 Pavillon, N. *et al.* Cell morphology and intracellular ionic homeostasis explored with a multimodal approach combining epifluorescence and digital holographic microscopy. *Journal of biophotonics* **3**, 432-436, doi:10.1002/jbio.201000018 (2010).
- 26 Jourdain, P. *et al.* Determination of transmembrane water fluxes in neurons elicited by glutamate ionotropic receptors and by the cotransporters KCC2 and NKCC1: a digital holographic microscopy study. *The Journal of neuroscience : the official journal of the Society for Neuroscience* **31**, 11846-11854, doi:10.1523/JNEUROSCI.0286-11.2011 (2011).
- 27 Jourdain, P. *et al.* Simultaneous optical recording in multiple cells by digital holographic microscopy of chloride current associated to activation of the ligand-gated chloride channel GABA(A) receptor. *PloS one* **7**, e51041, doi:10.1371/journal.pone.0051041 (2012).

- 28 CuChe, E., Marquet, P. & Depeursinge, C. Simultaneous amplitude-contrast and quantitative phase-contrast microscopy by numerical reconstruction of Fresnel off-axis holograms. *Applied optics* **38**, 6994-7001 (1999).
- 29 Colomb, T. *et al.* Numerical parametric lens for shifting, magnification, and complete aberration compensation in digital holographic microscopy. *Journal of the Optical Society of America. A, Optics, image science, and vision* **23**, 3177-3190 (2006).
- 30 Rappaz, B. *et al.* Comparative study of human erythrocytes by digital holographic microscopy, confocal microscopy, and impedance volume analyzer. *Cytometry. Part A : the journal of the International Society for Analytical Cytology* **73**, 895-903, doi:10.1002/cyto.a.20605 (2008).

CHAPTER V

DISCUSSION AND OUTLOOK

In the presented work, we established two technologies that offer unprecedented control to direct stem cell fate in three-dimensional *in vitro* microenvironments. Over the past decade, we observed the advent of various stem cell-derived organoid cultures that are able to recapitulate key organ functions in a near-physiological fashion. Such cultures are hyped to play a central role in the development of biologically accurate *in vitro* tissue models. Yet, as these cultures continue to be discovered for more tissues and organs of the body, one question seems to persist: How are we able to better control their generation and development to create more complex functions *in vitro* reproducibly?

Up until now, bioengineering approaches were mainly used to create engineered cell compatible scaffolds from natural and/or synthetic polymers to support cell survival and growth, as well as to systematically influence or direct cell behavior *in vitro*¹⁻⁴. However, such engineered matrices only provide cells with static and homogenous cues that are very often not representative to the dynamic environments cells are exposed to *in vivo*. To overcome this limitation, microfabricated devices that are compatible with the growth of some cell types, mostly immortalized cell lines, have shown the capability to deliver dynamic signals to two-dimensional monolayers of cells using microengineered gradients.

Recently, a major change in paradigm emerged through the discovery of stem cell-derived organoid cultures. Conventionally, stem cell scientists aimed at discovering different stem cell populations, characterizing them thoroughly and trying in vain to maintain and selectively multiply them *in vitro* without loss of their potency. Identifying that putting certain types of stem cells in a three-dimensional conformation enables them to proliferate, generate their niche and differentiate into all of the tissue-specific cell types opened exciting doors to fabricate pertinent tissues in a dish. These structures are highly dynamic and self-organize with remarkable *in vivo*-like accuracy. Yet while they can be maintained *in vitro* for extended periods of time, specific morphogenetic events correlating with embryonic development are inexact, desynchronized or altogether missing. Thus, the current bioengineering approaches have to be profoundly revisited to better assist and guide organoid development *in vitro*.

Both adult and pluripotent stem cells have been shown to grow and differentiate into organoids only when kept in a three-dimensional architecture and put in contact with varying amounts of extracellular matrix signaling. The extracellular matrix signaling in the current protocols is usually Matrigel, a reconstituted basement membrane extracted from a mouse sarcoma with high degrees of variability and uncharacterized growth factors. The reasons for the inherent variability of organoid cultures could therefore be exposure to this cocktail of largely unknown growth factors with unknown effects on the culture and the absence of spatio-temporal control of exposure to relevant growth factors. Hence, exposing a developing organoid to local and spatio-temporal signals must be performed in substrates that are defined but also compatible with the maturation of the organoid. To address this challenge, we developed a new technology that enables the fabrication of microfluidic networks in hydrogel materials with previously unattainable ease. Conventional tissue engineering uses hydrogel micromolding with either negative molds or sacrificial layers to create flow-permissive cavities in hydrogel substrates⁵⁻⁷.

However, these methods are too variable and labor intensive for routine use. Moreover, the range of material properties that can be utilized is limited and usually far from the properties needed to support organoid growth. Thus, we developed a technology based on laser micromachining to fabricate microfluidic networks in hydrogel substrates with ultra high precision. With short-pulsed lasers, extremely intricate microfluidic networks can be generated. Moreover, this approach permits the fabrication of three-dimensional microfluidics very easily. In addition to solving a major limitation found with conventional soft-lithography techniques, it is the first time that complex and stable three-dimensional microfluidics are shown within soft polymer substrate such as hydrogels. We also demonstrate that the initial network can be adapted over the period of the culture to follow and guide cellular growth and differentiation. Human placenta-derived mesenchymal stem cells (hMSC) were grown in a three-dimensional migration-permissive microenvironment and a laser-microfabricated channel was created in a selected region of the culture. When perfused with chemoattractants, the MSCs located close to the source migrated in its direction whereas the cells further away maintained their initial position. Also, we rendered this method suitable for the fabrication of vasculature-like constructs, when growing human umbilical vein endothelial cells (hUVECs) at the surface of 50 micrometer wide and 100 micrometer high collagen microchannels.

Our novel microfabrication approach offers unique features for the fast and easy fabrication of 3D microfluidic networks, and our method is adaptable to trigger and control specific morphogenetic events with precise spatial and temporal control in cultures of interest.

More elaborate organoid models derived from pluripotent stem cells, such as retinal, brain and inner ear organoids, do not require a mechanically sound three-dimensional matrix to grow and self-organize into specific tissues. However, these organoid cultures are nonetheless highly disorganized, uncontrolled and unreproducible⁸. In order to address this exciting challenge, we developed a novel microstructured high-throughput cell aggregation platform. When compared to previously described platforms^{9,10}, our arrays, composed of U-shaped microwells, display an extraordinary high level of versatility. Microwells of any size starting from ten micrometers to three millimeters in diameter can be imprinted onto any type of biocompatible polymer, such as naturally derived or synthetic hydrogels. Moreover, any shape of cavity can be imprinted with extremely high precision and reproducibility. Our arrays can be fabricated in substrates with physiological stiffness ranges between 150 Pa and 30 kPa (in average shear modulus, G'), allowing to fine-tune mechanical cues that are known to influence stem cell function¹¹. More importantly, when the microwell arrays are imprinted into synthetic polyethylene glycol substrates, the bottom of the microwells can be decorated with specific proteins tethered to the matrix due to the versatility of the substrate chemistry. In addition to this, they can be overlaid with a second layer of crosslinked hydrogel to create three-dimensional single or aggregated cell cultures within a single focal plane, allowing high-speed imaging of three-dimensional encapsulated cell cultures.

Cellular aggregates formed in our microwell arrays are significantly more monodisperse, homogenous and spherical than aggregates formed in conventional

96 U-bottom well plates or on Aggrewell™ surfaces. Also, single or very low numbers of cells can be grown in our microwells thanks to the high cell compatibility of our synthetic substrates. Finally, our approach showed that numerous cell types could be grown in a spherical architecture, including non-sphere forming cells types, such as the human breast cancer malignant cell line; MDA-MB231.

More importantly, growing complex organoid models demonstrated the power of our platform. Using 1.5 millimeter PEG milliwells, we could grow retinal organoids. There were multiple advantages of this system. First, the combination of controlled substrate stiffness together with defined soluble cues was critical to grow and improve the differentiation of retinal organoids. Optimized parameters synergistically improved the number of organoids differentiating towards cones and rods lineage from 60% using the conventional protocol to 90% using a stiff PEG hydrogel together with a neuro-lineage-specific supplemented medium. The retinas formed in our microwells differentiated towards the specific cell types of an *in vivo* developing retina, as demonstrated by histological sections and immunohistochemistry.

Finally, this platform is also adaptable to adult stem cell-derived organoids, such as intestinal organoids that are typically grown from single intestinal stem cells in Matrigel^{12,13}. These cultures suffer from myriad problems including the intrinsic variability of Matrigel and resulting heterogeneity within the same compartment, which make these cultures inconvenient for drug screening or for their use in the clinics. Most recently, it has been demonstrated that a single intestinal stem cell can generate intestinal organoids in synthetic PEG-based hydrogels (Gjorevski et al., Nature, accepted). Notably, the authors show that a dynamic matrix that softens over the course of the culture is needed as intestinal stem cells expand best in stiff microenvironments and intestinal colonies differentiate and undergo morphogenesis best in soft microenvironments.

Using our microwell platform to aggregate a small number of dissociated single intestinal stem cells, we demonstrate that a subsequent overlay with a non-dynamic soft matrix is sufficient to generate a homogenous population of intestinal organoids. These results illustrate that single intestinal stem cell expansion can be bypassed and organoids can be grown within six days directly from a small population of stem cells. In addition, the confinement given by the microwells facilitated tight control over and homogenization of the size of such organoid cultures. Finally, all the organoids are present in a single focal plane, which provides a major advantage for image-based read-outs.

However, we could see that even though the size of the organoids was nicely homogenous, the control of their budding was not possible using a large compartment of 500 μm in diameter. As any shape can be imprinted on our hydrogel surfaces, we could imagine imprinting shapes that resemble the final shape of intestinal organoids, for example with lateral extrusions of predetermined dimensions so the organoids crypts or buds can be deterministically placed with respect to the main organoid body.

In the last part of this work, we studied different methods to read out transepithelial membrane fluxes in 3D cultures. Intestinal organoids have been shown to be a relevant *in vitro* disease model for cystic fibrosis, a CFTR transmembrane transporter-related disease. So far, the only described method to analyze differential swelling behaviors between wild type and diseased organoids is based on changes in area^{14,15}. Tracking surface area assumes that the planar modifications are identical to height changes. As a result, the changes in surface area follow a linear function and do not represent accurately the dynamics of transmembrane fluxes. In order to extract behavioral changes of intestinal organoids with higher precision and definition, we studied an interferometry-based method that can measure the local density of any sample. When tracking the local density within the lumen of the organoids, we could extract key measures that represent the exact behavior of the transepithelial flux. Using this method, parameters such as the time to initiation of swelling, the dilution factor within the organoid lumen and the fluid uptake rate can be measured precisely. More importantly, these values are significantly different between wild type and $\Delta F508$ double mutant organoids. On the one hand, these parameters accurately represent changes in the three dimensions compared with analyzing changes solely in surface area. On the other hand, these macro-scale measures can be correlated to the native behavior of transmembrane transporters. We expect that, by precisely analyzing this set of parameters and normalizing them with the number of, for example, CFTR proteins present in a particular organoid population, even subtle changes can be observed between specific classes of mutations, allowing us to gain valuable information regarding the actions of pharmacological compounds on the mutated proteins.

Giving organoids directions

Based on our study, we could observe that despite improving the reproducibility of organoid cultures, significant variability still remains. For example, growth and differentiation of mouse retinal organoids were improved, but optic vesicles are still appearing stochastically from the surface of the neuroepithelium. We strongly believe that the induction of these morphogenetic events is driven by morphogen gradients that, for now, randomly establish over portions of the neuroepithelium. Our U-shaped microwell technology enabled the optimal growth and differentiation of these large retinal organoids within hydrogel substrates. Since hydrogel matrices are aqueous, any biomolecule, from small compounds to larger proteins, can diffuse freely within these matrices. Thus, our technology now allows us to generate morphogen gradients over these developing structures with ease. By interfacing hydrogel microfluidics and U-shaped microwells, we can locally deliver molecular effectors to guide the induction of optic vesicles and further the self-organization of optic cups into retinal organoids (see **Figure 1**).

Using this innovative type of gradient generator, we expect that major morphogenetic events involved in organoid development can be controlled and can appear deterministically. This format of gradient is of particular interest for induced pluripotent stem cells-derived organoids such as retina, brain and inner ear.

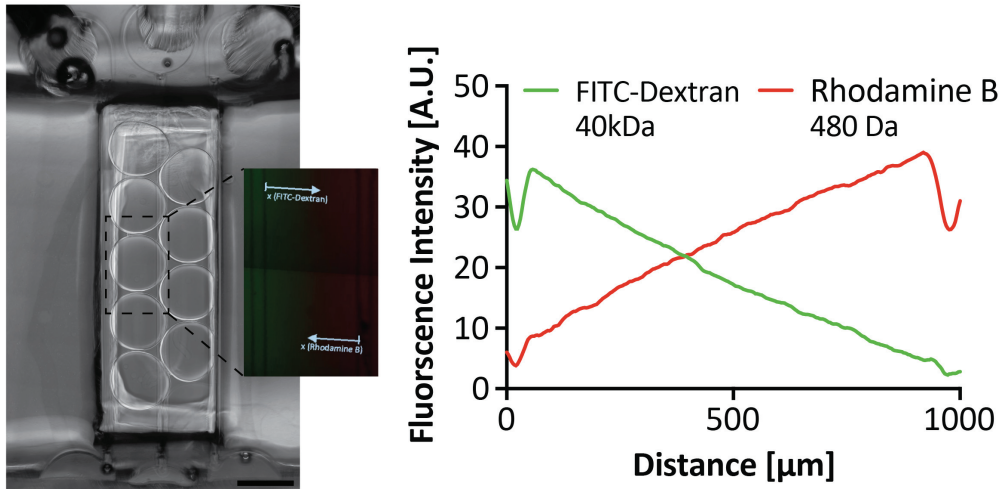


Figure 1: *left.* Brightfield image of 1.5 millimeters U-shaped microwells interfaced with microfluidic networks. When fluorescent model molecules, such as FITC-Dextran (40kDa) and Rhodamine B (480 Da) are actively perfused through the microfluidic network, the molecules equilibrate and form linear gradients over the microwells after about 8 hours. *Right.* Quantification of the equilibrated gradients. We could observe that the gradients are linear and that in both cases the fold difference between the sink and the source is about 8 folds. Scale bar: 1.5 mm.

In addition, the combination of laser-fabricated microfluidics together with U-shaped microwell arrays will become key for improving the throughput of drug screening using organoids. In the current format, the number of different conditions is limited to the number of wells of a 96-well microtiter plate. The integration of a microfluidic network beneath the array of microcavities could enable only a given population within the array to be influenced or establish concentration gradients of drugs over a specific field of organoids (see **Figure 2**).

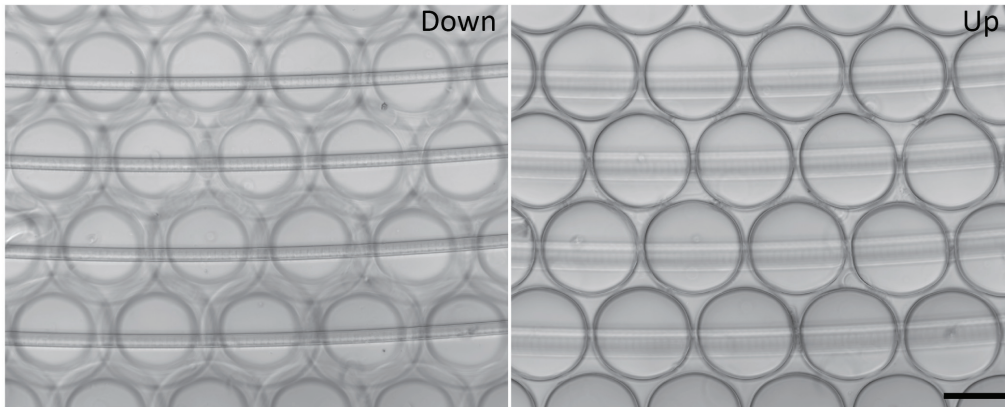


Figure 2: Brightfield microscopy image of U-shaped microwells of 500 μm in diameter interface with a microfluidic network beneath the bottom of the microwells. *Left.* The focal plane of the microfluidic network. *Right.* The focal plane of the microwells. Scale bar: 500 μm .

We expect this approach to improve the throughput of organoid-based drug screening as well as decrease the total amount of drugs used, especially with regard to the drug prices for some cystic fibrosis medications such as Orkambi, which costs \$258,000 per patient per year¹⁶.

Finally, we strongly believe that by growing organoids within cavities of defined geometry, organogenesis can be controlled precisely. Indeed, as shown by Gjorevski et al., asymmetric cell constructs are exposed to asymmetric signals in terms of soluble and mechanical cues^{17,18}. Thus, in order to deterministically control morphogenesis of organoid development, specific microcavities can be engineered to exert asymmetric signaling on developing stem cell constructs.

The future will be about “piloting” self-organization and “organoids-on-a-chip”

With the presented technologies, we can now miniaturize culture compartments and provide flow and dynamic signals to organoid compatible materials. We expect these approaches to enable the generation of a new kind of organoid, where we can pilot self-organization by topography and by delivering signaling molecules in a locally and temporally controlled fashion. Finally, the integration of these guided organoids within microdevices will give rise to a new era where organoids and specific tissues formed from stem cells can grow in a fully controlled microenvironment with precision approaching that of developing and self-renewing tissues.

References

- 1 Ehrbar, M. *et al.* Elucidating the role of matrix stiffness in 3D cell migration and remodeling. *Biophysical journal* **100**, 284-293, doi:10.1016/j.bpj.2010.11.082 (2011).
- 2 Ehrbar, M. *et al.* Enzymatic formation of modular cell-instructive fibrin analogs for tissue engineering. *Biomaterials* **28**, 3856-3866, doi:10.1016/j.biomaterials.2007.03.027 (2007).
- 3 Ehrbar, M. *et al.* Biomolecular hydrogels formed and degraded via site-specific enzymatic reactions. *Biomacromolecules* **8**, 3000-3007, doi:10.1021/bm070228f (2007).
- 4 Ranga, A. *et al.* 3D niche microarrays for systems-level analyses of cell fate. *Nature communications* **5**, 4324, doi:10.1038/ncomms5324 (2014).
- 5 Choi, N. W. *et al.* Microfluidic scaffolds for tissue engineering. *Nature materials* **6**, 908-915, doi:10.1038/nmat2022 (2007).
- 6 Morgan, J. P. *et al.* Formation of microvascular networks in vitro. *Nature protocols* **8**, 1820-1836, doi:10.1038/nprot.2013.110 (2013).
- 7 Miller, J. S. *et al.* Rapid casting of patterned vascular networks for perfusable engineered three-dimensional tissues. *Nature materials* **11**, 768-774, doi:10.1038/nmat3357 (2012).
- 8 Fatehullah, A., Tan, S. H. & Barker, N. Organoids as an in vitro model of human development and disease. *Nature cell biology* **18**, 246-254, doi:10.1038/ncb3312 (2016).
- 9 Ungrin, M. D., Joshi, C., Nica, A., Bauwens, C. & Zandstra, P. W. Reproducible, ultra high-throughput formation of multicellular organization from single cell suspension-derived human embryonic stem cell aggregates. *PloS one* **3**, e1565, doi:10.1371/journal.pone.0001565 (2008).
- 10 Vrij, E. J. *et al.* 3D high throughput screening and profiling of embryoid bodies in thermoformed microwell plates. *Lab on a chip* **16**, 734-742, doi:10.1039/c5lc01499a (2016).
- 11 Engler, A. J., Sen, S., Sweeney, H. L. & Discher, D. E. Matrix elasticity directs stem cell lineage specification. *Cell* **126**, 677-689, doi:10.1016/j.cell.2006.06.044 (2006).
- 12 Sato, T. *et al.* Single Lgr5 stem cells build crypt-villus structures in vitro without a mesenchymal niche. *Nature* **459**, 262-265, doi:10.1038/nature07935 (2009).
- 13 Sato, T. & Clevers, H. Growing self-organizing mini-guts from a single intestinal stem cell: mechanism and applications. *Science* **340**, 1190-1194, doi:10.1126/science.1234852 (2013).
- 14 Dekkers, J. F. *et al.* A functional CFTR assay using primary cystic fibrosis intestinal organoids. *Nature medicine* **19**, 939-945, doi:10.1038/nm.3201 (2013).
- 15 Dekkers, J. F. *et al.* Characterizing responses to CFTR-modulating drugs using rectal organoids derived from subjects with cystic fibrosis. *Science translational medicine* **8**, 344ra384, doi:10.1126/scitranslmed.aad8278 (2016).

- 16 Ferkol, T. & Quinton, P. Precision Medicine: At What Price? *American journal of respiratory and critical care medicine* **192**, 658-659, doi:10.1164/rccm.201507-1428ED (2015).
- 17 Gjorevski, N. & Nelson, C. M. The mechanics of development: Models and methods for tissue morphogenesis. *Birth defects research. Part C, Embryo today : reviews* **90**, 193-202, doi:10.1002/bdrc.20185 (2010).
- 18 Gjorevski, N., Piotrowski, A. S., Varner, V. D. & Nelson, C. M. Dynamic tensile forces drive collective cell migration through three-dimensional extracellular matrices. *Scientific reports* **5**, 11458, doi:10.1038/srep11458 (2015).

APPENDIX A

SUPPORTING INFORMATION FOR CHAPTER II: IN SITU PATTERNING OF MICROFLUIDIC NETWORKS IN 3D CELL-LADEN HYDROGELS

Supporting Figures:

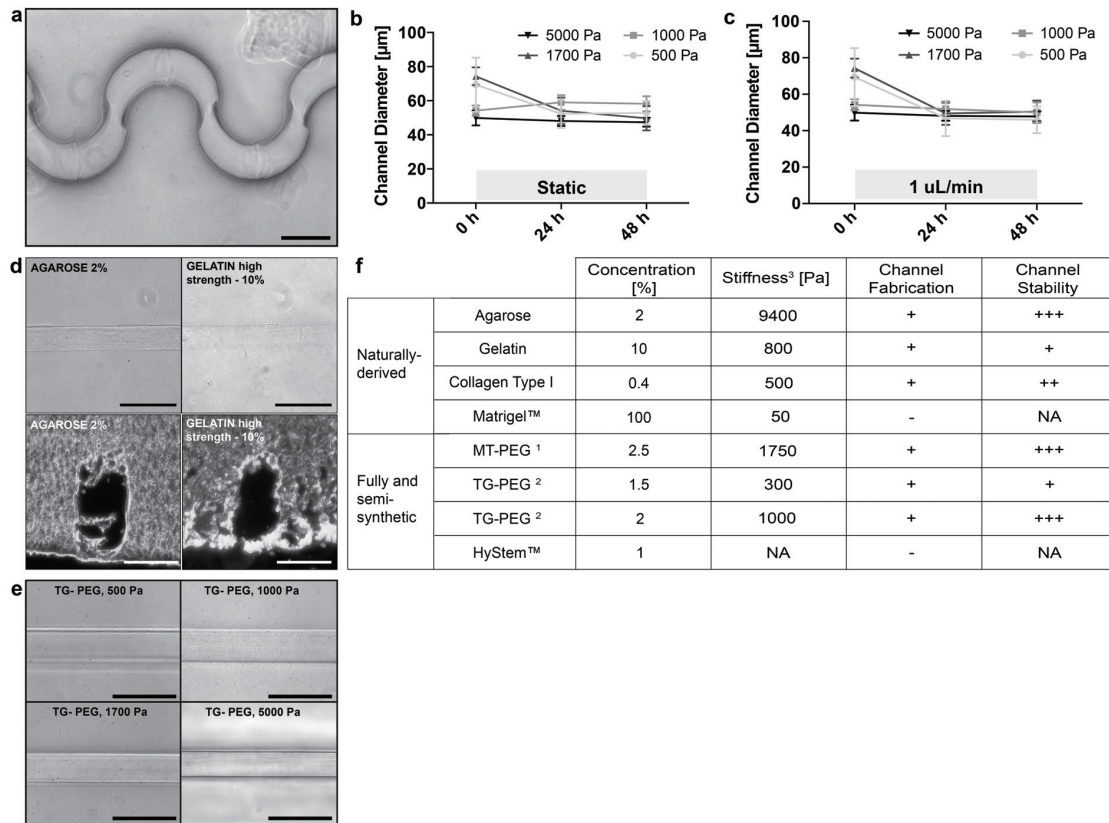


Figure S1: Characterization of laser-based generation of microfluidic channels. a) Undulating microfluidic channel. b, c) Dimensional stability of channels over 48 hours. The diameter of the fabricated structures was measured everyday for 48 hours without (b) or with (c) flow. Right after fabrication, the hollow structures tend to be slightly bigger but after relaxation and equilibration the channels are stable. d) Representative bright-field microscopy images of fabricated channels within agarose and high-strength gelatin gels. The lower panels show histology cryosections of microchannels fabricated in agarose and gelatin gels. e) Representative bright-field microscopy images of fabricated channels within FXIIIa-crosslinked PEG gels ('TG-PEG') of different stiffness (500, 1000, 1700, and 5000 Pa). f) Representative hydrogels that can be microfabricated via direct laser lithography. Qualitative assessment of channel stability in the different hydrogel types. ¹PEG hydrogels crosslinked via Michael-type addition ('MT-gels'), see ref. 17. ²PEG hydrogels crosslinked via transglutaminase FXIIIa ('TG-gels'), see ref. 18. ³Average shear modulus (G'), $n=3$ measurements. NA: Non-analysed. Scale bars: 100 μm .

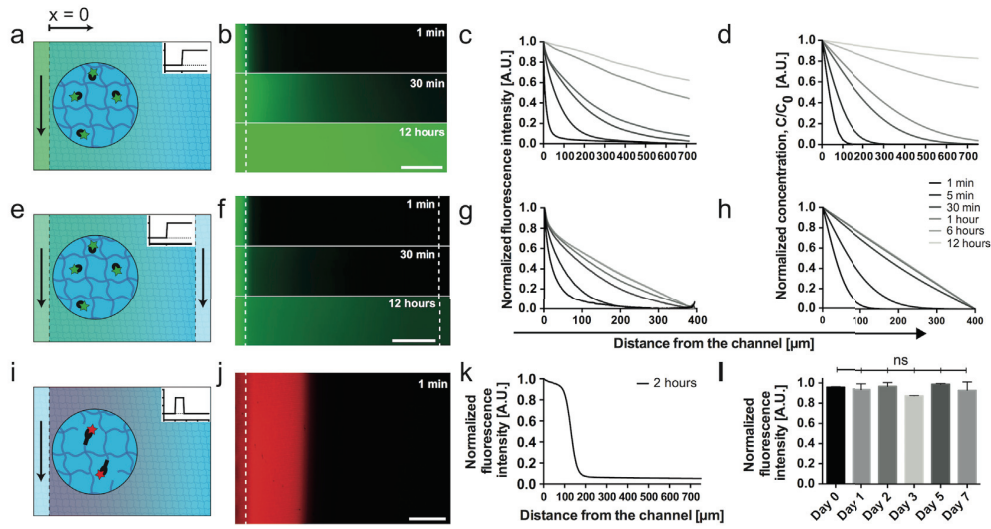


Figure S2: Characterization of mass transport. a) Schematic representation of a single source model. b) Representative fluorescent images of 70kDa FITC-dextran diffusion over time in PEG-based hydrogels (MT-PEG). The dashed line corresponds to the edge of the ablated microchannel. c) Single source model-based analysis of the diffusion profile. The effective diffusion coefficient (D_{eff}) estimated from curve fitting is $1.78 \times 10^{-7} \text{ cm}^2/\text{s}$. d) Theoretical diffusion profile obtained by a finite element solver software and D_{eff} . e) Schematic representation of a source-sink model. f) Representative fluorescent images of 70kDa FITC-dextran diffusion over time in MT-PEG gels in the sink-source configuration. g, f) Analysed (g) and modelled (h) diffusion profiles. The dashed line corresponds to the edge of the ablated microchannel. i) Schematic representation of a gradient system based on tethered biomolecules. j) Representative fluorescent images of reactive red fluorescent molecules diffusion over two hours in synthetic PEG hydrogels. The dashed line corresponds to the edge of the ablated microchannel. k) Intensity profile of tethered biomolecular gradient obtained after thorough washing of the non-specifically bound molecules. l) Stability of the tethered gradient over seven days ($n=3$). Scale bars: 100 μm .

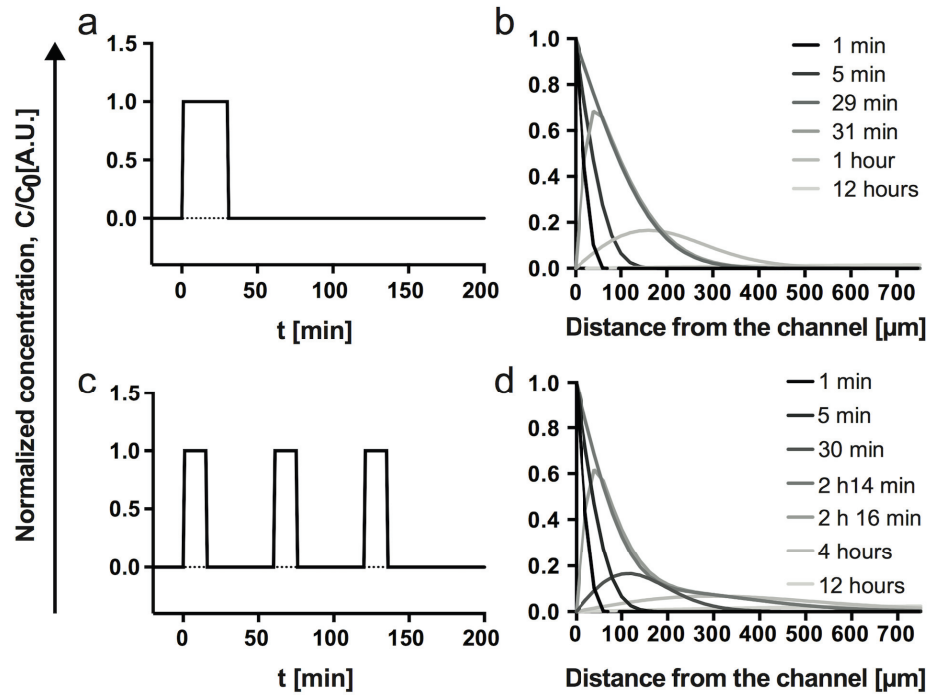


Figure S3: Mathematical modelling of the concentration variation within the hydrogel phase using pulsed biomolecule perfusion patterns. a) Single concentration pulse model. b) Resulting concentration profile in the hydrogel as a function of distance from the microchannel. c) Serial concentration pulses model. d) Resulting concentration profile in the hydrogel as a function of distance from the microchannel.

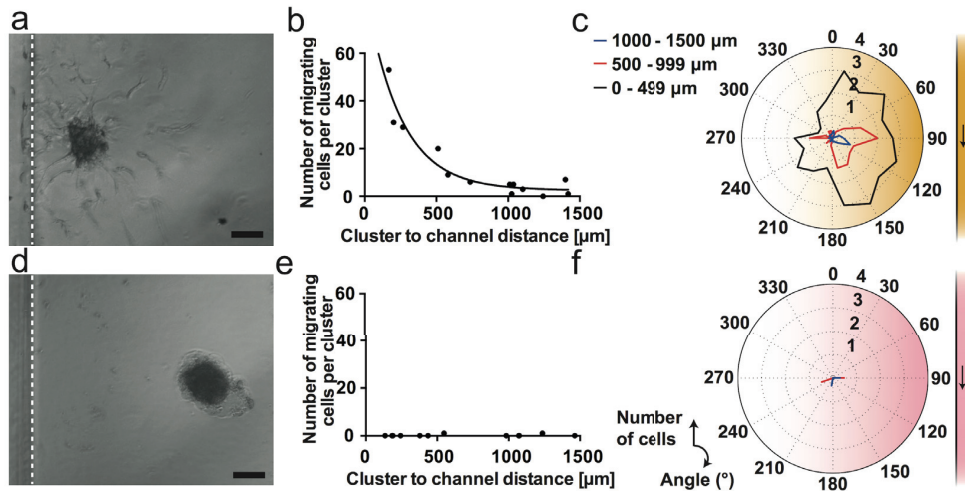


Figure S4: Microtissue-based 3D MSC chemotaxis model. a,d) Pre-starved hMSCs aggregates were exposed to PDGF gradients following a perfusion pattern based on a mathematical model and then tracked for 20 hours using time-lapse microscopy. The number of migrating cells away from the cluster and their directionality was quantified. b,e) Cells from the clusters located within 400 μm of the source were found to be significantly activated by PDGF exposure (b), in contrast to the control condition (e). c,f) Cells tended to migrate towards the source when activated (c), in contrast to the control condition (f).

Supporting Methods:

Fabrication of poly(dimethylsiloxane) (PDMS) mounts: PDMS mounts having a hydrogel chamber and connecting channels to the inlets and outlets of the device were fabricated as follows: SU-8 patterned silicon wafers were fabricated by standard lithography techniques, PDMS (ratio 1:10, SYLGARD® 184 SILICONE ELASTOMER KIT, Dow Corning) was poured on the wafer and incubated overnight at 75°C. After crosslinking, PDMS was de-moulded, the hydrogel chamber was cut manually, the inlets and outlets holes were punched with a 1.5mm puncher, and the resulting PDMS mounts were covalently bonded to glass coverslips using oxygen plasma.

Characterization of diffusion properties: To model the diffusion of molecules through PEG hydrogels from laser-ablated microchannels, two computational models (*i.e.* single source and a source-sink) were designed using COMSOL (COMSOL Multiphysics®). In these models we defined the system as the hydrogel, considered a steady-state flow within the microfluidic network and assumed that diffusive transport was outweighing convection in the hydrogel phase. Also, due to the high Peclet number in the microfluidic channel ($Pe \simeq 6500$), we assumed that convection outweighs diffusion in the aqueous phase into the channel. This assumption allows us to define that the molecule concentration at the channel surface is constant over time (Fig. S2a). Thus, the general mass transport equation can be simplified as

$$\frac{\partial c}{\partial t} = \nabla \cdot D \nabla c \quad (1)$$

which in our case, by taking advantage of the symmetry of the model, can be simplified to the analytical solution of a one dimensional problem, as follows:

$$\frac{c(x, t) - c_0}{c_s - c_0} = 1 - \operatorname{erf} \left(\frac{x}{2\sqrt{D_{\text{eff}} t}} \right) \quad (2)$$

where c is defined as the concentration of the molecule of interest, x , the distance from the source, the channel in our case, D_{eff} , is the effective diffusion coefficient through the hydrogel network¹ and t the time.

Diffusion was measured *in vitro* using both MT-PEG and TG-PEG at 2.5% polymer content. A 6 mM solution of fluorescein isothiocyanate (FITC)-labelled dextran (70 kDa, Sigma, cat. no. 46945-100MG-F) was perfused for 12 hours through a linear microfluidic channel in a single source and a source-sink fashion at 37°C, 5% CO₂. The fluorescent intensity through the gel was imaged for 12 hours using time-lapse microscopy. The first two hours were imaged with a time interval of one minute and the subsequent 10 hours with 15 minutes time intervals. The gradient generation was analysed with ImageJ. The intensity curves were fitted using Igor

Pro™ (Igor Pro™, Wavemetrics, USA) and the effective diffusion coefficient was calculated for FITC-Dextran in all conditions.

To establish a gradient of tethered molecules, Alexa-546 maleimide (Life Technologies, cat. no. A-10258) was perfused through the laser-etched microfluidic networks in MT-PEG hydrogels for two hours at 37°C, 5% CO₂. After two hours, the gel was thoroughly washed with PBS and imaged using a wide-field fluorescent microscope. Images were taken every 24 hours for seven days, and the overall gradient intensity for individual repeats was quantified.

Cell culture: C2C12 mouse myoblasts were maintained in Dulbecco's Modified Eagle Medium GlutaMAX™ medium (DMEM, high glucose, GlutaMAX™ Supplement, Gibco Life Technologies, cat. no. 10566-016) supplemented with 10% v/v FBS (fetal bovine serum, Life Technologies, cat. no. 10500064), 0.2 % penicillin/streptomycin solution (Gibco Life Technologies, cat. no. 15140-122), and 1 mM Sodium Pyruvate (Gibco Life Technologies, cat. no. 11360-070).

Human umbilical vein endothelial cells (HUVEC) were maintained in M199 GlutaMAX™ medium (Medium 199, GlutaMAX™ Supplement, Gibco Life Technologies, cat. no. 22571-020) supplemented with 10% v/v fetal calf serum (HyClone Cosmic Calf Serum, GE Healthcare Life Sciences, cat. no. SH30087.03), 1.3% v/v bovine brain extract (Lonza, cat. no. CC-4098), 10µg/mL hydrocortisone (Sigma, cat. no. H-0888), 100 ng/mL EGF (Peprotech, cat. no. 100-15) and 250 U/mL Heparin (Sigma, cat. no. H3149). For the vascularization experiments, HUVEC were cultured with the above medium and used between passages 2 and 7.

Primary human placenta-derived mesenchymal stem/progenitor cells (termed MSC) were maintained in Dulbecco's Modified Eagle Medium GlutaMAX™ medium (DMEM, high glucose, GlutaMAX™ Supplement, Gibco Life Technologies, cat. no. 10566-016) supplemented with 10% v/v fetal calf serum (HyClone Cosmic Calf Serum, GE Healthcare Life Sciences, cat. no. SH30087.03), 0.2% penicillin/streptomycin solution (Gibco Life Technologies, cat. no. 15140-122), 10 mM HEPES (Gibco Life Technologies, cat. no. 15630-056) and 1 mM Sodium Pyruvate (Gibco Life Technologies, cat. no. 11360-070). For the 3D chemotaxis assays, MSCs were cultured in serum-free conditions and used between passages 4 and 10.

MSC aggregate formation: MSCs were detached and re-suspended at specific densities (final concentration: 13'000 cells mL⁻¹, i.e. 400 cells per aggregates) in serum-free medium supplemented with 0.2% w/v methyl-cellulose (Sigma-Aldrich, cat. no. M0512). MSC aggregates were formed using hanging drops of 30µL volume. The drops were flipped and incubated overnight at 37°C, 5% CO₂.

Cell viability assay: C2C12 cells were encapsulated in TG-PEG hydrogels (2% w/v), supplemented with 50 mM of covalently attached RGD ligands²⁻⁴. After encapsulation, linear microfluidic channels were produced within the cell-laden hydrogel and cell viability was assessed one hour after fabrication. Samples were washed thoroughly with PBS and a solution of calcein AM and ethidium homodimer-

1 (EthD-1) (Life Technologies) in PBS was added to the sample following to the manufacturer's protocol. Samples were incubated 45 minutes at room temperature on an orbital shaker and cell viability was assessed by fluorescence microscopy. Cell-containing hydrogels with and without microfluidics, as well as standard 3D cultures were scanned and the cells were counted using the MTrackJ plugin of ImageJ.

Encapsulation of randomly distributed single cells and cell aggregates in PEG hydrogels: MSCs were detached according to standard protocols and MSCs clusters were harvested using a pipet tip to avoid perturbation of the cluster due to shear stress. Cell solutions or aggregates were re-suspended at the appropriate density to obtain final concentrations of 2×10^5 cell/mL or 400 clusters/mL, respectively, in the hydrogels. Cell solutions or cell clusters were then added to the gel precursor solution before addition of FXIIIa to induce crosslinking²⁻⁴. The final mix was then pipetted into the PDMS chamber. The chips were rotated gently to avoid sedimentation until initiation of crosslinking. The constructs were incubated for 30 minutes at 37°C, 5% CO₂, and appropriate media were added onto the hydrogel as well as in the inlet and outlet of the PDMS mount. Microfluidic channels were photo-ablated into cell-containing hydrogels to allow the localized delivery of growth factors during cell culture.

3D MSC invasion assays: Single, dispersed MSCs and MSC aggregates were embedded in MMP-sensitive TG-PEG hydrogels (2% w/v) supplemented with 50 mM of covalently bound RGD peptides⁴. After encapsulation, the cells were incubated for one hour and microfluidic networks were fabricated by laser ablation. In case of single MSCs, platelet-derived growth factor (PDGF-BB, Preprotech, cat. no. 100-14B-10ug) was perfused for 30 minutes and then washed away as schematically shown in Supplementary Figure S3a. Migratory cells were imaged for 20 hours after PDGF-BB washing using time-lapse microscopy. In case of MSCs aggregates, a microfluidic channel was etched in close proximity to a growing microtissue and PDGF-BB was perfused in a pulsed fashion, that is, a three times 15 minute perfusion followed by a sequence of 45 minutes of washing as schematically shown in Supplementary Figure 3c. Migratory cells were imaged for 20 hours after PDGF-BB washing by time-lapse microscopy. For both 3D migration assays, the cells were tracked using the MTrackJ plugin of ImageJ.

Generation of in vitro blood vessel-like constructs: Collagen type I hydrogels (0.4% w/v) were formed in the PDMS mounts and a linear microfluidic channel was photo-ablated in the collagen gel. HUVEC were harvested according to standard protocols and re-suspended at high concentration (12.5×10^6 cells/mL). To avoid cell sedimentation in the inlet and outlet, OptiPrep Density Gradient Medium (Sigma, cat. No. D1556-250ML) was added to the cell suspension. The cell suspension was then added at the entrance and the exit of the microfluidic channel. Finally, the construct was incubated for two hours at 37°C and 5% CO₂ and flipped after one hour to allow HUVEC to attach to the entire surface of the collagen channel (protocol adapted from previously reported work^{5,6}). After the cells attached to the collagen

surface, medium was added in the inlet and outlet in order to allow cells to proliferate over the full collagen channel. The construct was incubated for five days with no flow using expansion medium before fixation and analysis.

Immunostaining: Cellularized collagen constructs were washed with 1X PBS and fixed with 4% paraformaldehyde for 30 minutes at room temperature on an orbital shaker. The samples were washed thoroughly and the cells were permeabilized with 0.2 % TritonX in 1X PBS for 30 minutes at room temperature. After further washing, the samples were blocked with 2% BSA in 1X PBS for 2 hours at room temperature. Primary antibodies against CD-31 (host: mouse, dilution 1:50, BD Biosciences) and VE-cadherin (host: rabbit, dilution 1:50, ABCAM) were then added in the blocking buffer and incubated overnight at 4°C. The primary antibodies were then washed thoroughly and appropriate secondary antibodies were added and incubated overnight at 4°C.

REFERENCES

- 1 Choi, N. W. *et al.* Microfluidic scaffolds for tissue engineering. *Nature materials* **6**, 908-915, doi:10.1038/nmat2022 (2007).
- 2 Ehrbar, M. *et al.* Enzymatic formation of modular cell-instructive fibrin analogs for tissue engineering. *Biomaterials* **28**, 3856-3866, doi:10.1016/j.biomaterials.2007.03.027 (2007).
- 3 Ehrbar, M. *et al.* Biomolecular hydrogels formed and degraded via site-specific enzymatic reactions. *Biomacromolecules* **8**, 3000-3007, doi:10.1021/bm070228f (2007).
- 4 Ehrbar, M. *et al.* Elucidating the role of matrix stiffness in 3D cell migration and remodeling. *Biophysical journal* **100**, 284-293, doi:10.1016/j.bpj.2010.11.082 (2011).
- 5 Morgan, J. P. *et al.* Formation of microvascular networks in vitro. *Nature protocols* **8**, 1820-1836, doi:10.1038/nprot.2013.110 (2013).
- 6 Miller, J. S. *et al.* Rapid casting of patterned vascular networks for perfusable engineered three-dimensional tissues. *Nature materials* **11**, 768-774, doi:10.1038/nmat3357 (2012).

Supporting Movies:

Movie S1: Three-dimensional reconstruction from a confocal z-scan of a ramp-shaped microchannel.

Movie S2 Three-dimensional reconstruction from a confocal z-scan of a spiral-shaped microchannel.

Movie S3: Polystyrene microbeads (15µm in diameter) flowing through a Y-shaped microfluidic network.

Movie S4: Representative region of interest showing placenta-derived human mesenchymal stem cells (hMSCs) migrating towards the source microchannel, perfused with soluble placenta-derived growth factor (PDGF).

Movie S5: Representative region of interest showing placenta-derived human mesenchymal stem cells (hMSCs) non-activated beside the source microchannel, perfused with serum-free and growth factor-free medium (control condition).

Movie S6: Representative region of interest showing placenta-derived human mesenchymal stem cells (hMSCs) grown as aggregates migrating towards source the microchannel perfused with soluble placenta-derived growth factor (PDGF).

Movie S7: Representative region of interest showing placenta-derived human mesenchymal stem cells (hMSCs) grown as aggregates non-activated beside the source microchannel perfused with serum-free and growth factor-free medium (control condition).

APPENDIX B

SUPPORTING INFORMATION FOR CHAPTER III: STANDARDIZING COMPLEX ORGANOID CULTURES THROUGH MICROENGINEERED SUBSTRATES

Supporting Figures:

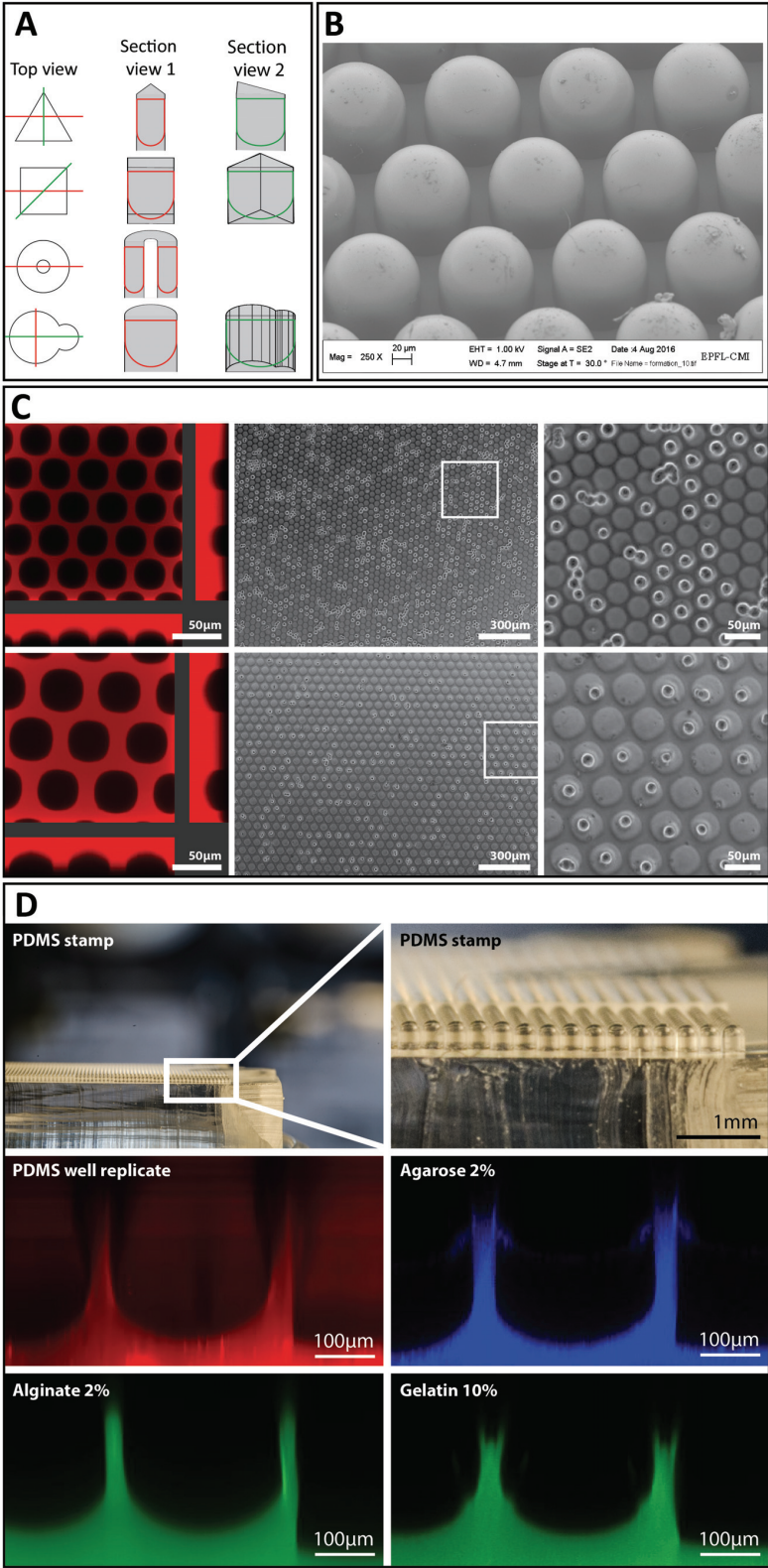


Figure S1: (A) Schematic representation of microwells having multiple geometrical shapes. Any shape, such as triangles, squared, tore-like structure, and fully irregular structures can be used to produce U-bottom microwells. These can be used for multiple applications; especially it can be a powerful tool for assessing the impact of the culture substrate's geometry on cellular functions. (B) Scanning electron microscope (SEM) representative image of microwells of 100 μ m in diameter and 120 μ m in width. (C) Microwells of sizes comprised between 10 and 50 μ m wells were moulded in 12.5kPa PEG hydrogel to create a single cell culture platform. Single cells were successfully seeded in separate well. (D) From the PDMS negative mold, diverse materials were imprinted with the above-described pattern. Soft, biocompatible polymers such as PDMS were used, as they are widely used for cell culture applications. More importantly, standard synthetic hydrogels such as polyethylene glycol (PEG) were demonstrated to be moldable as well as natural hydrogels, such as agarose, alginate, gelatin, Matrigel™ and collagens (data not shown).

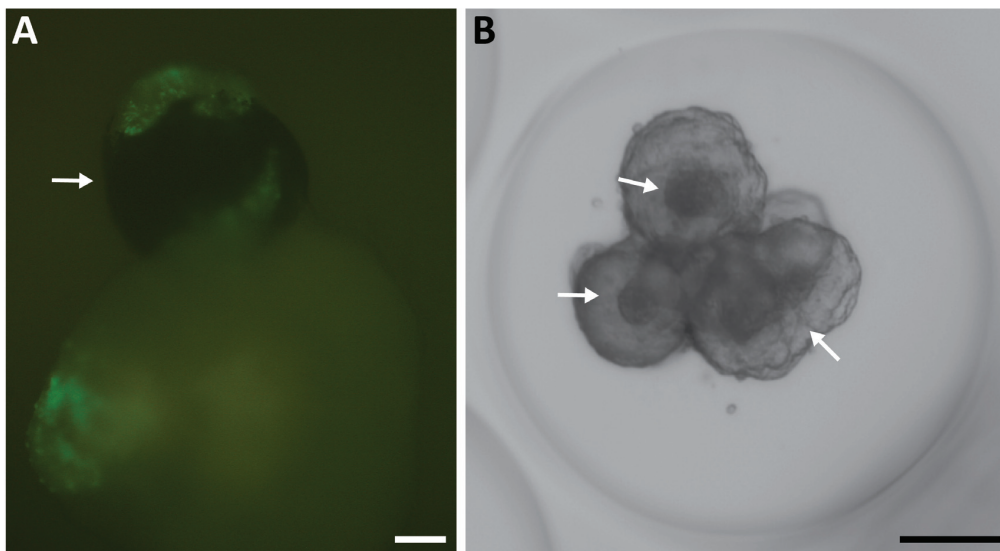


Figure S2: (A) Representative widefield fluorescent image of retinal pigmented epithelium (RPE) wrapping around the retinal tissue (white arrow). This colocalization is very rare but might be important for improving the survival of photoreceptors. (B) Intestinal organoid harbouring multiple lumen due to an excess of starting intestinal stem cells contributing to the organoid. Scale bars: 100 μ m.

APPENDIX C

CURRICULUM VITAE

Nathalie Brandenburg

Avenue de Floréal 2, 1006 Lausanne, Switzerland

Phone number: +41796789253 – Email address: nathalie.brandenberg@epfl.ch

Nationality: Swiss

EDUCATION

PhD in Biotechnology & Bioengineering 2016

Ecole Polytechnique fédérale de Lausanne (EPFL), Switzerland

Laboratory of Stem Cell Bioengineering, Prof. Lutolf's group

PhD thesis:

Advanced technologies to control stem-cell based organogenesis 2012-2016

Master of Science MSc in Bioengineering 2011

The University of Tokyo (東京大学), Tokyo, Japan and Ecole Polytechnique fédérale de Lausanne (EPFL), Switzerland

School of Life science and Technology

Master's thesis:

Cell bead based three-dimensional (3D) hepatic model toward high-throughput drug-induced toxicity screening 2010-2011

Bachelor of Science BSc in Life Science and Technology 2006-2009

Ecole Polytechnique fédérale de Lausanne (EPFL), Switzerland

School of Life science and Technology

PROFESSIONAL EXPERIENCE

SUN bioscience, SA, Lausanne, Switzerland 2016-present

Co-founder and COO of SUN bioscience SA (incorporation date, Jan. 2016)

SUN bioscience SA is an EPFL spin-off active in developing cell culture technologies for stem cell-derived organoids.

Bio Architecture Laboratory, Tokyo, Japan 2011-2012

Visiting scholar in Prof. Matsunaga's group research group

VOLUNTEERING EXPERIENCE

NADIA, Ishinomaki, Japan. 2011

Help for the victims of The Big Tohoku earthquake and tsunami, March 11th 2011

PUBLICATIONS

Hoehnel, S.*, **Brandenberg, N.***, et al, Arrays of reproducible intestinal organoids, *Nature Methods*, *in submission*.

Unzu C., Friedli M., Planet E., **Brandenberg N.**, Fusil F., Rougemont A., Cosset F.L., Lutolf M.P., Wildhaber B.E., and Trono D., Induced hepatic progenitor cells for the highly efficient expansion of primary human hepatocytes, *Nature Biotechnology*, *submitted*.

Brandenberg N., Lutolf M.P., Employing Microfluidic Devices to Induce Concentration Gradients, *Biology and Engineering of Stem Cell Niches* 1st Edition (Chapter 27), ISBN: 9780128027349, expected release Apr. 2017.

Brandenberg, N. & Lutolf, M. P. In Situ Patterning of Microfluidic Networks in 3D Cell-Laden Hydrogels. *Advanced materials*, 28(34):7450-7456, (2016).

Cosson, S., Aeberli, L. G., **Brandenberg, N.** & Lutolf, M. P. Ultra-rapid prototyping of flexible, multi-layered microfluidic devices via razor writing. *Lab on a chip*, **15**, 72-76, (2015).

PATENTS

Organoid tissue engineering, Gjorevski N., **Brandenberg N.**, Geraldo S., Tabata Y., Nikolaev M., Lutolf M., EP16199677.2 (Nov 18 2016).

Organoid arrays, Hoehnel S., **Brandenberg N.**, Lutolf M., EP16189510.7 (Sept 19 2016).

Devices for high-throughput aggregation and manipulation of mammalian cells, Hoehnel S., **Brandenberg N.**, Lutolf M., PCT/IB2014/067242 (Dec 22 2014).

